March 1982

CORNELL UNIVERSITY

Center for Radiophysics and Space Research

ITHACA, N. Y.

FINAL TECHNICAL REPORT

NASA Grant NGR 33-010-182

"16 to 40 Micron Spectroscopy from the NASA Lear Jet"

Funded

October 1, 1970 to October 31, 1980

Principal Investigator: J. R. Houck

FINAL TECHNICAL REPORT

NASA Grant NGR 33-010-182

"16 to 40 Micron Spectroscopy from the NASA Lear Jet"

Funded

October 1, 1970 to October 31, 1980

Principal Investigator: J. R. Houck

Department of Astronomy
Cornell University
Ithaca, New York 14853-0352

TABLE OF CONTENTS

Many scientific discoveries and technical innovations were made during the tenure or NASA Grant NGR 33-010-182. The program involved the design, fabrication and extensive use of two cryogenically cooled infrared grating spectrometers on the NASA Lear Jet Observatory. The first spectrometer was used to measure continuum sources such as dust in HII regions, the Galactic Center and the thermal emission from Mars, Jupiter, Saturn and Venus over the 16-40μm spectral range. The second spectrometer had higher resolution and was used to measure ionic spectral lines in H II regions (SIII at 18.7μm). It was later used extensively on NASA C-141 Observatory to make observations of numerous objects including HII regions, planetary nebulae,stars with circumstellar shells, the Galactic Center and extragalactic objects. It has only recently been superseded by an instrument of even higher resolution (built under NASA NGR 33-010-081).

In the remainder of this report the spectrometers are described including the major innovations and a list of the scientific contributions. In the final section a list of active participants on the project is presented. The appendix presents the major scientific paper published under the program. In addition, numerous scientific papers and colloquia were presented. No attempt has been made to list these presentations.

I. TECHNICAL INNOVATIONS

A. Cryogenically Cooled Spectrometers

Two small, liquid-helium-cooled grating spectrometers

for medium resolution astronomical spectrometry in the 16-40μ region have been designed and built. They have been used in conjunction with NASA's 31-cm Flying Infrared Telescope on the Lear Jet and the 91-cm telescope of the Kuiper Airborne Observatory.

A medium resolution is sufficient to allow observation of the broad spectral features associated with pressure-induced hydrogen absorption in the atmospheres of the Jovian planets. Interstellar dust found in HII regions can also be effectively studied with modest resolution. These instruments have been used to obtain spectra of the Orion Nebula and many other HII regions and obscured protostars.

The design objectives for the instruments were:

(1) a resolution $\frac{\lambda}{\Delta\lambda} \approx$ 30 to 200;

(2) entrance aperture corresponding to a beam on the sky of 2-6-arc minutes, with the Learscope (1-3-mm entrance aperture);

(3) cooled to liquid helium temperature to reduce the thermal background on the detector;

(4) simplicity of design and operation.

The etendue of the instrument was selected to match the Lear telescope (f/7.5) and the astronomical sources (<1-arc minute for the planets and 1-5-arc minutes for HII regions). An entrance aperture somewhat larger than the image size is desirable because of guiding jitter caused by the telescope stabilization system.

Simplicity of design and fabrication was desired in the instrument because of the

near impossibility of making adjustments while it is at liquid helium temperatures and to maximize the reliability of the instrument in the severe airborne environment. Since the optical requirements were not severe, a single pass Ebert-Fastie design is used.

B. Optical Design

The optical layout of one of the instruments is shown in Figure 1a. The radiation enters the entrance aperture (which lies above the plane of the paper) and is then reflected 90° into the plane of the paper by a 45° mirror. The radiation is collimated and then directed to the grating. Two parts of the diffracted beam are intercepted and sent to two separate detectors by concave mirrors that reduce the image size of the entrance aperture by a factor of 2.

Detector #1 is an arsenic-doped silicon photoconductor which is normally used in second order for wavelengths of 16-23μ. Detector #2 was a gallium-doped germanium photoconductor (it was later replaced by a zinc-doped germanium photoconductor) which is used in first order for wavelengths of 20-40μ. Thus for each grating position a short wavelength and a long wavelength are observed simultaneously; this procedure shortens the time necessary to measure a given spectrum and allows one to determine the extent of guiding jitter.

Detector #1 can be used in first order, if desired. Then, it will respond to radiation from wavelengths of 16-24μ.

The spectral orders are separated by an interference filter for the short wavelength detector (#1) and by the two

CaF_2 restrahlen mirrors for the long wavelength detector. The only transmission element in the system is the KRS-5 Dewar window.

The grating is a standard Bausch and Lomb replica; it has 21 grooves per millimeter and is blazed for 28.56μ. The ruled area is 26x26 mm, which is not quite fully illuminated. The focal length of the primary mirror is 125 mm, which gives a dispersion of 0.38μ/mm in first order and a nominal resolution of 1.0μ in first order and 0.5μ in second order with our 2.7-mm diameter entrance aperture.

The optical layout of the second instrument is shown in Figure 1b. The entrance aperture and collimating optics are similar to those described above. The dispersed beam is filtered by restrahlen reflection plate and an interference filter. The instrument was first flown with a four-element array of cooper-doped germanium detectors. Although the instrument performed well, the detectors had 2 or 3 times worse NEP's than corresponding Si:As elements. The performance was dramatically improved by the installation of a ten-element array of doped-silicon detectors (Si:Sb).

C. Mechanical Considerations

The spectrometer itself is 125 mm (5 in.) in diameter and 59.5 mm (2-11/32") tall and is mounted on the OFHC copper baseplace of a liquid helium can inside a helium Dewar as shown in Figure 2. The spectrometer is constructed entirely of aluminum (6061-T6) except for the detector cavities which are of OFHC copper.

The Ge:Ga (Ge:Zn) detector is heat sunk directly to the copper baseplate of the Dewar, while the silicon detectors are heat sunk to the baseplace of the spectrometer.

The primary mirror and the grating are mounted in spring loaded holders with copper cold straps to the body of the spectrometer.

All the small mirrors are attached to their mounting posts with either rubber cement or epoxy. These mirrors are supported only at one point to minimize distortion of their surfaces due to the differential thermal expansion between aluminum and glass or CaF_2. In many years of experience with more than 100 cool-down cycles, none of these joints has failed. No problems have been encountered with any of the optical components which can be associated with the helium temperature operation.

The grating carrier is attached to shafts which ride in ball bearings at the top and bottom of the spectrometer. On the bottom is a sector of a worm gear mounted on the grating shaft. A worm is also mounted on the bottom plate and meshes with the gear. The worm is connected via two flexible bellows couplings and a fiberglass shaft to the outside of the Dewar through a vacuum tight O-ring fitting. Once outside, the grating driveshaft is connected to a Superior Electric stepping motor by 1:1 bevel gears. A shaft encoder and a rotation counter on the worm shaft are used to monitor the grating position.

D. Spectrometer Performance - Lear Jet 30-cm Telescope

- 10-detector array spectrometer

  $\lambda\lambda 16\text{-}30$ $\quad \Delta\lambda = 0.5\mu$ $\quad$ Si:Sb detectors

  Beam size = 2.7'

  $A\Omega \simeq 3.6 \times 10^{-4} cm^2$ ster

In September-October, 1977, we observed VY CMa on several flights. From our flux calibration we estimate F_{23} (VY CMa) $\simeq 5 \times 10^{-15} W/cm^2\mu$ which corresponds to $F_\nu(23\mu$, VY CMa) $\simeq 8800$Jy. From an extensive series of noise measurements during several flights, we estimate an rms S/N ratio of approximately 22 for one second of integration time at wavelengths between atmospheric water vapor absorption.

If we define:

$$NEP_{system} = \sqrt{t}\ \frac{P}{S/N} \quad . \qquad (1)$$

and

$$NEFD_{system} = \sqrt{t}\ \frac{F_\nu}{S/N} \qquad (2)$$

where t = integration time, P - power from the source in the detector bandpass incident on the telescope, F_ν is the flux density of the source, S/N is the estimated rms signal-to-noise ratio. Then the above data imply a system performance at 23μ wavelength of:

$$NEP_{system} \simeq 8 \times 10^{-14} W/\sqrt{Hz}$$

and

$$NEFD_{system} \simeq 360\ Jy/\sqrt{Hz}$$

for each 0.5μ bandpass. The individual detectors are matched

to within ±10% of this performance.

For the observed in-flight detector performance, we estimate the spectrometer transmission to be ≈20%, the beam-splitter reflectivity to be ≈90%, and the chopper efficiency to be ≈90%. Then the observed detector performance in flight is approximately

$$NEP_{detector} \approx 1.3 \times 10^{-14} W/\sqrt{Hz}$$

for each of the 10 detectors.

●● Two-Detector Spectrometer

λλ16-23	Δλ = 0.5μ	Si:As detector
λλ21-38	Δλ = 1.0μ	Ge:Zn detector

beam size ≈ 3.3'

$A\Omega \approx 5.5 \times 10^{-4} cm^2$ ster

From measurements made on VY CMa in November 1976, we estimate, using equations (1) and (2), and the techniques outlined above, in flight performances of

	Si:As @ 19.3	Zn:Ge @ 31.2
NEP_{system}	$\approx 4 \times 10^{-13} W/\sqrt{Hz}$	$8 \times 10^{-13} W/\sqrt{Hz}$
$NEFD_{system}$	≈ 1500 Jy/$\sqrt{Hz}$	3900 Jy/$\sqrt{Hz}$
$NEP_{detector}$	$\approx 6.6 \times 10^{-14} W/\sqrt{Hz}$	$1.3 \times 10^{-13} W/\sqrt{Hz}$

E. Servo-Controlled Chopper Systems

The early choppers used on the Lear Jet employed solenoids and mechanical limit stops. As a result no adjustments could be made of the chopper during flight to either change the chopper throw or its offset. Because of the mechanical stops, the chopper was very microphonic and required frequent adjustment. These early choppers were replaced by a servo-controlled

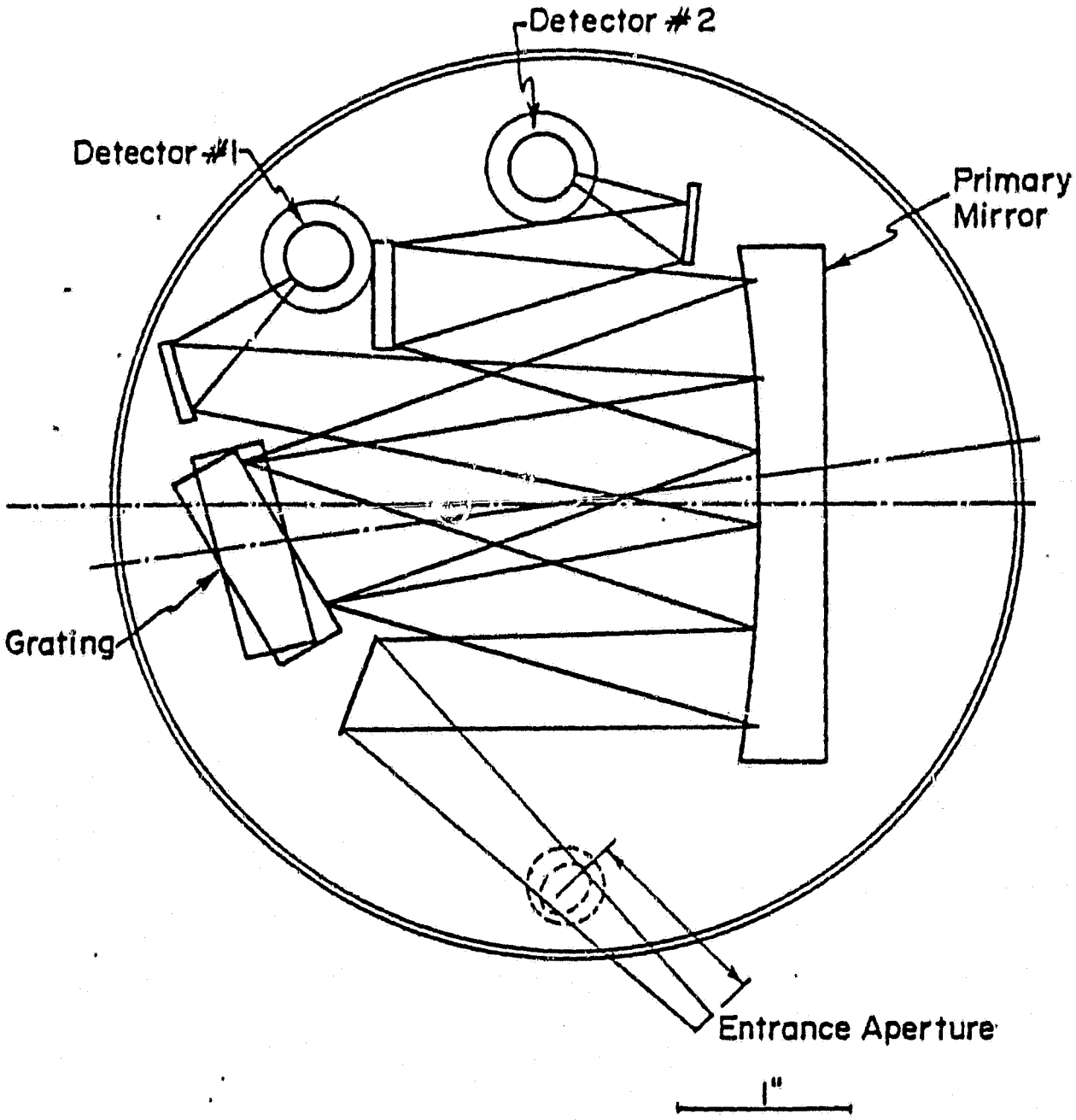

Fig. 1a Optical layout of the two-channel grating spectrometer.

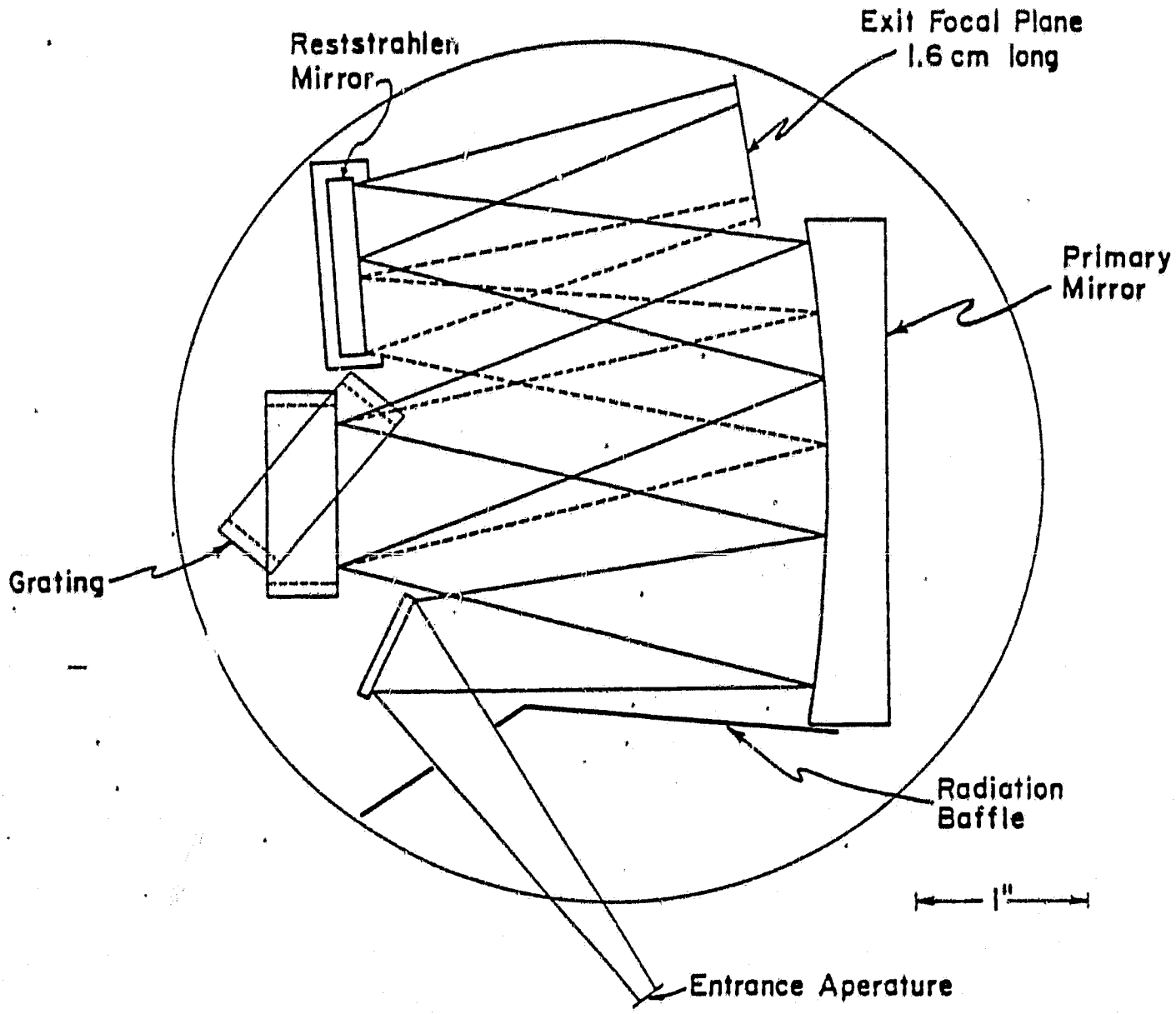

Fig. 1b. Optical layout of the multi-detector array spectrometer.

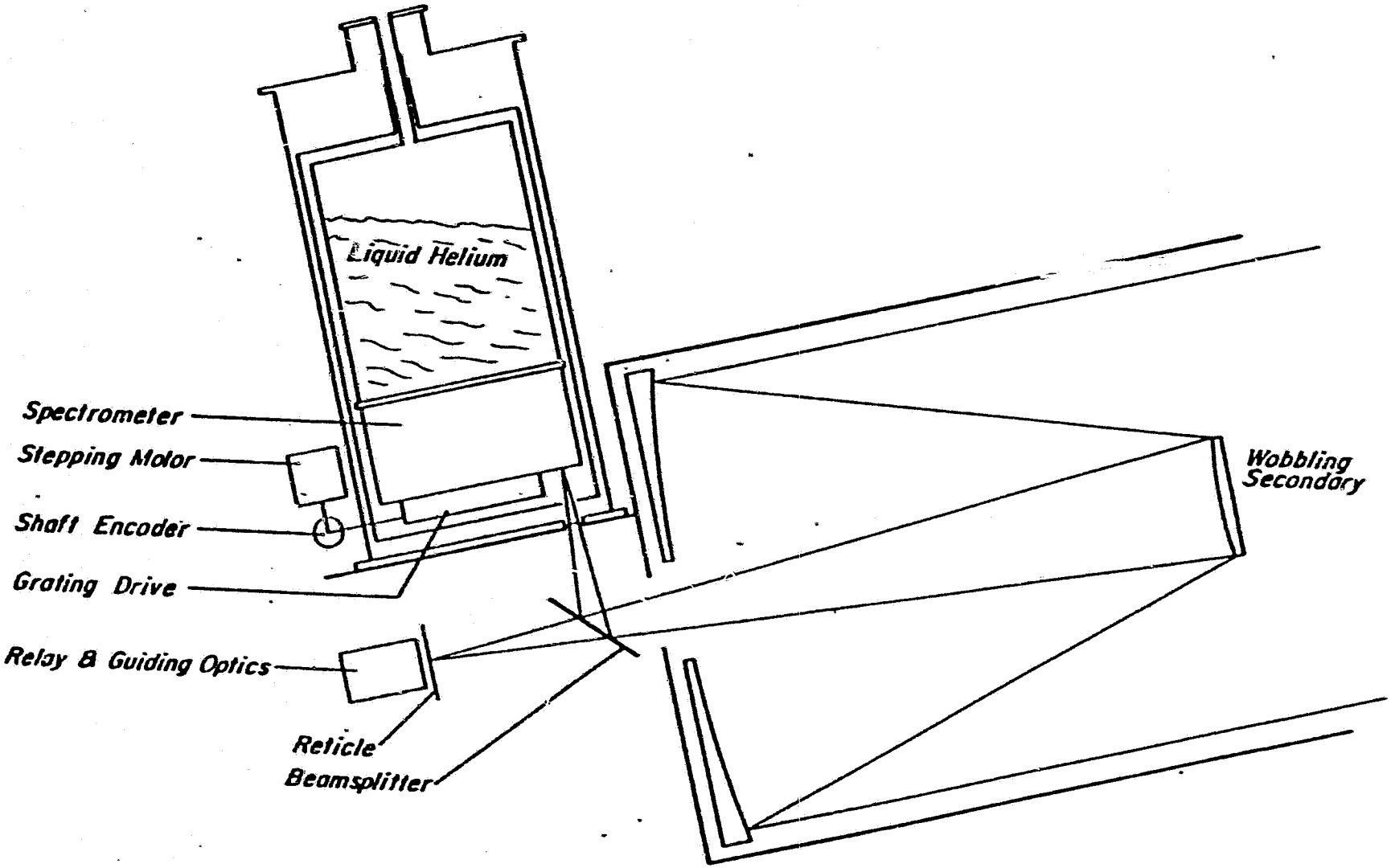

Fig. 2. Schematic of the spectrometer and liquid helium dewar mounted on the Lear Jet telescope.

chopper in 1975. The chopper was designed at Cornell and fabricated in the Ames model shop. The electronic drive unit was designed and built at Cornell. The system was optimized at Cornell and field-tested on the Lear Jet. It was subsequently turned over to the Ames personnel and has been maintained by them since 1976. Since then it has been the standard chopper for all Learscope observers who use choppers.

IV. SCIENTIFIC RESULTS

Numerous scientific results have been achieved using these spectrometers on the Lear Jet. In this section a very brief list of these is presented. The appendix includes a much more complete summary of our results.

Planetary Objects:

Jupiter - Determination at the He/H abundance ratio.

Saturn - Same as for Jupiter

Mars - Determination of continuum spectrum.

Venus - Detection of spectral features due to H_2SO_4 in the atmosphere.

Galactic HII Regions:

1) Determination of the shape of the "20μm silicate feature" in a large number of sources.

2) Measurement and interpretation of the SIII 18.7μm spectral line in nearly a dozen HII regions.

Stars: Determination of the long wavelength distribution of emission from VY Canis Majoris.

Galactic Center: Measurements of the 16 to 30μm continuum emission from the Galactic Center. Determination of the dust extinction toward the Galactic Center.

III. PERSONNEL

The success of this program is do to the efforts of many people. At Cornell these included three students who received their Ph.D.'s for research conducted on this program. Dr. W. J. Forrest was a post-doctoral research associate during much of the program and was the central figure in much of the work. Extraordinary technical support was provided by G. Stasavage, G. Gull and D. Briotta. The efforts of the Ames personnel were crucial to the success of the program. We particularly appreciate the assistance of the Lear Jet Manager, Robert Mason, and his staff. We also appreciate the Lear Jet pilots who spent many uncomfortable and often very cold hours in the middle of many nights helping us "get the data."

PH.D. THESES

David Francis Schaak, 1975, "Infrared Astronomical Spectroscopy from High Altitude Aircraft."

Robert Alan Reed, 1976, "The 16-to 40-Micron Spectra of Jupiter and Venus."

John Francis McCarthy, 1980, "Airborne Infrared Spectroscopy of Ionized Hydrogen Regions and the Galactic Center."

APPENDICES

THE ASTROPHYSICAL JOURNAL, 193:L139–L141, 1974 November 1

20 TO 40 MICRON SPECTROSCOPY OF THE ORION NEBULA

J. R. HOUCK,* D. F. SCHAACK, AND R. A. REED
Center for Radiophysics and Space Research, Cornell University
Received 1974 July 22

ABSTRACT

We present moderate-resolution (1.0 μ) spectra of the Orion Nebula. These observations are the first spectroscopic observations of the object between 20 and 40 μ. A comparison of our data with that of Harper, Solfer and Hudson, and Harvey *et al.* is presented. We find that the best fit to all of the data is provided by a model in which the dust within the molecular cloud has a clumpy distribution. The individual clumps have effective grain temperatures of 100° K and are optically thick for wavelengths shorter than 400 μ. The total dust mass required by this model is less than 20 $M_\odot$.

Subject headings: infrared — interstellar matter — Orion Nebula

I. INTRODUCTION

Two types of extended infrared sources have been detected in the Orion Nebula. The first type shows a strong 10-μ emission feature thought to result from circumstellar shells of silicate dust. The Ney-Allen (1969) object is of this type. The second class of objects shows the same feature in absorption (e.g., the Kleinmann-Low Nebula). These objects are thought to be "stars" embedded in much larger dust clouds. The former objects seem to cluster in the direction of the Trapezium while the latter are centered about the position of the molecular cloud (Zuckerman 1973).

As first shown by Harvey *et al.* (1974), the bulk of the submillimeter radiation also comes from the direction of the molecular cloud. At 1 mm the apparent size of the cloud is $\sim$2′. We present new observational data between 20 and 40 μ. Several models are presented in an attempt to account for all of the observations from 20 μ to 1 mm.

Analysis of the 28.2-μ line of molecular hydrogen will be presented in another paper.

II. OBSERVATIONS

The Orion nebula was observed on the nights of 1973 November 14–21 using the 31-cm telescope mounted on the NASA Lear jet. This telescope is very similar to the one developed by Low. The aircraft was flown to an altitude of 14 km (45,000 feet). At this altitude about 3 to 10 precipitable microns of water per air mass remain above the observer. The telescope viewed the source at elevation angles between 14° and 28° (4.1 to 2.1 air mass). The spectral scans were made using a liquid-helium-cooled grating spectrometer (Schaack and Houck 1974). This instrument employs a 12.5-cm focal length Ebert-Fastie spectrometer with two detectors in the focal plane. A Ge:Cu photoconductor scans the 16–28 μ band while a Ge:Ga photoconductor covers 20–40 μ. The resolutions of the two channels are 0.5 and 1.0 μ, respectively. We report here only the results of the 20–40 μ channel. The instrument operates at f/7.5 and has a 2.7-mm entrance aperture corresponding to 4′.7 on the sky. A wobbling secondary chopper was used. The beam separation was 15′. The chopping frequency was 48 Hz.

The instrumental response was determined by normalizing spectra of the Moon and Mars as if they were blackbody radiators at 350° and 220° K, respectively. The instrumental profile determined in this way was used to normalize the Orion data. The resulting spectrum is shown in figure 1. The spectrum was normalized to the 30–45 μ broad-band photometric point determined by Harper (1974). This is consistent with an absolute calibration of the system by intercomparing Lear-jet and ground-based observations of Jupiter. It is also consistent with the low-spatial-resolution 20-μ ground-based map of Orion obtained by Lemke, Low, and Thum (1974). The major noise source was tracking error associated with the pointing system of the Learscope.

III. DISCUSSION

Figure 2 shows representative far-infrared observations of Orion. The dashed curve is the result of a model in which the source is a uniform 2′ diameter cloud as suggested by the observations of Harvey *et al.* It has been assumed that the grain emissivity is proportional to the reciprocal wavelength squared. This is the form

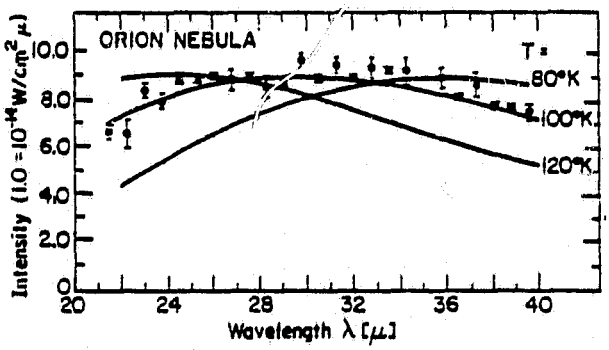

FIG. 1.—Spectrum for the Orion region from 20 to 40 μ. The beam diameter was 4′.7. The curves are of blackbody radiation at various temperatures.

* Alfred P. Sloan Foundation Fellow.

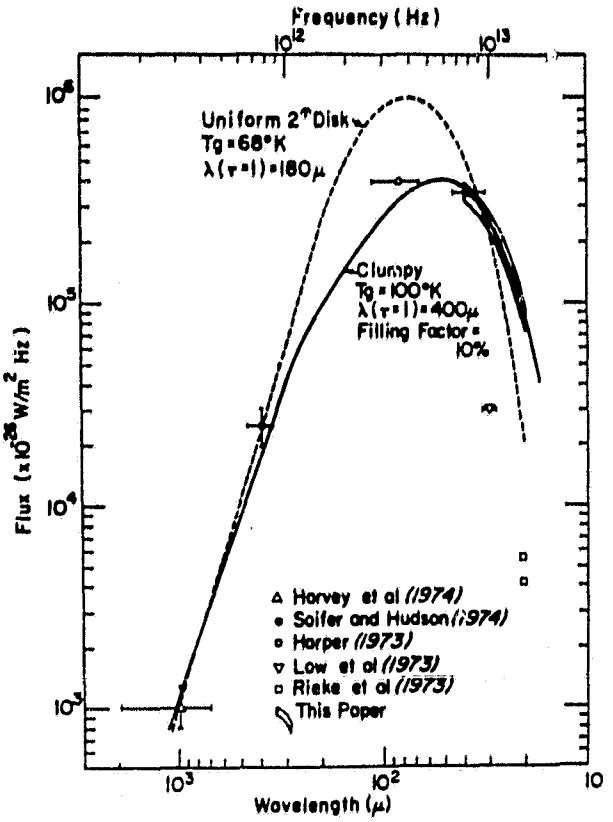

FIG. 2.—Results of several studies of Orion. *Dashed curve*, a uniform disk model; *Solid curve*, a clumpy model with a filling factor of 10%.

which results from using the optical constants for lunar material and the scattering theory for small particles (Knacke and Thompson 1973). Hoyle and Wickramasinghe (1962) have also suggested this frequency dependence for graphite grains. The model was fitted to the data points at 30 and 1000 μ. This two-parameter fit determined the grain temperature T_g and the wavelength at which the cloud becomes optically thick, λ_T:

$$F_{\rm OBS} = B(\lambda, T_g)\Omega_{\rm NEB}[1 - \exp - (\lambda_T/\lambda)^2] , \qquad (1)$$

where $F_{\rm OBS}$ is the observed flux, $B(\lambda, T)$ the Planck function, $\Omega_{\rm NEB}$ the solid angle of the nebula ($\Omega_{\rm NEB} = 2.1 \times 10^{-7}$ sr for a 2′ disk). For this model $T_g = 68°$ K and $\lambda_T = 180$ μ.

The solid curve results from a model in which the emissivity again is proportional to λ^{-2}. In this case, however, an attempt was made to fit the shape of the observed data disregarding temporarily the absolute flux comparison. Under these conditions the best fit is obtained by $\lambda_T = 400$ μ with $T_g = 100°$ K. A direct application of equation (1) predicts 10 times more flux at each wavelength than is observed. Strong clumping within the source would of course reduce the flux below that predicted by equation (1). In this case one would conclude that only 10 percent of the 2′ beam was filled by sources each with $T_g = 100°$ K and $\lambda_T = 400$ μ.

Rieke, Low, and Kleinmann (1973) have mapped the region around the Kleinmann-Low nebula at 5, 10, and 20 μ with very high spatial resolution (5″–10″). They find that the region is divided into at least five separate sources. These clearly separated sources are too faint to account for the flux observed between 30 and 45 μ by Harper (1974) from the Lear jet by a factor of 10 to 20, assuming the small sources have the same spectral shape as the entire region. Rieke *et al.* also find evidence at 10 μ for an underlying smooth (or unresolved distribution of sources) flux distribution. Even including this radiation, the ground-based observations detect only 10–20 percent of the large beam flux observed from aircraft. This discrepancy is probably due to the self-cancellation inherent in beam-switched observation of extended sources. Typical beam throws for airborne observations are 10′, whereas they are is seldom larger than 1′ for ground-based observations. Therefore, ground-based observations support a clumpy model, but we are unable to make a clear connection between ground-based and airborne observations.

The "uniform cloud model" is pressed to explain any small-scale features. If the cloud has $\lambda_T \approx 180$ μ, then the optical depths at 20, 10 and 5 μ are 15, 20, and 15, respectively, if the data of Knacke *et al.* are used. Under these conditions the sources seen by Rieke *et al.* would have to be very near the surface of the cloud to be seen at all. The sources would be confined to $\lesssim 5$ percent of the volume of the cloud.

A third model involves a "uniform cloud" with 10 percent of the area of the 2′ source seen by Harvey *et al.* with $T_g = 100°$ K and $\lambda_T = 400$ μ. This model would result in an enormously bright object 40″ in diameter that is inconsistent with ground-based surveys.

A fourth model is one in which Q varies as λ^{-2} for $\lambda \geq 400$ μ and $Q \approx$ constant for $\lambda \leq 400$ μ. Such a behavior would be quite unlike that of lunar material. However, the results of Knacke *et al.* are derived from room temperature measurements of materials that have undergone sufficient heating to acquire recognizable mineralogical forms. For the Orion cloud the temperature is certainly much less than room temperature. Further, it is quite likely that the grains have much less regular structure than lunar fines. Hoyle and Wickramasinghe (1969) suggested that the impurities (including structural imperfections) would lead to enhanced emission at long wavelengths. One would therefore invoke enhanced emission due to a variety of impurities to maintain $Q \approx$ constant with $\tau \approx 0.1$ from 20 to 400 μ. This degree of enhancement would be possible based on the detailed analysis of impurity mode emission by Field (1969). At wavelengths longer than 400 μ one would still expect a λ^{-2} dependence as shown by the arguments of Gezari, Joyce, and Simon (1973) and Gezari *et al.* (1974).

The mass of dust involved is best determined by fitting the parameters of the source and dust at 1 mm where the optical depth is small for all models:

$$M_{\rm grains} = \tfrac{4}{3}\left(\frac{a}{Q}\right)\frac{F_{\rm OBS}R^2\rho}{B(\lambda, T)} \quad \text{for } \tau < 1 ,$$

where R is the distance to the nebula, 460 pc; Q is the ratio of effective emitting cross-section to geometrical cross-section; and a is the grain radius (taken to be 0.2 μ). The value of Q/a ranges between 0.3 cm^{-1} (Knacke and Thomson 1973) to 400 cm^{-1} (Werner and Salpeter 1969). The higher value corresponds to the maximum allowable value based on the inclusion of impurity oscillators.

For the clumpy model the mass of the dust is 0.02–20 $M_\odot$ depending on the choice of Q/a. The uniform disk model requires 50 percent more dust because of the lower temperature. Using dynamical considerations, Zuckerman (1973) has estimated the total molecular hydrogen mass to be $\lesssim 10^4 M_\odot$. The above estimates are therefore consistent with cosmic abundances.

We wish to thank J. L. Pipher and B. T. Soifer for many helpful discussions. We are also grateful for the efforts of the NASA Ames Airborne Science Office. This work was supported by NASA grant NGR 33-010-182.

REFERENCES

Field, G. B. 1969, *M.N.R.A.S.*, **144**, 411.
Gezari, D. Y., Joyce, R. R., Richini, G., and Simon, M. 1974, preprint.
Gezari, D. Y., Joyce, R. R., and Simon, M. 1973, *Ap. J.* (*Letters*), **179**, L67.
Harper, D. A. 1974, preprint.
Harvey, P. M., Gatley, I., Werner, M. W., Elias, J. H., Evans, N. J., Zuckerman, B., Morris, G., Sato, T., and Litvak, M. M. 1974, *Ap. J.* (*Letters*), **189**, L87.
Hoyle, F., and Wickramasinghe, N. C. 1962, *M.N.R.A.S.*, **124**, 417.
———. 1969, *Nature*, **223**, 459.
Kleinmann, D. E., and Low, F. J. 1967, *Ap. J.* (*Letters*), **149**, L1.
Knacke, R. F., and Thompson, R. K. 1973, *Pub. A.S.P.*, **85**, 341.
Lemke, D., Low, F. J., and Thum, C. 1974, *Astr. and Ap.*, **32**, 231.
Low, F. J., Rieke, G. H., and Armstrong, K. R. 1973, *Ap. J.* (*Letters*), **183**, L105.
Ney, E. P., and Allen, D. A. 1969, *Ap. J.* (*Letters*), **155**, L193.
Rieke, G. H., Low, F. J., and Kleinmann, D. E. 1973, *Ap. J.* (*Letters*), **186**, L7.
Schaack, D. F., and Houck, J. R. 1974, preprint.
Soifer, B. T., and Hudson, H. S. 1974, preprint.
Werner, M. W., and Salpeter, E. E. 1969, *M.N.R.A.S.*, **145**, 249.
Zuckerman, B. 1973, *Ap. J.*, **183**, 863.

J. R. Houck, R. A. Reed, and D. F. Schaack: Center for Radiophysics and Space Research, Cornell University, Ithaca, NY 14850

Jupiter: Its Infrared Spectrum from 16 to 40 Micrometers

Abstract. *Spectral measurements of the thermal radiation from Jupiter in the band from 16 to 40 micrometers are analyzed under the assumption that pressure-broadened molecular hydrogen transitions are responsible for the bulk of the infrared opacity over most of this spectral interval. Both the vertical pressure-temperature profile and the molecular hydrogen mixing ratio are determined. The derived value of the molecular hydrogen mixing ratio, 0.89 ± 0.11, is consistent with the solar value of 0.86.*

The abundance of H_2 and He in the Jovian atmosphere has a direct influence on a number of astronomical problems. Jupiter's low atmospheric temperature and great mass prevent even the lightest atoms from escaping from the top of the atmosphere. Therefore, Jupiter as a whole is a sample of the elemental abundance at the time of the formation of the planet. Modern theories of explosive nuclear synthesis show that most of the He presently in the universe was formed during the Big Bang (*1*). Further, it has been shown that the relative abundance of H_2 and He depends strongly on the temperature and density during the early stages of the evolution. To the extent that the Jovian atmosphere is representative of the planet as a whole, a measure of the H_2 mixing ratio $\alpha_{H_2} = N(H_2)/[N(H_2) + N(He)]$, where $N(x)$ is the number density of x in the atmosphere, is useful for the determination of the conditions during the early stages of the Big Bang. There are, however, several effects which may systematically distort the atmospheric value of α_{H_2}.

Opik has suggested a model for the formation of Jupiter in which first "hydrogen snow" collects to form a core and then a He-rich atmosphere is captured (*2*). Salpeter has suggested that there may be internal differentiation with the He sinking toward the center of the planet, resulting in a H_2-rich atmosphere (*3*).

We observed Jupiter on the nights of 14 November and 16 November 1973 and 21 January 1974, using a 31-cm telescope mounted on the National Aeronautics and Space Administration Ames Research Center Lear jet. The aircraft was flown to an altitude of 14 km (45,000 feet). At this altitude about 3 to 10 precipitable micrometers of water remain above the observer. The telescope viewed the source at elevation angles between 14° and 28°. The spectral scans were made with two different grating spectrometers cooled to liquid helium temperatures (*4*). These instruments employ an Ebert-Fastie spectrometer (12.5-cm focal length) with two detectors in the focal plane. Instrument 1 has a Ge:Cu photoconductor to scan the 16- to 28-μm band, and a Ge:Ga photoconductor covers the range from 20 to 40 μm. The resolution of the two channels is 0.5 and 1.0 μm, respectively. Instrument 2 has two Ge:Cu photoconductors and covers the range from 16 to 28 μm with a 2.7-mm entrance aperture corresponding to 4.7 minutes of arc. Jupiter had a diameter of about 0.5 minute of arc during the observing periods. The chopping frequency was 48 hertz.

We determined the instrumental response by normalizing spectra of the moon and Mars as if they were blackbody radiators at 350° and 240°K, respectively. The instrumental profile determined in this way is consistent with the laboratory profile and the absorption expected by the atmosphere. It was used to normalize the Jupiter data. The resulting spectrum (Fig. 1a) shows the presence of three absorption features at 18, 23.5, and 28 μm. The first and last are, respectively, the $J = 1$ and $J = 0$ rotational transitions of H_2. The 23.5-μm feature shown in Fig. 1a may be due to sulfur, silicate dust, or complex hydrocarbons in the atmosphere (*5*). However, recent data of greater resolution and signal-to-noise ratio indicates that the brightness temperature falls smoothly from a maximum at 21 μm to a broad minimum around 28 μm. The regions of the spectrum used to determine the ratio of H_2 to He are substantially unchanged. However, the reality of the 23.5 μm is somewhat in doubt. A discussion of all the observational data will be given by Pollack *et al.* (*6*).

The observed spectrum of Jupiter contains information about both a portion of its vertical temperature structure and its ratio of He to H_2. Before describing our numerical method for deriving this information, we describe the physical connection between these quantities and the observed spectrum. The brightness temperature found at a given wavelength is approximately equal to the value of the physical temperature in the Jovian atmosphere at an optical depth of unity. As the wavelength changes, the altitude at which the optical depth is unity also varies. Thus, spectral observations over a range of wavelengths provide information on the temperature conditions over a corresponding range of altitudes in the atmosphere. For the spectral band measured, H_2 is the principal source of opacity. The Jovian atmosphere is probed from pressures of about 0.15 to 0.6 atm, a region which includes a temperature minimum and the top of the convection zone.

In carrying out the analysis described below, we excluded data close to the 23.5-μm feature. In addition to opacity due to the rotational and translational transitions of H_2, we allowed for opacity due to NH_3, which is important only at the long-wavelength edge of our data. We carried out calculations both without and with an optically thick NH_3 cloud present in the zone regions of Jupiter, located at the level of the atmosphere where NH_3 saturation occurs. The NH_3 clouds were assumed to behave as blackbody emitters.

In accord with radio temperature measurements we assumed that the temperature gradient equaled the adiabatic value at pressures greater than the bottom altitude boundary of the region we sense (*7*). Our derived temperature profiles are consistent with this assumption. Above our top altitude boundary we made use of the temperature gradients derived by Orton (*8*) from an analysis of measurements in the region of the 7.7-μm CH_4 band.

Our ability to gain information about the ratio of He to H_2 follows from the dependence of the pressure-induced transitions of H_2 on this ratio. This dependence is illustrated in Fig. 1b, which shows the values of the absorption coefficient of H_2 when the rotational transitions occur in the

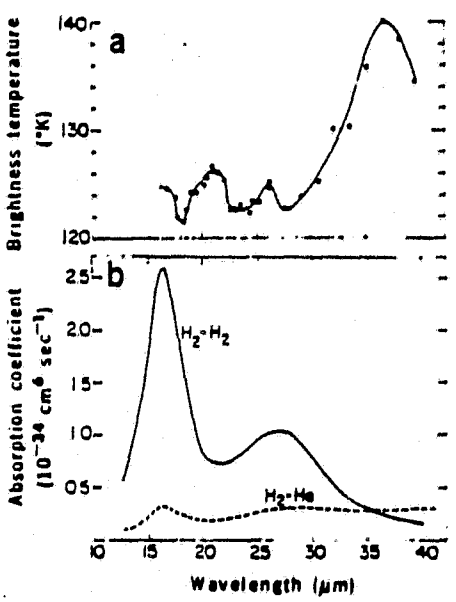

Fig. 1. (a) The brightness temperature of Jupiter for wavelengths from 16 to 40 μm. (b) The pressure-induced absorption coefficients for H_2-He collisions. The curves shown represent the sums of both translational and rotational transitions.

Reprinted from SCIENCE, 29 August 1975, volume 189, pages 720-722

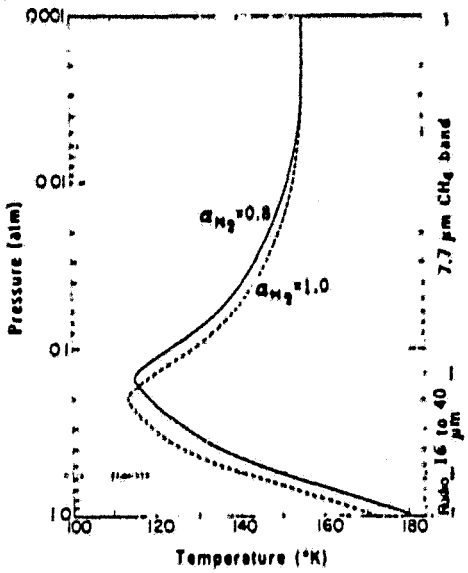

Fig. 2. A plot of the derived pressure-temperature profile for the Jovian atmosphere. The pressure level most directly measured by various observational techniques is shown.

presence of a nearby molecule of H_2 (H_2-H_2), and in the presence of a nearby He atom (H_2-He). We see from Fig. 1b that the absorption coefficient shows a different spectral variation for the (H_2-He) case than for the (H_2-H_2) case.

The numerical method used to obtain the desired information from the observed spectrum of Jupiter begins with an assumed trial value of α_{H_2}. For this choice of the mixing ratio, the observed spectrum is inverted to determine the pressure-temperature structure by means of an iteration technique developed by Smith (*9*) and applied to planetary atmospheres by Ohring (*10*). This method is similar to the method developed by Encrenaz and Gautier (*11*) and Gautier and Grossmann (*12*). It involves starting with a trial temperature profile, computing a predicted spectrum with this profile, and correcting the profile on the basis of the difference between the observed and calculated flux values, the flux residuals. The improved guess is used to repeat this process and, after a small number of iterations, the root-mean-square of the flux residuals approaches an asymptotic value. This procedure is repeated for other trial values of α_{H_2}. An estimate of α_{H_2} was obtained from the locations of the minimum in the value of the flux residual as a function of mixing ratio.

Figure 2 shows the vertical temperature structure of Jupiter determined from our spectrum for α_{H_2} values of 0.8 and 1.0. These results refer to models containing no NH_3 cloud opacity. However, very similar curves were obtained for measurements with optically thick clouds. Our results have been smoothly joined with the temperature gradients found above and below our region of sensing. Figure 2 also indicates the location of the regions probed in our measurement, at radio wavelengths, and within the 7.7-μm CH_4 band. The temperature values found from these various determinations are quite consistent near their boundaries. The temperature gradient becomes adiabatic at the higher-pressure domain of our sensing region, which is consistent with the temperature lapse rate implied by the radio results. We find that the lapse rate first reaches the adiabatic value and therefore that the convection zone begins at approximately 0.4 atm. This result is in good agreement with the theoretical predictions of Pollack and Ohring (*13*), which were based on a radiative equilibrium model. Our measurements also suggest the presence of a temperature minimum and the start of an inversion layer at the lower-pressure levels of our region. This aspect of the temperature profile is suggested by the small displacement of the observed minimum in our brightness temperature spectrum from the center of the $J = 1$ H_2 rotational transitions. These results are in accord with Orton's analysis (*8*) of measurements made in a spectral region containing the 7.7-μm fundamental of CH_4. The value of our temperature minimum (115°K) is also in good agreement with Orton's value of about 118°K.

The temperature profiles shown in Fig. 2 are in conflict with the structure found from a preliminary analysis of the Pioneer 10 S-band occultation experiment (*14*). The results from the occultation experiment indicate a much warmer atmosphere than our results at pressures above several millibars. Our infrared observations could be reconciled with the S-band data if we postulate the presence of an optically thick cloud near the 1-mbar region. However, in this case the pressure-induced opacity of H_2 would be negligible and we would not expect to detect the $J = 0$ and $J = 1$ rotational transitions in our spectrum. The presence of these features in our spectrum suggests that further study of the S-band occultation results is needed. These conclusions are also supported by the consistency of our temperature profile with values obtained at shorter infrared wavelengths and in the radio domain, as discussed above.

For models containing no NH_3 cloud opacity in the zones of Jupiter, we find that the α_{H_2} is 0.85 ± 0.07, whereas we obtain a value of $1.0^{+0}_{-0.04}$ for the cases involving an optically thick NH_3 cloud. These error bars reflect only the formal random errors of our results. The cloud-free models had a smaller value for the minimum fractional flux residual than the set incorporating a thick cloud (0.039 versus 0.043). Combining the above two estimates, we conclude that α_{H_2} equals 0.89 ± 0.11. This range of values encompasses the solar value of 0.86.

JAMES R. HOUCK
Center for Radiophysics and Space Research, Cornell University, Ithaca, New York 14853
JAMES B. POLLACK
Space Science Division, Ames Research Center, Moffett Field, California 94035
DAVID SCHAACK, ROBERT A. REED
Center for Radiophysics and Space Research, Cornell University
A. SUMMERS
Space Science Division, Ames Research Center

References and Notes

1. R. V. Wagoner, *Science* **155**, 1369 (1967).
2. E. Opik, *Icarus* **1**, 200 (1962).
3. E. E. Salpeter, *Astrophys. J.* **181**, L83 (1973).
4. D. F. Schaack and J. R. Houck, in preparation.
5. R. F. Knacke and R. K. Thompson, *Publ. Astron. Soc. Pac.* **85**, 341 (1973); F. F. Bentley, L. D. Smithson, A. L. Rozek, Eds., *Infrared Spectra and Characteristic Frequencies, 700–300 cm*$^{-1}$ (Interscience, New York, 1968); J. S. Lewis and R. G. Prinn, *Science* **169**, 472 (1970); B. N. Khare and C. Sagan, *ibid.* **189**, 722 (1975).
6. J. B. Pollack, J. R. Houck, D. Schaack, R. Reed, A. Summers, in preparation.
7. S. Gulkis and R. Poynter, *Phys. Earth Planet. Interiors* **6**, 36 (1972).
8. G. Orton, personal communication [see also G. Ohring (*10*)].
9. W. Smith, *Appl. Opt.* **9**, 1993 (1970).
10. G. Ohring, *Astrophys. J.* **184**, 1027 (1973).
11. T. Encrenaz and D. Gautier, *Astron. Astrophys.* **26**, 141 (1973).
12. D. Gautier and K. Grossmann, *J. Atmos. Sci.* **29**, 788 (1972).
13. J. B. Pollack and G. Ohring, *Icarus* **19**, 34 (1973).
14. A. Kliore, D. L. Cain, G. Fjeldbo, B. L. Seidel, S. I. Rasool, *Science* **183**, 322 (1974).
15. We thank P. Gierasch, C. Sagan, and G. Orton for helpful discussions; D. Card for contributions to the statistical analysis of our data; and B. Baldwin for help with the computer programming. The outstanding efforts of the pilots and staff of the Airborne Science Office of Ames Research Center greatly facilitated the observations. This work was supported by NASA grant NGR 33-010-182. J.R.H. was also supported by an Alfred P. Sloan research fellowship.

20 February 1975

THE ASTROPHYSICAL JOURNAL, 208:L133–L136, 1976 September 15

16–40 MICRON SPECTROSCOPY OF THE TRAPEZIUM AND THE KLEINMANN-LOW NEBULA IN ORION

W. J. FORREST, J. R. HOUCK, AND R. A. REED
Center for Radiophysics and Space Research, Cornell University
Received 1976 April 26; revised 1976 July 2

ABSTRACT

Observations of the 16–40 μ spectra of the Trapezium region and the Kleinmann-Low nebula in the Orion Nebula with a resolution $\lambda/\Delta\lambda \sim 30$–40 are reported. The Trapezium spectrum shows a single broad emission feature peaking at 18.5 μ; this is interpreted as the O–Si–O bending-mode resonance in silicate grains. The spectrum is compared with a simple model of small heated silicate grains. The Kleinmann-Low Nebula shows a continuum with the color temperature approximately equal to brightness temperature (~85 K). The weakness of the 20 μ absorption feature is attributed to radiation transfer effects in the molecular cloud. A decrease in brightness temperature to longer wavelengths indicates that the center of the molecular cloud is being observed at 28 μ. The cloud mass and visual optical depth derived using this information are in good agreement with molecular determination while the derived central density is an order of magnitude larger.

Subject headings: infrared: spectra — nebulae: Orion Nebula

I. INTRODUCTION

A general description of the Orion Nebula sources and the importance of 20 μ spectroscopy is given in the accompanying *Letter* (Forrest and Soifer 1976, herein referred to as FS). The present spectra are important in extending the wavelength coverage beyond 24 μ. With the entire 16–40 μ spectrum a more complete picture of the emissivity properties and temperature and optical depth of the dust in these sources is formed. In addition, the present spectra should aid in the interpretation of the longer wavelength observations of these sources.

II. INSTRUMENTATION

The observations were made with a helium-cooled Ebert-Fastie spectrometer (Houck *et al.* 1976). An As:Si detector was used for the 16–23 μ band. The 20–40 μ band used a Ge:Ga photoconductor built by W. J. Moore. The short- and long-wavelength bandpasses were 0.5 μ and 1.2 μ FWHM, respectively. The spectrometer was used in conjunction with the 91 cm telescope of the NASA Gerard P. Kuiper Airborne Observatory. The beam size was 25″, and the beam throw was ~90″ in an E-W direction. The C141 aircraft was flown at an altitude of 12.7 km (41,000 feet). The total observing time available for the observations reported here was 2½ hours (plus 1 hour's observation of Mars).

III. OBSERVATIONS

The Kleinmann-Low Nebula (Kleinmann and Low 1967, herein referred to as KL) was observed on two flights, 1975 October 29–30 and October 30–31. The Trapezium region (Ney and Allen 1969) was observed only on the second flight. Mars was used as a calibration source and was observed on both flights. An on-board water-vapor column-density meter indicated 7–15 μ of precipitable water vapor above the aircraft during the first night, and the Martian spectrum on the second night was in good agreement with the first flight spectrum, with no indication of differing terrestrial water vapor. The typical night to night reproducibility of the KL spectra was ~5 percent. The observed signals were converted to flux levels by using Mars as a calibration source. Its ephemeris diameter and a blackbody temperature of 240 K were assumed.[1] A small ~20 percent wavelength-dependent correction for $\lambda \lesssim 17$ μ was used to account for CO_2 absorption in the Martian atmosphere. This correction was determined by comparing spectra of Mars and the Moon using the spectrometer on NASA's 31 cm Lear Jet telescope. Figure 1 shows the derived spectra under these assumptions.

Also included on Figure 1 are ground-based broad-band measurements of these sources made by other observers with comparable beam sizes. The agreement with the 18 and 20 μ measurements of Ney, Strecker, and Gehrz (1973, 25″ beam) and Ney and Allen (1969, 26″ beam) is fair. The early 22 μ measurement of KL by Kleinmann and Low (1967) seems too low—since these observers used a 30″ beam, the disagreement cannot be ascribed to beam-size effects. The 34 μ measurements by Low, Rieke, and Armstrong (1973) with a 25″ beam also seem systematically low compared to the present observations. Part of this discrepancy

[1] Wright (1976) has proposed a model for the thermal emission from the whole disk of Mars. At the time of these observations, the model gives a Martian brightness temperature of 240 K at ~30 μ but a slightly higher (~260 K) color temperature from 20 to 40 μ. This would not materially affect the conclusions reached here.

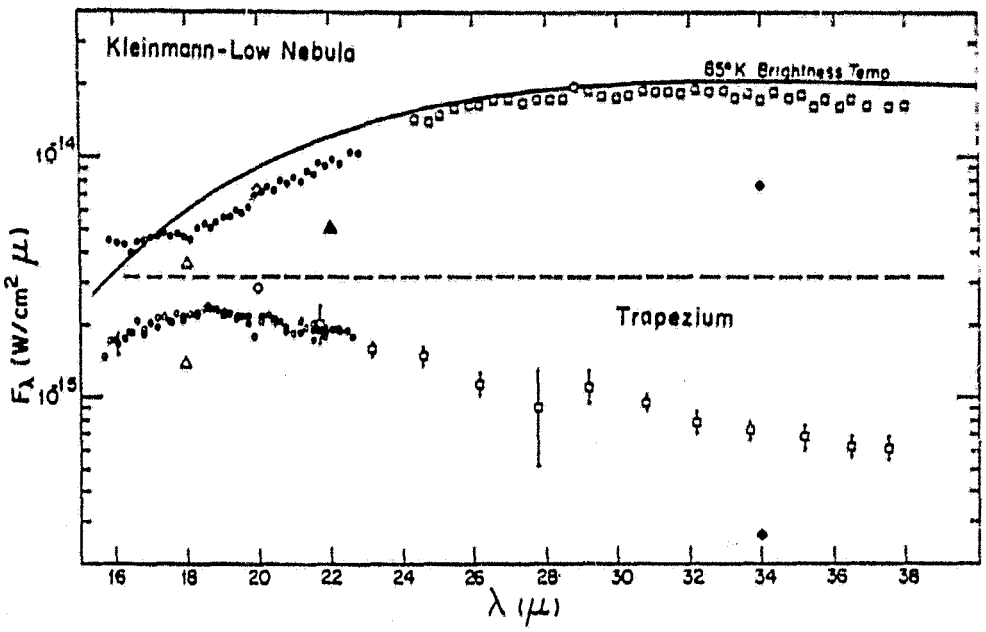

FIG. 1.—The 16–38 μ spectra of the Kleinmann-Low (KL) nebula and the Trapezium region in the Orion Nebula. The smooth curve represents an 85 K blackbody filling the 25″ beam. For the KL spectrum the statistical errors may be estimated from the scatter of adjacent points. For the Trapezium spectrum the statistical errors from 16 to 23 μ (channel 1) can be estimated from the agreement of the second spectrum obtained (*closed circles*) with the first (*open circles*); for channel 2 (20–38 μ, *open squares*), data over approximately 2 μ passbands have been averaged and error bars representing 1 σ of the mean are shown. Broad-band data from Ney and Allen (1969, *open diamonds*), Ney *et al.* (1973, *open triangles*), Low *et al.* (1973, *filled diamonds*), and Kleinmann and Low (1967, *solid triangle*) are included.

for the Trapezium could be due to the smaller beam throw (~45″) these authors employed. The discrepancies at 34 μ are believed to be larger than the systematic errors in the present experiment.

IV. THE TRAPEZIUM

The spectrum of the Trapezium (Fig. 1) shows a broad emission feature peaking at ~18.5 μ with flux decreasing out to the longest wavelengths. No emission or absorption lines are evident to within ~10 percent of the continuum level. This spectrum agrees quite well in shape with the spectrum presented in the accompanying paper (FS); the only real difference is that the present spectrum appears to decrease slightly less rapidly longward of 19 μ. The emission feature is narrower than a blackbody; therefore, it indicates a resonance in the emissivity of the dust grains near 18.5 μ. This is in qualitative agreement with the expected behavior of silicate grains.

Figure 2 shows a plot of both the long (16–40 μ) and short (8–13 μ) wavelength spectra of the Trapezium region. The short wavelength data represent the spectrum reported by Forrest, Gillett, and Stein (1975) scaled to a 25″ beam; the adopted 10 μ flux level agrees with the measurements of Gehrz, Hackwell, and Smith (1975) with a 26″ beam. The dashed curve is a model of 160 K silicate grains fitted to the data. The emissivity as a function of wavelength is for Moon rock No. 14321 (Perry *et al.* 1972) in the form of 0.2 μ grains taken

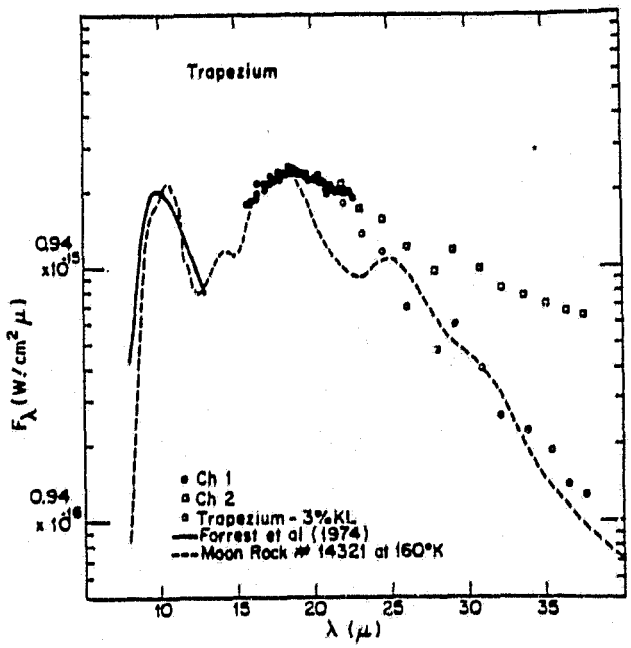

FIG. 2.—A simple silicate model (*dashed curve*) fit to the Trapezium data as described in the text. The open squares and closed circles are the present data from Fig. 1, and the open circles are the present data with 3% of the flux from KL (Fig. 1) subtracted. The solid line represents the 10 μ spectrum reported by Forrest *et al.* (1975).

from Knacke and Thomson (1973). The optical depth of this model is $\sim 0.3 \times 10^{-2}$ at 20 μ.

The actual temperature of the dust radiating at 20 μ is difficult to deduce, as it is related to the relative strengths of the 10 μ and 20 μ emission features. In addition, Day (1976) has shown that the relative strengths of these bands can vary with grain temperatures, the 20 μ band becoming stronger at lower temperatures. For ratios $\epsilon_{18\mu}/\epsilon_{10\mu}$ from $\frac{1}{3}$ to 1, the dust temperature would range from 150 K to 200 K. These temperatures are significantly lower than the 250 K temperature deduced from the 10 μ emission profile (Gillett *et al.* 1975). This discrepancy could possibly be explained as an effect of a temperature distribution within the Trapezium, or it may indicate that the cosmic silicates have a larger 20–10 μ emissivity ratio than has been reported from laboratory measurements. Since Ney, Strecker, and Gehrz (1973) found only a small ($\sim$25 K) range in the 10–20 μ color temperature for several regions in the Trapezium, the latter effect would seem to be more important.

It is seen from Figure 2 that the simple model gives a fair representation of the overall shape of the observed spectrum from 8 to 20 μ. Longward of 20 μ there is increasing disagreement in that the observed spectrum falls less rapidly than the single-temperature silicate model. There are several possible explanations for this discrepancy. The grain emissivity could be falling less rapidly than the lunar silicates for which $\epsilon_\lambda \sim \lambda^{-1}$ here; for 160 K grains it requires an emissivity approximately constant from 25 to 40 μ. There could be an admixture of cooler grains. To explain the observed 40 μ flux with grains with emissivity similar to Moon rock 14321 at 40 μ would require a mass in colder grains more than 6 times larger than the dust which is responsible for the 10–20 μ flux.

An alternative explanation is that the observed spectrum is contaminated at the longest wavelengths by diffuse background radiation from the nearby Orion molecular cloud. Maps of this region (Low, Rieke, and Armstrong 1973; Werner *et al.* 1976) indicate that the contamination in our beam can be several percent of the peak KL flux in the 30–50 μ range. To indicate how this would affect the observed spectrum, we have subtracted 3 percent of the KL spectrum (Fig. 1) from the Trapezium data; this is also shown in Figure 2. After allowing for a reasonable amount of molecular cloud contamination, the fit between the simple silicate dust model and the data is quite good longward of 25 μ.

The simple model disagrees with the observed spectrum in one further detail: the local minimum in emissivity of the lunar silicate around 23 μ is not present in the Trapezium spectrum. A similar feature is seen in all the lunar silicates studied by Knacke and Thomson (1973). Terrestrial silicates also show fine structure in the 20 μ region. Thus either the fine structure is masked by a mixture of different silicates or the cosmic material is different from that in lunar and terrestrial silicates. Day (1974) has found a similar lack of structure in the 20 μ region in an artificially produced amorphous silicate and in carbonaceous chondrite silicate material, but they peak at longer wavelengths than the Trapezium. Recently Penman (1976) has measured the optical constants of several meteoritic silicate materials; a combination of the Vigarno and Murchison carbonaceous chondrite materials would peak at 18.5 μ and show no further structure in the 20 μ region. It would seem that these amorphous, dirty silicate materials may provide a closer representation of the observed Trapezium spectrum.

V. THE KLEINMANN-LOW NEBULA

The 16–40 μ spectrum of the Kleinmann-Low Nebula (Fig. 1) shows a broad continuum with no sharp features. In the region of overlap, the spectral shape is in quite good agreement with the data presented in the accompanying paper (FS). The approximate equality of 20 μ color temperature and brightness temperature with the radio determinations of gas temperatures in the molecular cloud (Liszt *et al.* 1974) leads us to conclude that the actual physical temperature of dust grains is approximately 80 K in the region of the molecular cloud which is seen at these wavelengths (FS). The absence of the rotational lines of molecular hydrogen near 17 and 28 μ is not unexpected, because of the coarse resolution ($\lambda/\Delta\lambda \approx 30$) of the present experiment. For an optically thick line of width 10 km s^{-1}, gas at temperatures from 0 to 100 K would result in at most a $\sim$0.1 percent feature in the present spectrum.

The small residual absorption feature at $\sim$20 μ is ascribed to the effects of radiation transfer in the cloud coupled with the wavelength-dependent opacity of the dust grains (FS; Knacke and Thomson 1973; Kwan and Scoville 1975); because of the reduced opacity at 16 and 24 μ we see to a physically deeper layer in the cloud than at 20 μ and find that the dust temperature is higher there. Most dust models and the spectrum of the Trapezium (Fig. 1) indicate that the dust emissivity decreases with wavelength longward of 20 μ. Therefore, we should see deeper and deeper into the molecular cloud at wavelengths longer than 20 μ. The observed fact that the brightness temperature peaks at $\lambda \sim 28$ μ and then decreases to longer wavelengths indicates that at $\lambda \sim 28$ μ we are seeing to the central, hottest portion of the nebula and thereafter we see beyond the center where the dust is cooler. Thus we conclude that $\tau_{28\mu} \approx 1$ to the center of the Orion molecular cloud.

The 28 μ optical depth may be used to estimate the total mass and central density in the Orion molecular cloud (OMC-1). Following the discussion of Gillett *et al.* (1975), if the density in the cloud goes as $\rho \propto 1/R^2$ (Larson 1969), the central gas density ρ_0 (gas) and total cloud mass M_{tot} will be related to the observed optical depth τ_λ by

$$\rho_0(\text{gas}) = 1/f\left(\frac{\tau_\lambda}{\kappa_\lambda R_0}\right), \quad (1)$$

and

$$M_{tot} = 1/f\frac{4\pi\tau_\lambda}{\kappa_\lambda} R_0 R_1, \quad (2)$$

where R_0 and $R_1 \gg R_0$ are the inner and outer radii, respectively, of the region observed, $1+f$ is the mass ratio of gas to dust, and κ_λ is the mass absorption of the coefficient of the dust. For normal galactic abundances, $1/f \gtrsim 300$ for silicate material. For the lunar silicates studied by Knacke and Thompson (1973), $\kappa_{23\mu} \approx \frac{1}{4}$ $\kappa_{10\mu} \approx 4 \times 10^3 \text{cm}^2\,\text{g}^{-1}$. In the present case, we identify the inner radius R_0 with the 12".5 beam radius which, at the Orion distance of 500 pc, corresponds to 0.9×10^{17} cm. Then ρ_0, expressed as a number density of molecular hydrogen atoms, is $n_0(\text{H}_2) \gtrsim 2 \times 10^6\ \text{cm}^{-3}$ for the central 25" region of the molecular cloud. If the outer radius R_1 is identified with the $\sim 4' \times 9'$ emission ridge seen in the CO and CS molecular maps of Liszt *et al.* (1974), the total mass within this region is given by $M_{\text{tot}} \gtrsim 600\ M_\odot$. From considerations of the formaldehyde emission in Orion observed with a 1' beam, Harvey *et al.* (1974) estimated an H_2 density of $\sim 10^5$ cm^{-3} and a total mass of $\sim 500\ M_\odot$ within a $2' \times 5'$ region. The mass estimates are in quite good agreement; the larger density inferred here would be due to the smaller beam size employed in the present study and the assumption here that $\rho \propto 1/R^2$ in this cloud. The assumption of a steep density gradient has recently been supported by a study of the 1 mm continuum emission from Orion and three other molecular clouds by Westbrook *et al.* (1976).

Since $\kappa_{10\mu}/\kappa_{23\mu} \sim 7$ for lunar silicates, we would also infer that $\tau_{10\mu} \sim 7$ to the center of the molecular cloud. Gillett *et al.* (1975) found a ratio of visual extinction to 10 μ optical depth $A_v/\tau_{10\mu} \gtrsim 15$ from a study of compact H II regions embedded in molecular clouds. This would imply a visual extinction of $\gtrsim 100$ mag to the central region of the molecular cloud. This amount of extinction is in good agreement with that deduced from microwave observations of formaldehyde in the same region of the Orion Nebula (Thaddeus *et al.* 1971).

VI. CONCLUSIONS

The Trapezium spectrum shows a broad emission feature peaking at about 18.5 μ. This supports the identification of silicates as a major component of the dust in this source. At longer wavelengths the spectrum may be contaminated by radiation from the nearby Orion molecular cloud.

The Kleinmann-Low nebula shows a smooth spectrum with only a small residual absorption feature near 20 μ and a gradual decrease in brightness temperature longward of 28 μ. The observed spectrum can be understood as a result of radiation transfer in the molecular cloud; this indicates the hottest, central region of the Orion molecular cloud is being observed at approximately 28 μ.

We wish to thank W. J. Moore of the Naval Research Laboratory for providing the Ge:Ga detector which gave always welcome increased sensitivity from 20 to 40 μ.

We wish to acknowledge helpful conversations with B. T. Soifer, J. L. Pipher, M. Harwit, and D. B. Ward. We also wish to thank the staff of the Gerard P. Kuiper Airborne Observatory for their assistance. This work was supported in part by NASA grant NGR 33-010-081.

REFERENCES

Day, K. L. 1974, *Ap. J.* (*Letters*), **192**, L15.
———. 1976, *ibid.*, **203**, L99.
Forrest, W. J., Gillett, F. C., and Stein, W. A. 1975, *Ap. J.*, **195**, 423.
Forrest, W. J., and Soifer, B. T. 1976, *Ap. J.* (*Letters*), **208**, L129 (FS).
Gehrz, R. D., Hackwell, J. A., and Smith, J. R. 1975, *Ap. J.* (*Letters*), **202**, L35.
Gillett, F. C., Forrest, W. J., Merrill, K. M., Capps, R. W., and Soifer, B. T. 1975, *Ap. J.*, **200**, 609.
Harvey, P. M., Gatley, I., Werner, M. W., Elias, J. H., Evans, N. J., II, Zuckerman, B., Morris, G., Sato, J., and Litvak, M. M. 1974, *Ap. J.* (*Letters*), **189**, L87.
Houck *et al.* 1976, in preparation.
Kleinmann, D. E., and Low, F. J. 1967, *Ap. J.* (*Letters*), **149**, L1 (KL).
Knacke, R. F., and Thomson, R. K. 1973, *Pub. A.S.P.*, **85**, 341.
Kwan, J., and Scoville, N. Z. 1975, preprint.
Larson, R. B. 1969, *M.N.R.A.S.*, **145**, 271.
Liszt, H. S., Wilson, R. W., Penzias, A. A., Jefferts, K. B., Wannier, P. G., and Solomon, P. 1974, *Ap. J.*, **190**, 557.
Low, F. J., Rieke, G. H., and Armstrong, K. R. 1973, *Ap. J.* (*Letters*), **183**, L105.
Ney, E. P., and Allen, D. A. 1969, *Ap. J.* (*Letters*), **155**, L193.
Ney, E. P., Strecker, D. W., and Gehrz, R. D. 1973, *Ap. J.*, **180**, 809.
Penman, J. M. 1976, *M.N.R.A.S.*, **175**, 149.
Perry, C. H., Agrawal, D. K., Anastassakis, E., Lowndes, R. P., Rastogi, A., and Tornberg, N. E. 1972, *Moon*, **4**, 315.
Thaddeus, P., Wilson, R. W., Kutner, M., Penzias, A. A., and Jefferts, K. B. 1971, *Ap. J.* (*Letters*), **168**, L59.
Werner, M. W., Gatley, I., Harper, D. A., Becklin, E. E., Loewenstein, R. F., Telesco, C. M., and Thronson, H. A. 1976, *Ap. J.*, **204**, 420.
Westbrook, W. E., Werner, M. W., Elias, J. H., Gezari, D. Y., Hauser, M. G., Lo, K. Y., and Neugebauer, G. 1976, *Ap. J.*, **209**, in press.
Wright, E. L. 1976, preprint.

W. J. Forrest and J. R. Houck: Center for Radiophysics and Space Research, Space Sciences Building, Cornell University, Ithaca, NY 14853

R. A. Reed: Research, Plant 35, Grumman Aircraft, Bethpage, NY 11714

Furthermore, if the Martian $^{13}C/^{12}C$ ratio is in fact no greater than the terrestrial value, then the present results put an upper limit of ~30% on the fractional abundance or argon in the atmosphere. Strong emission features were found in the centers of the 950 cm^{-1} $^{12}C^{16}O_2$ absorption lines. These have Gaussian profiles and imply a kinetic temperature of ~170 K at mesospheric altitudes. The absolute intensities of the emission features are, however, from two to ten times greater than expected from gas in LTE at this temperature. The emission appears to result from CO_2 excitation by solar near-infrared radiation. This work was supported in part by NASA-Grant NGL-05-003-272 and NGR-05-003-452.

32.04.02 The Far Infrared Spectrum of Jupiter. D. GOLDVITCH, E.F. ERICKSON, D.W. STRECKER, J.P. SIMPSON, J.D. SCARGLE, L.C. CAROFF, and F.C. WITTEBORN, NASA-Ames Research Center, Moffett Field, CA 94035. - The spectrum of Jupiter has been measured from 28-120 microns from an altitude of 13 km (~ 43000 ft) using the 91-cm telescope on board NASA's Kuiper Airborne Observatory. The spectrometer is a Michelson interferometer with a useful bandpass from 80-350 cm^{-1}. The resolution of the spectra is about 5 cm^{-1}. From 50 to 100 microns, the main opacity source is due to the rotational spectrum of NH_3 plus the H_2 translational continuum. Synthetic spectra have been calculated using both the NH_3 & H_2 opacity and the equation for radiative transport. Several reported pressure temperature profiles for the Jovian atmosphere and the saturated vapor pressure as a function of temperature for NH_3 are used. In the unsaturated regions a mixing ratio of 1.5×10^{-4} is used for the partial pressure of NH_3. For the pressures used, the NH_3 line shapes are given by the Lorentzian profile with broadening due to H_2, He and NH_3 included. The synthetic spectra are compared to the observations and discussed. The amount of NH_3 in the line-of-sight is deduced.

32.05.02 Curves of Growth for the 0-0 S(J) H_2 Quadrupole Lines for Jupiter and Uranus. D. GOLDVITCH and C. CHACKERIAN, JR., NASA-Ames Research Center, Moffett Field, CA 94035. - Since high altitude platforms, such as the C-141, balloons, and the Shuttle are becoming available for carrying telescopes above the tropopause, the 0-0 S(J) quadrupole lines of H_2 once obscured by telluric H_2O can be observed in the atmospheres of the outer planets with high resolution instruments. The development of narrow frequency lasers operating in the infrared has made possible the extension of radioastronomical techniques to this region of the spectrum. We have calculated the curve of growth and the line shape for the 28, 17, and 12μ lines for Jupiter and Uranus using the Galatry profile. For each line, we calculated the curve of growth using the cool, nominal and warm models of T.N. Divine (NASA SP-8069) and F.D. Palluconi (NASA SP-8103) for Jupiter and Uranus, respectively. These three models represent different H_2/He ratios which can be supported by observations. The atmospheres are divided into about 30 layers and the absorption is calculated for emission up through these layers. The line strengths were taken from the literature, the diffusion constant and pressure broadening coefficient are calculated taking into account the interactions between hydrogen and helium. Also a semi-empirical line shift was included which tends to lessen the saturation. We present the curve of growth for the strongest line 0-0 S(1) at 17μ for both Jupiter and Uranus nominal model.

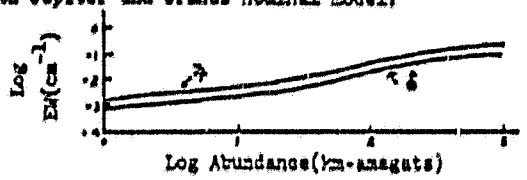

32.06.02 Venus: The 16-40 Micron Spectrum. R.A. REED, Cornell U. & Grumman Aircraft, J.B. POLLACK, NASA/Ames, J.R. HOUCK & F.J. FORREST, Cornell U. - We report on observations of Venus made in the spectral interval 17-39 microns with a resolution of approximately 1 micron. The observations were obtained with a two channel grating spectrometer at an altitude of 14 km using the NASA Learjet 31 cm open port telescope. The Venus spectrum exhibits three broad and shallow absorption features near 17 microns, 22 microns, and 36 microns. The spectrum is consistent with emission from a haze of aqueous sulfuric acid droplets.

32.07.02 17-25μ Spectra of Jupiter and Saturn. A. TOKUNAGA, R. F. KNACKE, & T. OWEN, SUNY-Stony Brook- Spectra of Jupiter and Saturn in the 17-25μ spectral region have been obtained at resolutions of 0.02μ and 0.4μ, respectively, with a ground-based Michelson spectrometer. Theoretical spectra are compared to the observations. The shape of the continuum appears to be consistent with recent atmospheric models and the pressure-induced opacity of H_2. There is no compelling evidence for sulfur or other absorbers in Jupiter in this data.

32.08.02 Far Infrared Lamellar Grating Observations from the Gerard P. Kuiper Airborne Observatory. J.L. PIPHER, M.F. SAVEDOFF, & J.G. DUTHIE, U. Rochester. - A lamellar grating interferometer has been successfully used on the Gerard P. Kuiper Airborne Observatory to obtain spectra between 100μ and 600μ of Jupiter and the Kleinmann-Low Nebula. We present our first spectra of these objects at a resolution of 3.2 cm^{-1} and 13.1 cm^{-1} respectively using Mars as a calibration standard. The Jupiter spectrum exhibits brightness temperatures consistent with existing broadband measurements, and we compare it to theoretical models. We failed to detect NH_3 at these wavelengths. The

Bull. A.A.S. 8, 357 (1976)

ICARUS 33, 554–557 (1978)

Venus: The 17- to 38-Micron Spectrum

R. A. REED,[1] W. J. FORREST, AND J. R. HOUCK

Center for Radiophysics and Space Research, Cornell University, Ithaca, New York 14853

AND

J. B. POLLACK

NASA Ames Research Center, Moffett Field, California 00000

Received March 18, 1977; revised July 27, 1977

The Venus emission spectrum was measured from the NASA Lear Jet on five nights in June 1975. A cooled grating spectrometer with a resolution of $\lambda/\Delta\lambda \simeq 25$ over the spectral interval 17 to 38 μm was used. The main features in the observed spectrum are consistent with the theoretical emission spectrum of a haze of aqueous sulfuric acid droplets suspended in a CO_2 atmosphere.

INTRODUCTION

The thermal emission spectrum of a planet contains information on the chemical composition and thermal structure of the planetary atmosphere. In the case of Venus, the peak surface temperature of ~750°K is observed only in the radio region; the 200–250°K temperatures observed in the thermal infrared originate from a much higher level in the Venus atmosphere. It has been proposed (Sill, 1972; Young, 1973, 1974; Pollack *et al.*, 1974) that a haze cloud of sulfuric acid droplets exists in the primarily CO_2 atmosphere of Venus at the levels observed in the thermal infrared. The present 17–38-μm spectrum of Venus will allow a further test of this hypothesis.

OBSERVATIONS

The spectrum of Venus has been obtained from an altitude of 14 km with the 30-cm telescope of the NASA Lear Jet. The instrument employed was a cooled grating spectrometer utilizing both the first- and second-order spectra from the grating to achieve a resolution of 25 over the wavelength range 17–38 μm (Houck *et al.*, 1975; Schaack, 1975). The beam size of 3.6 arcmin included the whole disk of Venus. The instrumental response was calibrated using the emission of Mars in conjunction with the model of Wright (1976), which at this time gave brightness temperatures of 256 and 248°K at wavelengths of 20 and 34 μm, respectively (Wright, personal communication, 1976). The observed spectrum, shown in Fig. 1, is the average of five nights of observation in June 1975. Data points have been taken at a density of three per resolution element so that the statistical errors may be estimated from the scatter of adjacent points. The spectrum is characterized by an overall continuum level, with noticeable absorption shortward of 20 μm and longward of 30 μm, compared to a 245°K blackbody. This spectral shape has

[1] Present address: Grumman Aircraft, Bethpage, N. Y. 11714.

0019-1035/78/0333-0554$02.00/0

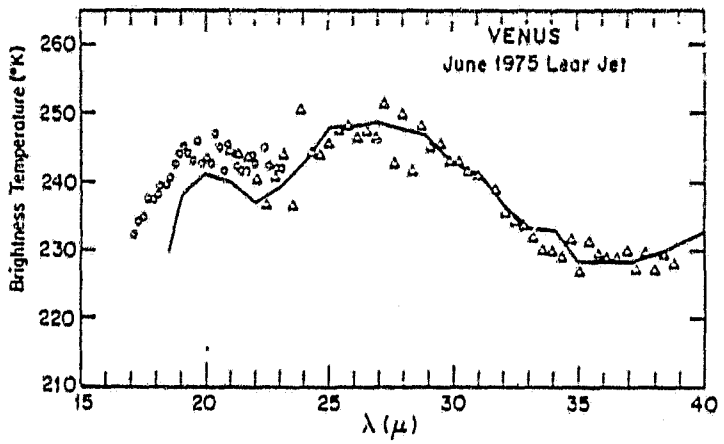

FIG. 1. The comparison of the Venus emission spectrum (points) with the synthetic H_2SO_4 spectrum (solid line) as described in the text. The triangles and circles are from the first and second-order spectrometer channels, respectively.

been confirmed by later observations by Forrest and McCarthy, who used a slightly modified instrument (Forrest and McCarthy, 1976). Mariner 10 broad-band measurements give a disk brightness temperature of 245°K in the 35–55 μm-band (Chase *et al.*, 1974). The Venera 9 and 10 spacecraft measured a somewhat lower (8–40 μm) brightness temperature of 232°K (day side) and 241°K (night side) (Keldysh, 1977).

The continuum level observed here implies a continuous source of opacity in the Venus atmosphere over the entire 17–38-μm range with increased opacity shortward of 20 μm and longward of 30 μm. Possible sources of opacity at these wavelengths are gaseous CO_2, water vapor, and the cloud material. The wings of the 15-μm CO_2 band may provide some of the short wavelength opacity but the opacity decreases rapidly longward of 17 μm. Water vapor could supply opacity at longer wavelengths but the absence of structure, particularly at the position of the strong H_2O band at ~35.5 μm (Traub and Stier, 1976) indicates this is not the primary source of continuum opacity. In the following section it is shown that a haze of sulfuric acid droplets can provide the necessary opacity and explain the depressions seen longward of 30 μm and shortward of 20 μm.

SULFURIC ACID MODEL

A number of recent observations indicate that the Venus clouds are composed of aqueous sulfuric acid. Among these are: (1) the wavelength dependence of polarization of visible light (Hansen and Hovenier, 1974), (2) the shape of Venus' reflectivity in the 3–4 μm region (Pollack *et al.*, 1974), and (3) the 8- to 13-μm spectrum (Sinton and Strong, 1960; Gillett, Low and Stein, 1968; Hanel *et al.*, 1968; Samuelson *et al.*, 1975). The far-infrared observations of Venus presented here offer another observational test of this hypothesis because sulfuric acid has absorption maxima at 17, 22, and longward of 30 μm.

The radiative transfer method of Young (1974) was applied to the Venus atmosphere in order to generate a synthetic spectrum. This method makes the simplifying assumptions of a constant temperature lapse rate and a cloud scale height invariant with altitude. The data of Jones (1975) and of Palmer and Williams (1975) for 75% H_2SO_4 were used to obtain the Mie scattering and absorption cross sections of the

haze droplets. This data should be representative of the Venus clouds because the aerosol is believed to be between 75 and 85% H_2SO_4 (Young, 1975) and the far infrared optical constants of aqueous sulfuric acid vary little within this range (F. W. Taylor, personal communication, 1976). It was assumed that the droplets are small, with radius ≤ 1 μm, so that scattering is negligible at these wavelengths. Such an assumption is consistent with the value of 1 μm for the mean droplet radius as inferred by Hansen and Hovenier (1974). Because of strong CO_2 absorption near the 15 μm fundamental only observations at 20 μm and longer were used to obtain the best-fit model parameters. In addition, the model was terminated below the $T = 230$°K level as this is the freezing point of 75% H_2SO_4 (Young, 1973). The two free parameters in the resulting model spectrum are an overall normalization constant and T_1, the temperature lapse rate per unit cloud scale height. It was found that values of T_1 between approximately 35 and 45°K provided the best fit to the observed data.

The synthetic brightness temperature spectrum for $T_1 = 35$°K is compared against the data in Fig. 1. It is seen that the principal features of the Venus emission spectrum can be accounted for by this simple model. This supports the sulfuric acid hypothesis for the Venus clouds. The precise shape of the spectrum, however, is sensitive to parameters of the Venus atmosphere such as the size distribution of the aerosol and the vertical variation of the aerosol mixing ratio. It is also sensitive to uncertainties in the infrared emission spectrum of Mars. One of us (J.B.P.) is pursuing a more detailed analysis of the data.

Using our absolute calibration and the spacecraft data for the Venus atmosphere, we deduce a pressure level for our spectrum of roughly 200 mbar. This figure is confirmed by an alternate analysis using the optical properties of sulfuric acid and the 25- to 75-mbar pressure level for visible optical depth unity determined by Hansen and Hovenier (1974). (The extinction efficiency Q_e is between 10 and 15 times larger in the visible than in the 20–40-μm region.) At this level in the atmosphere, the data of McClatchey *et al.* (1975) lead us to believe that the 17–20-μm opacity is due to both the 17-μm absorption maximum of sulfuric acid and CO_2.

The value derived for $T_1 \sim 40$°K deserves further discussion because it gives new information about the Venus atmosphere at deeper levels than are accessible at shorter wavelengths. This value is approximately twice the value expected on the basis of direct extrapolation downwards from overlying levels of the atmosphere (Lacis, 1975). From this it can be inferred that below a level corresponding to $P \gtrsim 200$ mbar, the cloud aerosol may no longer be characterized by a simple scale height law. The present analysis gives little indication of what the actual distribution is, but it is interesting to consider that a failure of the simple scale height law may be related to the detailed cloud structure observed below ~65 km altitude by the Venera 9 and 10 spacecraft (Keldysh, 1977).

ACKNOWLEDGMENTS

We wish to thank A. D. Jones for making his results on the optical properties of H_2SO_4 available, F. W. Taylor for helpful discussion, and an anonymous referee for helpful comments on this paper. The pilots and staff of the NASA Lear Jet contributed greatly to the success of this program. This work was supported by NASA Grant NGR 33-010-182.

REFERENCES

CHASE, S. C., MINER, E. D., MORRISON, D., MUNCH, G., AND NEUGEBAUER, G. (1974). Preliminary infrared radiometry of Venus from Mariner 10. *Science* **183**, 1291–1292.

FORREST, W. J., AND MCCARTHY, J. F. (1976). Personal communication.

GILLETT, F. C., LOW, F. J., AND STEIN, W. A. (1968). The absolute spectrum of Venus from 2.8 to 14 microns. *J. Atmos. Sci.* **25**, 594–595.

HANEL, R., FOREMAN, M., STAMBACH, G., AND

MEILLEUR, T. (1968). Preliminary results of Venus observations between 8 and 13 microns. *J. Atmos. Sci.* **25**, 586–593.

HANSEN, J. E., AND HOVENIER, J. W. (1974). Interpretation of the polarization of Venus. *J. Atmos. Sci.* **31**, 1137–1160.

HOUCK, J. R., POLLACK, J. B., SCHAACK, D. F., REED, R. A., AND SUMMERS, A. (1975). Jupiter: Its infrared spectrum from 16 to 40 microns. *Science* **189**, 720–722.

JONES, A. D. (1975). The optical constants of sulphuric acid in the far infrared. JPL preprint.

KELDYSH, M. V. (1977). Venus exploration with the Venera 9 and Venera 10 spacecraft. *Icarus* **30**, 605–625.

LACIS, A. A., AND HANSEN, J. E. (1974). The atmosphere of Venus: Implications of Venera 8 sunlight measurements. *Science* **184**, 979–982.

LACIS, A. A. (1975). Cloud structure and heating rates in the atmosphere of Venus. *J. Atmos. Sci.* **32**, 1107–1124.

MCCLATCHEY, R. A., AND SELBY, J. E. A. (1975). Atmospheric transmission from 0.25 to 25 microns: Computer Code LOWTRAN3. AFCRL-TR-75-0255.

PALMER, K. F., AND WILLIAMS, D. (1975). Optical constants of H_2SO_4: Application to the clouds of Venus? *Appl. Opt.* **14**, 208–219.

POLLACK, J. B., ERICKSON, E. F., WITTEBORN, F. C., CHACKERIAN, C., JR., SUMMERS, A. L., VAN CAMP, W., BALDWIN, B. J., AUGASON, G. C., AND CAROFF, L. J. (1974). Aircraft observations of Venus' near infrared reflection spectrum: Implications for cloud composition. *Icarus* **23**, 8–26.

SAMUELSON, R. E., HANEL, R. A., HERATH, L. W., KUNDE, V. G., AND MAGUIRE, W. C. (1975). Venus cloud properties: Infrared opacity and mass mixing ratio. *Icarus* **25**, 49–63.

SCHAACK, D. F. (1975). PhD. thesis. Cornell University.

SILL, G. T. (1972). Sulfuric acid in the clouds of Venus. *Commun. Lunar Planet. Lab.* **9**, 191–198.

SINTON, W. M., AND STRONG, J. (1960). Radiometric observations of Venus. *Astrophys. J.* **131**, 470–490.

TRAUB, W. A., AND STIER, M. T. (1976). Theoretical atmospheric transmission in the mid- and far-infrared at four altitudes. *Appl. Opt.* **15**, 364–377.

WRIGHT, E. L. (1976). Recalibration of the far-infrared brightness temperatures of the planets. *Astrophys. J.* **210**, 250–253.

YOUNG, A. T. (1973). Are the clouds of Venus sulfuric acid? *Icarus* **18**, 564–582.

YOUNG, A. T. (1974). Venus clouds: Structure and composition. *Science* **183**, 407–409.

YOUNG, A. T. (1975). The clouds of Venus. *J. Atmos. Sci.* **32**, 1125–1132.

REPRINT

A LIQUID-HELIUM-COOLED GRATING SPECTROMETER FOR FAR INFRARED ASTRONOMICAL OBSERVATIONS

J. R. HOUCK AND DENNIS WARD

Reprinted from the *Publications of the Astronomical Society of the Pacific*
(Vol. 91, No. 539, February 1979)

Publications of the Astronomical Society of the Pacific
91:140-142, February 1979

A LIQUID-HELIUM-COOLED GRATING SPECTROMETER FOR FAR INFRARED ASTRONOMICAL OBSERVATIONS

J. R. HOUCK AND DENNIS WARD*
Center for Radiophysics and Space Research, Cornell University

Received 1978 October 5

Key words: infrared spectrometer

A liquid-helium-cooled grating spectrometer has been constructed and used to make low-resolution far-infrared spectrometric observations of astronomical sources from the U.S. National Aeronautics and Space Administration (NASA) Lear Jet. A grating instrument was chosen for this application because it is simply constructed, is insensitive to vibration, weighs little, and is small. These are important considerations for observations with the 30-cm Lear Jet telescope. Moreover, since our detectors behave as though background limited, the sensitivity of a cooled grating instrument is competitive with a multiplexing spectrometer.

The instrument is shown schematically in Figure 1. The focus end of the spectrometer is bolted to the cold work surface of a liquid helium Dewar; the rest of the instrument is covered by a vapor-cooled radiation shield. The warmest parts of the frame are kept at a temperature < 20 K under operating conditions. This keeps the background flux on the detectors, from inside the instrument, small compared to radiation entering through the polyethylene window from the atmosphere and telescope. To eliminate scattered light, the inside of the instrument is coated with an absorbing paint, and the direct reflection from the secondary mirror to the detectors is blocked by a black mask on the secondary.

The spectrometer has a focal ratio of *f*6.5, and a 40-cm focal length. The entrance slit is 2.2×2.9 mm^2, which defines a beam of $4'.5 \times 6'$ on the sky when used on the Learscope. The focal ratio and length can be conveniently changed by substituting different secondary mirrors.

The instrument frame is constructed entirely from aluminum, and occupies a cylindrical volume approximately 13 cm in diameter and 26 cm in length within the Dewar. The primary and secondary pyrex mirrors are spherical and coated with aluminium. They are spring or clip mounted to avoid breakage during cool-down, but the instrument retains its alignment well even after many cryogenic cycles. The Dewar capacity is 2.5 liters, and its hold time is approximately eleven hours.

After a liquid nitrogen precooling phase, three helium transfers (about 12 liters, including transfer losses) over a period of two to three hours are required to bring the system to liquid helium temperature.

The spectrometer is scanned in wavelength by rotating the grating with a stepping motor located on the outside bottom of the Dewar. The motor connects via a fiberglass shaft that runs through a vacuum coupling to a pair of bevel gears, a worm, and a sector gear

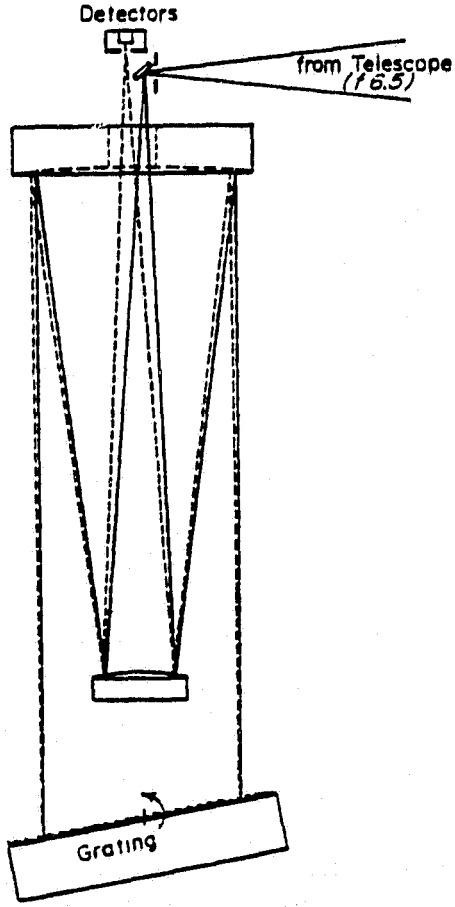

FIG. 1—Schematic drawing of the spectrometer.

*Present Address: David Dunlap Observatory, University of Toronto, Toronto, Ontario, Canada, L4C 4Y6.

which combine to rotate the grating mount. The spectral resolution and wavelength coverage are determined by the slit sizes and grating blaze angle. We have employed gratings with groove spacings ranging from 0.10 to 1.75 mm, blazed at ~ 90 μ. Both custom-made aluminum gratings and standard Bausch and Lomb replica gratings have been used. The instrument has been used over the wavelength range from 45 μ to 115 μ, at resolving powers ranging from 10 to 150. The theoretical maximum resolving power of the instrument is ~ 700 at 90 μ, but the limited guiding accuracy of the Lear telescope has constrained us to use fairly large slits and a correspondingly lower resolving power.

The instrument uses two Ge:Ga photoconductive detectors (Moore and Shenker 1965) which have been produced following the procedures of Pipher (1971). These detectors are mounted directly to the cold work surface of the Dewar, and operate at ~ 4.2 K. One detector works in the wavelength range from 45 μ to 80 μ in first and second order of the grating, with a CaF_2 filter; a diamond scatter filter (Armstrong and Low 1973) cuts off short wavelength light and KRS-5 acts as a long-wavelength cut-off filter. The second detector works longward of 60 μ in first order, with BaF_2 plus the CaF_2 and scatter filter blocking light at shorter wavelengths.

The spectrometer employs very simple cooled MOSFET coupled transimpedance preamplifiers (Wyatt, Baker, and Frodsham 1974), for which the circuit is shown in Figure 2. The MOSFETs and the feedback resistors are mounted as close as possible to the detectors. Microphonic noise is not a problem in spite of the relatively high vibration levels encountered in the aircraft. Linearity of the response is sufficient to permit use of the moon to give a spectral calibration even for faint infrared sources. The accuracy of this approach was confirmed by observations of Mars, whose brightness as a function of wavelength and time of observation has been calculated by Wright (1976). The noise of the preamplifier is about 1.5 microvolts-Hz$^{-0.5}$, which is far less than detector noise under normal operating conditions.

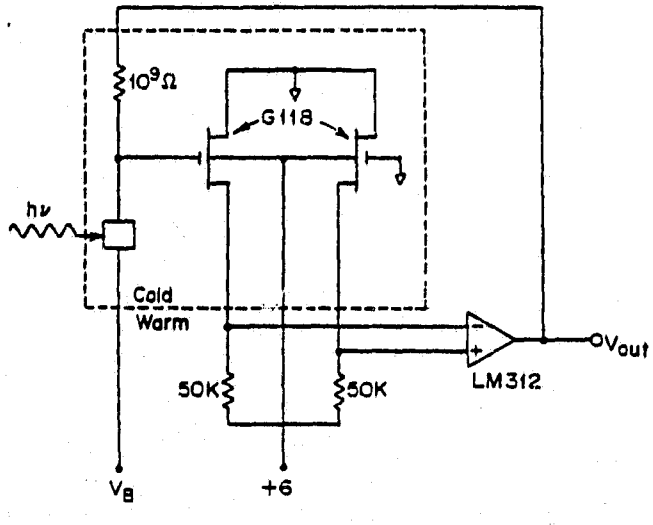

FIG. 2—The simple MOSFET coupled transimpedance preamplifiers used in the spectrometer.

In laboratory tests without an integrating cavity at ~ 85 μ effective wavelength and backgrounds of ~ 10^{-8} watts, these detectors gave measured photon NEP's of 1×10^{-13} w-Hz$^{-0.5}$. This is about a factor of 10 larger than the theoretical background limit for a photoconductor under these conditions. The current responsivity was approximately one ampere per watt at the optimum bias voltage.

In actual observations of M42 and Venus on the aircraft, the observed system NEP at a resolving power of 150 was about 4×10^{-13} watts-Hz$^{-0.5}$ at 88 μ and 9×10^{-13} watts-Hz$^{-0.5}$ at 52 μ. No corrections were made for telescope, chopper, and atmospheric losses. Noise contributions from guiding errors which generally dominated over the detector noise were included. The derived system efficiency is ~ 10%, again including telescope, chopper, and atmospheric losses.

Normally a calibration spectrum is obtained with a laboratory source prior to each Lear Jet flight. For this calibration the spectrometer views a liquid-nitrogen-cooled blackbody source placed ~ 70 cm from the polyethylene vacuum window. The solid angle subtended by the source has a diameter of ~ 8°. It equals the angular diameter subtended by the wobbling secondary mirror at the entrance slit of the spectrometer during flight. Figure 3 compares preflight and in-flight spectra obtained on typical days. The inflight spectrum was obtained at a cruising altitude of 13.5 km. The preflight spectrum was taken at sea level, at Moffett Field, California. The spectral resolving power is ~ 120 in both spectra. The lunar spectrum shows somewhat shallower absorption features than the spectrum of water vapor in 70 cm of normal air traversed at sea level. The water vapor features are pressure broadened in the lower atmosphere. A more detailed comparison of the two curves would require a curve-of-growth analysis of the water vapor features.

The spectral resolving power attained by the instrument varies with the source viewed. Compact sources whose images do not fill the entire entrance slit width produce spectra with a resolving power of ~ 150 while extended sources like the moon provide a resolving power of 120. Similarly a small shift in the position of a spectral feature is produced if a small source is imaged first at one side and then the other of the entrance slit. Both of these problems could be overcome to a large extent by using a field lens in front of the entrance slit.

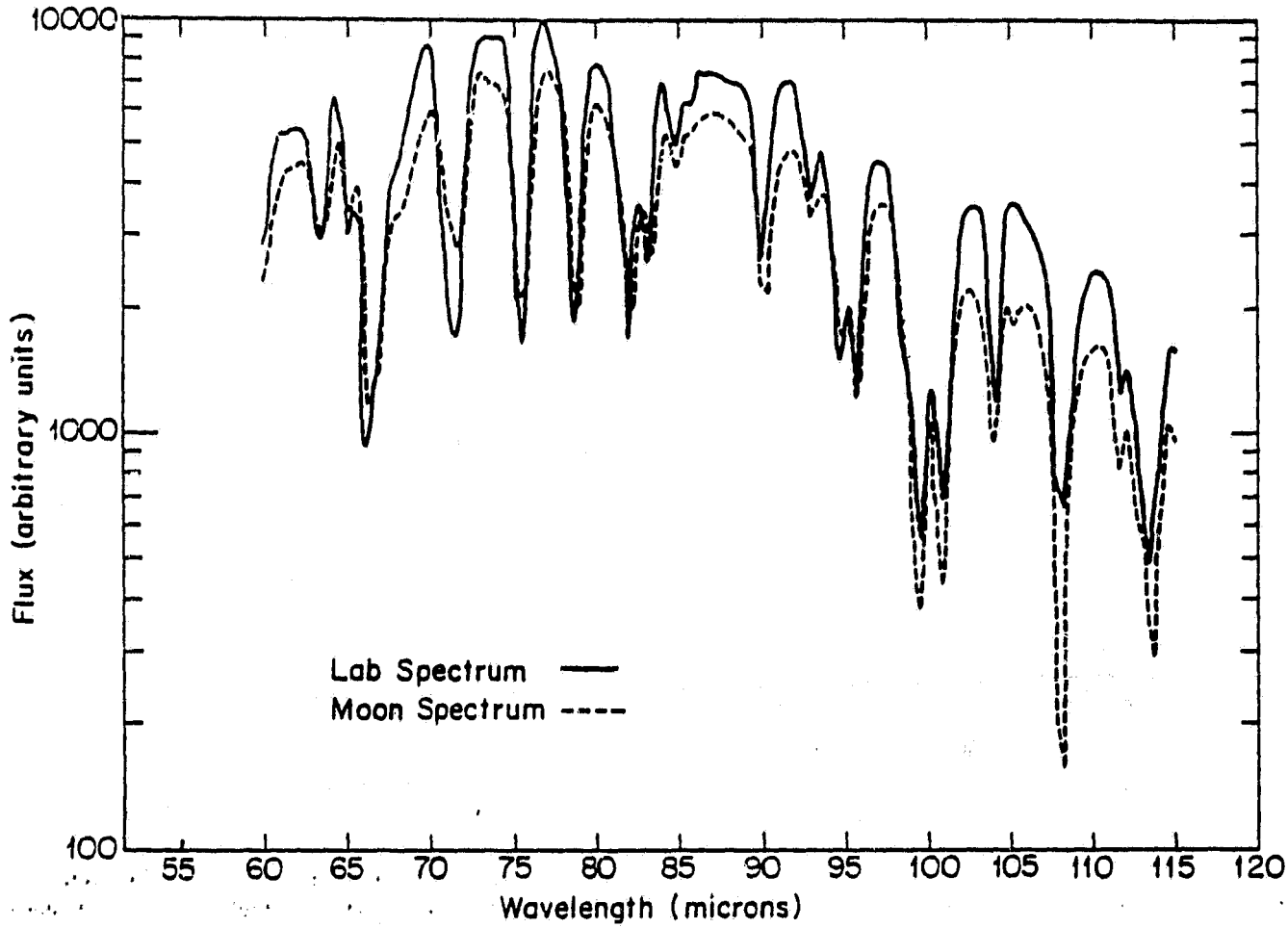

FIG. 3—Spectrum of the moon as seen from a Lear Jet altitude of 13.5 km and a preflight calibration spectrum of a laboratory source seen through a path length of 70 cm of air at sea level.

The reader can gain a clear understanding of the capability of the instrument from published spectra. Low-resolution spectra ($\lambda/\Delta\lambda \sim$ 10–30) are given by Ward, Gull, and Harwit (1977*a*,*b*). High-resolution spectral line data are given by Ward et al. (1975) and Dain et al. (1978) ([O III] 88.16 μ), and Melnick et al. (1978) and Melnick, Gull, and Harwit (1978) ([O III] 51.8 μ and [O I] 63 μ).

We would like to thank Martin Harwit, George Gull, and Carl Frederick for their extensive contributions to the development and use of this instrument. The excellent support of the Airborne Sciences Office at NASA Ames made the observational phase of this project possible. This work was supported by NASA contracts NGR 33-010-146 and NGR 33-010-182.

REFERENCES

Armstrong, K. R., and Low, F. J. 1973, *Appl. Opt.* 12, 2007.
Dain, F. W., Gull, G. E., Melnick, G., Harwit, M., and Ward, D. B. 1978, *Ap. J. (Letters)* 221, L17.
Melnick, G., Gull, G. E., and Harwit, M. 1970*a*, *Ap. J. (Letters)* 227, L29.
——— 1979*b*, *ibid.* 227 L35.
Melnick, G., Gull, G. E., Harwit, M., and Ward, D. W. 1978, *Ap. J. (Letters)* 222, L137.
Moore, W. J., and Shenker, H. 1965, *Infrared Physics* 5, 99.
Pipher, J. L. 1971, Dissertation, Cornell University.
Ward, D. B., Dennison, B., Gull, G. E., and Harwit, M. 1975, *Ap. J. (Letters)* 202, L31.
Ward, D. B., Gull, G. E., and Harwit, M. 1977*a*, *Icarus* 30, 295
——— 1971*b*, *Ap. J. (Letters)* 214, L83.
Wright, E. L. 1976, *Center for Astrophysics Preprint Series* No. 480.
Wyatt, C. L., Baker, D. J., and Frodsham, D. G. 1974, *Infrared Physics* 14, 165.

THE ASTROPHYSICAL JOURNAL, 231:711–719, 1979 August 1

OBSERVATIONS OF [S III] 18.71 MICRON EMISSION IN GALACTIC H II REGIONS

J. F. MCCARTHY, W. J. FORREST, AND J. R. HOUCK
Center for Radiophysics and Space Research, Cornell University
Received 1978 December 15; accepted 1979 February 12

ABSTRACT

Emission of [S III] 18.71 μm radiation has been detected in the Orion Nebula, M17, NGC 2024, and W51, and an upper limit has been set for Sgr A. The line flux from M17 has been mapped with a resolution of 2'.7. A simple theory for predicting the [S III] flux from radio continuum observations is presented and compared with the data. It is found that Orion and M17 are in satisfactory agreement with the observations, and that NGC 2024 is consistent with a low excitation source behind a reasonable amount of 18 μm dust extinction. In W51 the low observed flux may be explained either by low S^{++} abundance or, more likely, by dust extinction. In Sgr A attenuation by dust is the most plausible explanation.

Subject headings: infrared: sources — infrared: spectra — nebulae: general

I. INTRODUCTION

Infrared fine-structure lines can be used to investigate the properties of the dust and ionized gas of H II regions. If the ionized nebula suffers little visual extinction, as in the Orion Nebula, the observed fluxes from fine-structure lines can be used to determine electron densities, temperatures, and ionic abundances, which in turn can be interpreted to yield information about the exciting star and elemental abundances. On the other hand, in the case of heavily obscured nebulae, such as W51, the attenuation due to dust is not negligible, and the comparison of observed fluxes with predictions based on simple models can be useful in estimating the optical constants of the dust, which at present are poorly known.

In the mid-infrared spectra of galactic H II regions, the 18.71 μm line of [S III] is among the strongest observed. It arises from transitions between the $^3P_2$ and $^3P_1$ levels in the split ground state of the S^{++} ion. Collisions with electrons populate these levels, and for low enough densities ($n_e \lesssim 6000\ \mathrm{cm}^{-3}$) emission of 18.71 μm radiation is the dominant de-excitation mechanism. For higher densities, de-excitation due to collisions with other electrons becomes dominant, and the emissivity divided by ionic and electron densities drops off as $1/n_e$. The line's location near the center of the 16–20 μm silicate absorption band makes it an ideal probe of the properties of silicate grains, thought to be a major constituent of interstellar dust. Knowledge of the strength of the 20 μm band would be a further constraint on the chemical composition of the grains and would allow better theoretical models of the spectra of cool stars and H II regions where dust emission is important. Furthermore, since the $S^+ \rightarrow S^{++}$ ionization potential (23.3 eV) is close to that of $He^0 \rightarrow He^+$ (24.6 eV), comparison with radio recombination line observations can give clues to the ionization structure.

Earlier work has detected [S III] 18.71 μm in the Orion Nebula (Baluteau *et al.* 1976), in W3A (Moorwood *et al.* 1978), and in G333.6−0.2, NGC 7027, and BD+30°3639 (Greenberg, Dyal, and Geballe 1977). This paper reports on detections of [S III] 18.71 μm in Orion, M17, W51, and NGC 2024, and on an unsuccessful search for line emission in Sgr A. We have also mapped line and continuum emission in M17.

II. OBSERVATIONS AND INSTRUMENTATION

The spectra reported here were obtained over a 3 week period in 1977 September and October, using the NASA Lear Jet 30 cm telescope operating at an altitude of 45,000 feet (13.7 km). The circular beam was 2'.7 in diameter and the chopper throw was 8'.1 in azimuth, except for the M17 map, where the amplitude was increased to 16'.2. Except for the Orion Nebula and M17, the 8'.1 throw was large enough to ensure that the reference beam was in empty sky, and in those two cases the line flux in the reference beam is estimated from radio maps (Schraml and Mezger 1969) to be 10% or less of the flux in the main beam.

Spectra of the subsolar point of the Moon were used to correct for the instrumental response and the transmission of the Earth's atmosphere by assuming that the Moon's intrinsic spectrum was a blackbody of temperature 395 K. The absolute flux calibration was based on observations of Mars and Wright's (1976) model for its brightness temperature at 20 μm. (A recent more detailed model [Christensen 1979] of Mars would lower the calibrated fluxes by 1.17.) The flux calibration was checked by observing VY CMa, the 20 μm flux of which agreed with Morrison and Simon (1973). The uncertainty in this calibration is hard to estimate but may be of order ±10%. Night-to-night gain variations were ±10% or less. The wavelength calibration was based on laboratory measurements of water lines and was frequently checked by examining the position of zero order.

During this flight series our limiting source of noise

was guiding inaccuracies. Since our dewar samples several closely spaced wavelengths simultaneously, it was possible to make a correction for this guiding noise. This was performed by assuming that when the grating was in one position the average of the 10 channels should be constant within limits set by the other sources of noise, e.g., sky noise and background fluctuations. When an average fell outside these limits, all contributing channels were multiplied by the correction factor necessary to make the average agree with a predetermined value. In the case of sources at the peak of infrared maps, like W51 and M17 S, this value was the maximum observed, while for sources like M17N and θ^2 Ori, which are on the slopes of much stronger sources, the averages were corrected to agree with the mean of all the averages. Typically these guiding corrections were made to about one-third of the integrations and were of order 10%. They improved the shape of the spectrum, thus aiding in identifying the line. However, these corrections also introduced an additional uncertainty into the absolute flux calibration.

These observations were carried out with a new 10-channel liquid-helium–cooled grating spectrometer. The 10 Si:Sb photoconductor detectors are mounted in the focal plane of the f/7 single pass Ebert-Fastie configuration, and together they cover a 5 μm band with a FWHM spectral resolution of 0.5 μm. The entire 16–30 μm region can be sampled at a density of three points per resolution element with a total of only nine grating movements. From observations of VY CMa, the in-flight system NEP at 23 μm has been estimated to be 8×10^{-14} W Hz$^{-1/2}$ in each 0.5 μm bandpass, with all the detectors equaling this performance within $\pm 10\%$. By allowing for spectrometer transmission, beam splitter reflectivity, and chopper efficiency, we estimate the in-flight detector NEP to be 1.3×10^{-14} W Hz$^{-1/2}$ for each detector.

Detector output currents first pass through G118 FET transimpedance amplifiers on the cold spectrometer baseplate, thereby avoiding long high impedance leads which are susceptible to microphonic pickup. The signals are next amplified by operational amplifier (op amp) circuits with several available gain settings and then filtered by low pass filters with 100 Hz roll-off. At this point the 10 channels are also averaged by an op amp summing circuit, and this "sum channel" is synchronously demodulated by a lock-in amplifier and displayed on a strip chart. In the absence of correlated noise, this channel gains a $\sqrt{10}$ improvement in signal-to-noise ratio and can be very useful in finding source peaks. All data channels are fed into an IMSAI 8080 microcomputer where they are sampled by a 16-channel 12 bit analog to digital converter. The synchronous demodulation process is carried out in software, using an INTEL 8080 assembly language program, which normally samples and demodulates 12 channels in 1.56 ms (640 Hz). The phase lags between the chopper reference signal and the detector outputs are the same within $\pm 3°$, and the synchronous demodulation routine will accept a single phase delay of up to 32 ms or 180°, whichever is smaller. The computer can also step the grating according to an easily modified table in its memory, and the results of all integrations are written onto floppy disks and printed on a small data logger. The observer controls the system by means of sense switches which call master routines, and by using a keyboard to enter alphanumeric data. At all times the program's status is displayed on a television monitor and on the front panel LEDs. On board the Kuiper Airborne Observatory, the entire data-acquisition process is automated, with the IMSAI acting in the role of master computer and using the on-board minicomputers as slaves for real-time data analysis and for nodding the telescope. The data-acquisition program occupies 8K bytes of memory plus an additional 4K bytes for a disk operating system.

III. RESULTS

a) Full Spectra

[S III] 18.71 μm emission was detected from three beam positions in the Orion Nebula (Trapezium, KL, and θ^2 Ori), M17 S, M17 N, NGC 2024, and W51. No line emission was seen in Sgr A. Between 17.2 and 20.2 μm, the spectra were fitted to a quadratic baseline and a Gaussian line profile of FWHM = 0.5 μm and central wavelength $\lambda_c = 18.71$ μm. The results are plotted in Figure 1 and summarized in Table 1. Where large enough to plot, the errors shown in individual data points are standard deviations of the mean derived from the scatter of separate integrations. The quoted errors on line fluxes derive from the fitting procedure and do not include uncertainties in calibration or gain changes. The relatively high χ^2 values in the Orion and M17 S fits can be attributed to two causes. First, there appear to be small systematic point-to-point variations in the spectra which show up as jitter and scatter and which are not described by the statistical errors. Such scatter might be caused by incomplete cancellation of the instrumental response or by guiding noise. If the statistical error of the spectrum of the Trapezium were increased to 2% of the flux, the χ^2 of the fit would be decreased to a more acceptable 1.05. Second, in these high signal-to-noise spectra the line profile suggests a non-Gaussian shape. No attempt was made to eliminate these effects, since it was felt that the desired quantity, the line flux, was sufficiently well determined.

b) M17 Map

Fourteen positions in M17 were examined for [S III] emission; the line was detected in 12 of them. The positions were separated by 1'.8 and are roughly oriented along and perpendicular to the axis between M17 S and M17 N. Offsetting was from the star BD $-16°4816$ by means of an xy stage. The chopper throw during the mapping was 16'.2, ensuring that the reference beam was completely off the H II region as shown in the radio maps (Schraml and Mezger 1969). The spectra were sampled at a density of one point per resolution element, and due to the lower density the

TABLE 1

[S III] 18.71 MICRONS IN H II REGIONS

Object	Galactic Designation	χ^2 per degree of freedom	Fitted Line Flux (10^{-16} W cm^{-2})	S_ν* (Jy)	Predicted Line Flux (10^{-16} W cm^{-2})	Observed / Predicted	Comments
Trapezium	G209.0-19.4	12.2	23.8±0.8	116	29.3	0.81	
KL			20.1±1.2	81	20.4	0.99	a
θ^2Ori		2.1	14.1±0.6	66	16.7	0.84	
M17S	G15.0-0.7	3.3	17.2±0.4	91	23.0	0.75	
	G15.1-0.7	0.6	12.0±0.5	66	16.7	0.72	
[illegible]	G49.5-0.4	1.8	3.3±0.6	66	16.7	0.20	
NGC 2024	G206.6-16.4	0.7	3.1±0.3	23	5.8	0.53	
Sgr A		1.2	< 2.3	26	5.8	< 0.40	b

*All fluxes at 15.4 GHz except Sgr A, which is at 5 GHz.

a- The spectrum of KL consists of only a single integration at each wavelength, so no meaningful χ^2 can be calculated. For fitting purposes, $\sigma_\lambda = 0.02F_\lambda$ was assumed, giving $\chi^2 = 1.2$.

b- Value for line flux is a 3σ upper limit.

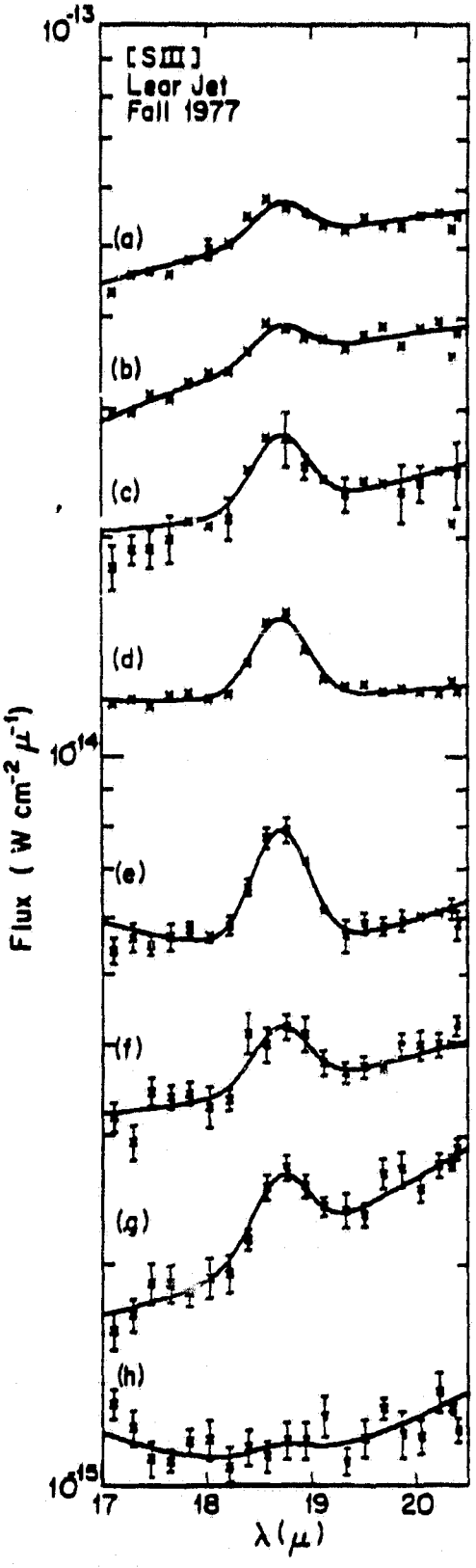

FIG. 1.—Observed [S III] 18.71 μm lines. Sampling is three data points per resolution element, and $\Delta\lambda = 0.5$ μm. The error bars are 1 standard deviation of the mean, and the solid lines are fits to the data. The spectra have been normalized for legibility. Object and normalization factor: (*a*) Trapezium × 1.33. (*b*) KL Nebula × 1. (*c*) θ^2 Orionis × 2. (*d*) M17 S × 1. (*e*) M17 N × 1. (*f*) W51 × 1.125. (*g*) NGC 2024 × 0.9. (*h*) Sgr A × 0.33. The curve through the Sgr A data represents the fitted value of the line strength, which is much less than a 3 σ detection.

fitting function was simplified to a linear baseline plus a Gaussian line profile with FWHM = 0.5 μm and a central wavelength of 18.71 μm. The results are listed in Table 2 and plotted in Figures 2*b* and 2*c*.

IV. CALCULATION OF EXPECTED LINE STRENGTHS

In the absence of extinction, the expression for the [S III] flux from a cloud of ionized gas may be written (Simpson 1975)

$$F = \frac{j}{n_{S\,III} n_e} \frac{n_{S\,III}}{n_p} \frac{n_p}{n_e} E\Omega ,$$

where $(j/n_{S\,III}n_e)$ is the emissivity of the ion, $n_{S\,III}$, n_e, n_p are the number densities of the S^{++} ions, electrons, and protons, E is the emission measure of the region integrated over the beam, and Ω is the solid angle of the beam.

The emissivity of the ionized gas depends on the electron density and temperature. For $n_e \lesssim 6300$ cm^{-3}, collisional de-excitation is negligible, and the emissivity is essentially independent of density and only weakly dependent on temperature (Simpson 1975). Due to collisional de-excitation, the emissivity decreases with increasing n_e for $n_e \gtrsim 6300$ cm^{-3} and falls to half of its low density value at $n_e = 2.5 \times 10^4$ cm^{-3}. Observations of Sgr A (Ekers *et al.* 1975; Pauls *et al.* 1976) indicate that collisional de-excitation is negligible in that source. According to Schraml and Mezger (1969), the electron densities of all our other regions are also below 6300 cm^{-3}. However, in at least one case, W51, higher-resolution observations show that most of the radio continuum flux originates from compact, high density sources. On the other hand, high density sources are absent or a small fraction of the total flux in M17 (Matthews, Harten, and Goss 1978; Webster, Altenhoff, and Wink 1971) and in Orion (Webster and Altenhoff 1970). The effects of high density regions on individual sources are considered in more detail below. For the purposes of our simple theory we have assumed $T_e = 10^4$ K and $n_e \lesssim 6300$ cm^{-3} throughout, which gives $(j/n_{S\,III}n_e) = 5.2 \times 10^{-22}$ ergs cm^3 s^{-1} sr^{-1}.

The abundance of S^{++} was taken to be the average of 12 positions in the Orion Nebula which were measured by Peimbert and Torres-Peimbert (1977) giving $n_{S\,III}/n_p = 1.4 \times 10^{-5}$. When corrections for unobserved ionization states (e.g., S IV) are made, it is found that roughly half the sulfur is in S^{++}, most of the rest being S^{+++}. The variations within the nebula are roughly a factor of 2 above and below the mean. For the purposes of this simple theory, we

TABLE 2

M17 Map

#	Position RA(1950)	Dec(1950)	18.7 μm Continuum Flux (10^{-16} W cm^{-2} μ^{-1})	Observed Line Flux (10^{-16} W cm^{-2})	S_ν(15.4GHz) (J_y)	Predicted Line Flux (10^{-16} W cm^{-2})	Observed / Predicted	Comments
1	$18^h17^m32.^s7$	−16°13'03"	118.8±0.1	20.2±0.5	88	22.3	0.91±0.02	a
2	37.^{s}4	11'40"	49.1±0.7	11.4±1.5	62	15.8	0.72±0.09	
3	42.^{s}1	10'16"	51.7±0.6	14.7±1.1	55	13.9	1.06±0.08	b
4	46.^{s}9	08'52"	24.2±0.7	5.6±1.1	22	5.6	1.00±0.20	
5	28.^{s}0	14'28"	27.3±0.7	4.9±1.0	44	11.1	0.44±0.09	
6	23.^{s}3	15'52"	< 2.3	< 3.0	5.5	1.4	< 2.1	d,e
7	48.^{s}0	11'24"	34.6±0.7	10.3±0.9	48	12.1	0.85±0.07	c
8	53.^{s}8	12'32"	14.8±0.5	5.6±1.4	29	7.4	0.76±0.19	
9	59.^{s}6	13'40"	4.7±0.6	< 9.2	14	3.5	< 1.8	d
10	36.^{s}3	09'08"	48.8±0.9	9.1±1.3	44	11.1	0.82±0.12	
11	30.^{s}5	08'00"	22.9±0.8	5.8±1.4	26	6.5	0.89±0.22	
12	26.^{s}9	11'56"	76.0±0.7	10.6±1.6	51	13.0	0.82±0.12	
13	38.^{s}5	14'12"	72.1±0.7	15.3±2.1	81	20.4	0.75±0.10	
14	44.^{s}4	15'20"	29.2±0.1	7.6±1.3	44	11.1	0.68±0.12	

[a] M17 S (Lemke and Low 1972).

[b] About 50" to east of M17 N (Lemke and Low 1972), and 80" to east of G15.1−0.7 (Schraml and Mezger 1969).

[c] About 50" to west of M17 E (Lemke and Low 1972).

[d] Line flux is 3 σ upper limit.

[e] Continuum flux is 3 σ upper limit. Beam position is south of M17 S, on fringes of molecular cloud.

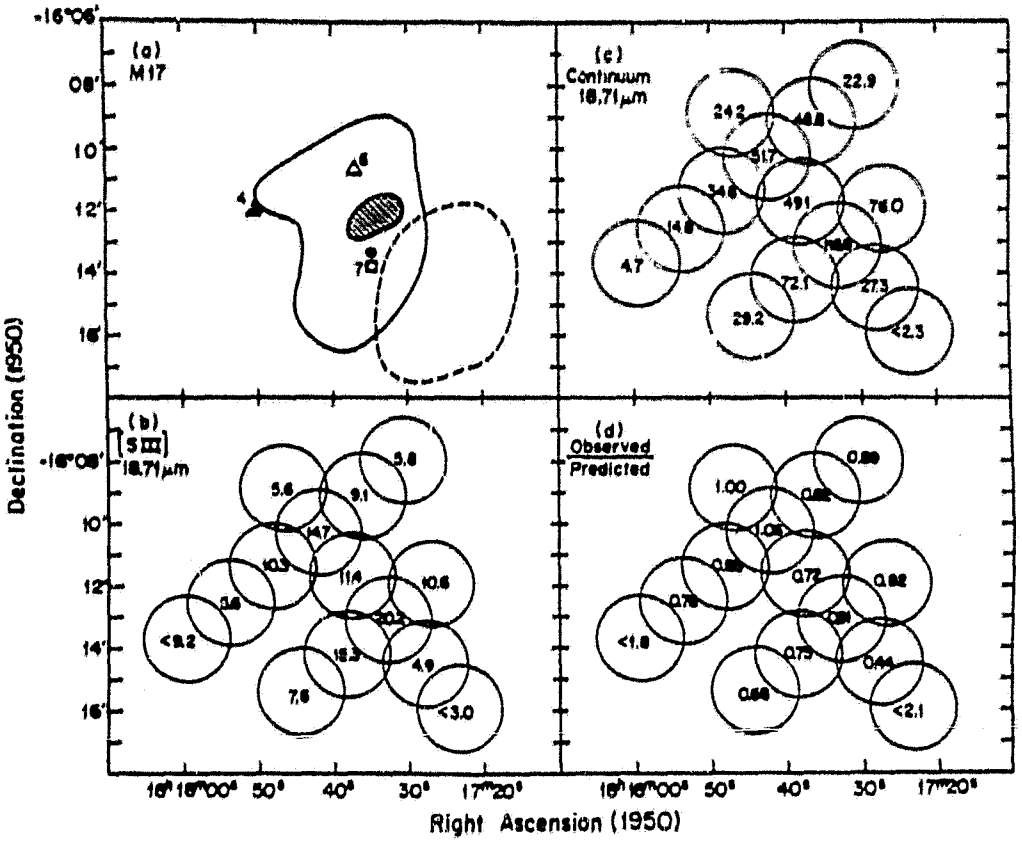

FIG. 2.—(*a*) Features in the H II region M17. *Asterisk*, the foreground star BD −16°4816 which was used for offset guiding. *Square* and *open triangle*, positions of radio peaks G15.0−0.7 and G15.1−0.7 (Schraml and Mezger 1969). *Solid line*, half-power contour of 15.4 GHz map, 2′ beam (Schraml and Mezger 1969). *Dotted line*, half-power contour of $^{13}C^{18}O$ emission (Lada, Dickinson, and Penfield 1974). *Filled triangle*, peak of Hα emission (Dickel 1968). *Hatched ellipse*, center of heavily obscured star cluster (Beetz *et al.* 1976). Numbers give values of A_v to H II region as derived by Dickel (1968) by comparison of radio and Hα fluxes. (*b*) Map of the integrated [S III] 18.71 μm line flux. Units are 10^{-16} W cm^{-2}, and typical errors are $\pm 1.3 \times 10^{-16}$ W cm^{-2}. (*c*) Map of the 18.71 μm continuum. Circles represent the beam positions, and the central numbers give the flux in the 2′.7 beam at that position. Units of flux are 10^{-16} W cm^{-2} μm^{-1}, and typical errors (1 standard deviation, derived from the fitting procedure) are $\pm 0.7 \times 10^{-16}$ W cm^{-2} μm^{-1}. (*d*) Map of the ratio of the observed [S III] 18.71 μm line flux to that predicted by the theory described in the text. Typical errors in the ratio are ±0.12.

have assumed that this abundance is constant for all the regions observed. Finally, the ratio n_e/n_p was taken to be 1.10, since most of the helium should be singly ionized in the region where S^{++} is found.

Except for Sgr A, the emission measure was estimated from the maps of Schraml and Mezger (1969). By assuming that the brightness temperature was constant over the Lear Jet beam, the antenna temperature at the center of the beam was used to calculate the radio flux in the Lear Jet beam. The resulting fluxes are given in Tables 1 and 2. This method overestimates the flux from a point source and underestimates for a source about the size of the radio beam (2′). The error is believed to be no more than a factor of 1.5.

In the case of Sgr A, aperture synthesis observations (Ekers *et al.* 1975) have separated the thermal source, Sgr A West, from the probable supernova remnant, Sgr A East. The integrated flux from Sgr A West is 26 ± 4 Jy at 5 GHz, and since the FWHM of the source is only 1′ × <0′.6, all of this flux was included in our Lear Jet beam.

Given the radio flux in the beam, the emission measure can be calculated if a value for T_e is assumed. Under these assumptions, one can then write a simple relation between the [S III] 18.71 μm flux and the optically thin radio free-free continuum, S_ν:

$$F(18.71\ \mu\text{m}) = 2.04 \times 10^{-16} f(T_e, \nu)(S_\nu/1\ \text{Jy})\ \text{W cm}^{-2}$$

where

$$f(T_e, \nu) = (T_e/10^4\ \text{K})^{1/2}\,[\ln (4.96 \times 10^7 T_e^{3/2}\nu^{-1})]^{-1},$$

and is a slowly varying function of the electron temperature and the radio frequency. For $T_e = 10^4$ K and $\nu = 10$ GHz, $f(T_e, \nu) = 0.118$. The total uncertainty due to temperature is small. In the low density limit $T_e = 5000$ K would lower the predicted flux by 5%, while $T_e = 2 \times 10^4$ K would raise it by 10%.

Several of our sources lie behind large column densities of dust, and if this dust contains silicates one can expect attenuation of the [S III] radiation by the 18 μm resonance. Because the strength of the 18 μm feature is uncertain, we have chosen not to include this

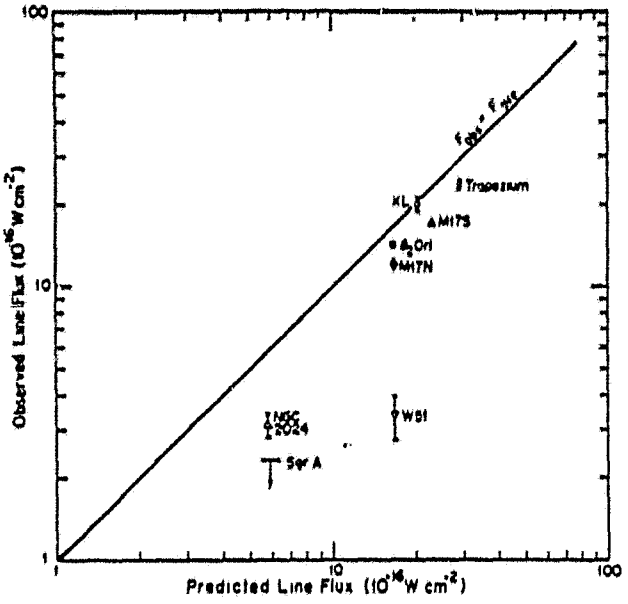

FIG. 3.—Comparison of observed [S III] line flux with that predicted by the simple theory described in the text. Error bars are 1 standard deviation and are derived from the fitting procedure.

extinction in our calculations, but instead to consider the 18 μm optical depth as a quantity which can be measured by comparing the observed flux with that expected in the absence of extinction.

The results of these calculations are given in Tables 1 and 2 and graphed in Figures 2*d* and 3.

V. DISCUSSION

There is a systematic trend for the predicted [S III] fluxes to be too high by an average factor of about 1.3, excluding W51 and observed upper limits. This could be due to one or more of several effects. First, our flux calibration could be low, but the agreement of our spectrum of VY CMa with ground-based measurements argues against this being the major factor. Second, the method of estimating the radio flux may have systematic errors. In order to estimate the magnitude of such errors, models of sources with Gaussian surface-brightness profiles were constructed and the computed fluxes (estimated using the method outlined above) were compared to the exact values. For the source and beam sizes involved, the estimated flux was low by 12% at most, which has the sense of increasing the disagreement. Finally, the assumed ionic abundance may be too high by a factor of 1.3. Given the variations of a factor of 2 in the Orion Nebula (Peimbert and Torres-Peimbert 1977), this seems quite possible.

Orion.—Since the 20 μm silicate feature is seen in emission from the Trapezium (Forrest, Houck, and Reed 1976), the dust optical depth is small, and these observations serve as a useful check on the consistency of the theory. In all three of our beam positions the agreement between predicted and observed fluxes is good.

Our flux from the Trapezium corresponds to a surface brightness of $(4.9 \pm 0.2) \times 10^{-9}$ W cm^{-2} sr^{-1} averaged over our 2'.7 beam. This value is a factor of 1.75 times higher than observed by Baluteau *et al.* (1976) (see also Moorwood *et al.* 1978) with a 55" beam and does not require a lower value of the sulfur abundance than assumed by Simpson (1975). For a 2'.7 circular beam centered on the Trapezium, Simpson's model predicts a [S III] flux of 27.4×10^{-16} W cm^{-2} (Simpson, private communication), which is also in good agreement with our observations.

M17.—In this source the agreement between predicted and observed fluxes is good. The [S III] flux generally follows the radio flux fairly closely with the possible exception of position 5. Here the beam is at the interface between the H II region and the molecular cloud, so the excitation may be lower or the extinction may be greater. At most of the other points the predicted flux is within 25% of that expected, and the variations are within the errors. There is no strong evidence for systematic changes in the ratio of the predicted to the expected [S III] flux over the nebula.

NGC 2024.—This source appears to have low excitation. The radio recombination lines of He are anomalously weak and the size of the He^+ source is significantly smaller than that of radio continuum source, as well as being offset by about 1' (MacLeod, Doherty, and Higgs 1975). Optical observations (Balick 1976) show that forbidden lines of high ionization species are weak or absent, and that the ratio of He^+/He integrated over the nebula is less than 0.2. This evidence indicates that the source of the ionizing radiation is cool. Balick models the H II region with $n_e = 10^3$ cm^{-3} and a single star of $T = 33{,}500$ K.

Our predicted flux is approximately twice what is observed, but the interpretation is confused by the presence of substantial dust column densities in the line of sight. Grasdalen (1974) measured $A_v = 8.3 \pm 0.2$ mag toward NGC 2024 No. 1 and $A_v = 32 \pm 6$ toward NGC 2024 No. 2. NGC 2024 No. 1 is on the edge of the dark lane overlying the core of the H II region, so its visual extinction may be used as a lower limit to the mean extinction of the source. We can estimate an upper limit to the 18.71 μm optical depth by assuming that all the sulfur is in S^{++} and that the total sulfur abundance is $S/H = 2.6 \times 10^{-5}$ [log S = 7.41 by number] as given by the average of the positions in Orion (Peimbert and Torres-Peimbert 1977). From this we find τ (18.71 μm) $\lesssim 1.3$, which leads to $A_v/\tau(18.71\ \mu\text{m}) \gtrsim 6$. The ratio $A_v/\tau(9.7\ \mu\text{m})$ toward VI Cyg No. 12 is 14 (Gillett *et al.* 1975*b*), and for most silicates the 20 μm resonance is weaker than the 10 μm one, so this lower limit on $A_v/\tau(18.71\ \mu\text{m})$ is entirely reasonable.

Using Balick and Sneden (1976) to derive S^{++}/S based on Balick's (1976) model of NGC 2024, one finds that $S^{++}/S \approx 0.7$ and $\tau(18.71\ \mu\text{m}) \approx 1$. The observed [S III] flux is therefore consistent with the Balick model.

W51.—For this giant H II region, our simple theory predicts 5 times more [S III] flux than observed. At least three effects can be proposed as the cause of this discrepancy: collisional de-excitation in compact regions, low S^{++} abundance, and attenuation by dust.

Much of the radio flux in our beam probably comes from the two compact components seen in the high-resolution radio observations of Martin (1972), Felli, Tofani, and D'Addario (1974), and Scott (1978). These compact H II regions will be referred to by the names given to them by Wynn-Williams, Becklin, and Neugebauer (1974), W51 IRS 1 and W51 IRS 2. In order to estimate the [S III] 18.71 μm line fluxes expected from these sources, the observed radio fluxes have been fitted to a thermal bremsstrahlung model to derive the "optically thin" flux at 5 GHz. This leads to an estimate of approximately 45 ± 10 Jy from W51 IRS 1 and 14 ± 2 Jy for W51 IRS 2. Scott (1978) estimates the electron densities to be $n_e \approx 10^4$ cm^{-3} for W51 IRS 1 and $n_e \approx 2.5 \times 10^4$ cm^{-3} for W51 IRS 2. Then, using the formulation of Petrosian (1970) and Simpson (1975) for the expected strength of the [S III] 18.71 μm line with a S III abundance of 1.4×10^{-5} with respect to protons, the [S III] 18.71 μm line flux should be approximately 8.9×10^{-16} W cm^{-2} from W51 IRS 1 and 1.7×10^{-16} W cm^{-2} from W51 IRS 2 or a total of $\sim 10.6 \times 10^{-16}$ W cm^{-2} for the compact components alone. The observed line flux of $3.3 \pm 0.6 \times 10^{-16}$ W cm^{-2} is approximately a factor of 3 lower than this. Therefore density effects alone are not enough to explain the smaller observed [S III] flux.

Due to the enormous visual obscuration of W51, it is not possible to directly measure the S^{++} abundance as in Orion. Instead one must rely on indirect methods. Based on continuum measurements, Beiging (1975) finds that one or more O4 stars are the exciting stars in these sources. O4 V stars have temperatures of about 50,000 K (Panagia 1973), which is hot enough that about 90% of the sulfur is in S^{+++} (Balick and Sneden 1976). One can next try to observe [S IV] 10.5 μm to check on this. Using Simpson's (1975) emissivity for $T_e = 10^4$ K and $n_e = 10^4$ cm^{-3}, a total sulfur abundance of $12 + \log N_s = 7.4$ (Peimbert and Torres-Peimbert 1977), and Martin's emission measure of 72.5×10^6 pc cm^{-6} and size (14″ × 31″) for IRS 1, we predict F ([S IV] 10.5 μm) $= 3.4 \times 10^{-15} f e^{-\tau}$, where $e^{-\tau}$ is the attenuation due to dust and f is the fraction of sulfur in S^{+++}. If we take $f = 1$ and $\tau = 3.9$ (Gillett *et al.* 1975*a*), we predict F ([S IV] 10.5 μm) $= 6.8 \times 10^{-17}$ W cm^{-2}. Gillett *et al.* (1975*a*) did not detect [S IV], and an upper limit of about 6×10^{-16} W cm^{-2} can be set to the line flux. It appears that S^{+++} is less abundant than expected. This is puzzling because [O III] 88 μm is observed at close to the expected strength, assuming an O^{++} abundance like Orion's (Dain *et al.* 1978), but O^{++} and S^{+++} require similar photon energies for their creation. Either S V or S III must be the dominant form. Orion is ionized by θ^1 C Ori, which is an O6 or O5 star (Bečvář 1964; Smithsonian Astrophysical Observatory 1966), so according to Balick and Sneden, $S^{+++}/S > 0.8$ and $S^{++}/S \lesssim 0.05$. Yet the [S III] flux from Orion requires that much of the S be S^{++}, and the [S IV] 10.5 μm line is undetected and weaker than predicted by a factor of 4 (Moorwood *et al.* 1978). By analogy it is plausible that S^{++} is the dominant ion of sulfur in W51 as well. It is unclear why this should be so. Possibilities include (1) the stellar atmosphere models are incorrect; (2) selective ultraviolet extinction by dust cools the radiation field in the H II region; (3) charge exchange reactions are important for sulfur but not for oxygen; and (4) W51 is ionized by a cluster of stars of spectral type later than O4. For a discussion of this point, see Rank *et al.* (1978).

The visual extinction toward W51 IRS 1 and IRS 2 is estimated to be more than 60 and 24 mag, respectively, and both sources show deep 10 μm silicate absorption features (Gillett *et al.* 1975*a*). Our continuum spectrum shows a shallow 20 μm absorption feature, so large column densities of dust are clearly present. If we assume that the observed flux is lower than expected because of dust extinction, we derive $\tau(18.71\ \mu\text{m}) = 1$ or greater, over most of the source.

Sagittarius A.—In this H II region, which is believed to lie at the galactic center, [S III] emission was not detected and a 3 σ upper limit of 2.3×10^{-16} W cm^{-2} may be set, which is a factor of 2.5 below the expected flux. From radio synthesis maps of the thermal component, Sgr A (West), Ekers *et al.* (1975) derived $n_e = 10^3$ cm^{-3}, well below the value of 6000 cm^{-3} at which collisional de-excitation begins to lower the emissivity. Plausible arguments that most of the sulfur is in S^{++} may be made from other observations. Mezger and Smith (1976) found that the integrated strength of the He109α recombination line was 0.095 ± 0.04 times that of H, indicating that almost all He is singly ionized as long as the He abundance is normal. Similarly, observations of [Ne II] 12.8 μm (Aitken *et al.* 1976; Wollman *et al.* 1977) are consistent with most Ne being in Ne^+, under the assumptions that the Ne abundance is normal and that $\tau(12.8\ \mu\text{m}) \approx 1$. On the other hand, [O III] 88 μm radiation is weaker than expected, indicating that O^{++} is underabundant relative to Orion (Dain *et al.* 1978). On the basis of the coincidence of ionization potentials, one can argue that the radiation field is hot enough to make Ne^+, S^{++}, and He^+ the dominant ions of their elements, but that the ultraviolet flux is not hard enough to create abundant O^{++} or to turn S^{++} into S^{+++}. Therefore we feel our assumption that most of the sulfur is in S^{++} is justified. By elimination, one is left with attenuation by dust for an explanation. The 16–20 μm continuum absorption feature is the deepest one ever seen in our Lear Jet observations, leading one to suspect that extinction is important here. If we interpret the discrepancy between predicted flux and observed upper limit as due solely to dust extinction, then we derive $\tau(18.71\ \mu\text{m}) > 0.9$. Further observations with a smaller beam (McCarthy, Forrest, and Houck 1979) allow setting a more stringent limit to the [S III] flux and permit comparison with other wavelengths.

VI. CONCLUSIONS

[S III] 18.71 μm radiation has been detected in the Orion Nebula, M17, NGC 2024, and W51, but not in Sgr A. A simple method of predicting the [S III] flux from the radio continuum flux has been applied, and it has been shown that Orion and M17 agree with the expected flux. The observed line flux in NGC 2024 is consistent with Balick's model for the exciting source, plus a moderate amount of extinction by silicate dust grains. In the case of W51, the low observed flux may be due to either a lower S^{++} abundance than in Orion or dust extinction or both. The most plausible explanation for the low [S III] emission from the galactic center Sgr A is attenuation by dust.

We would like to thank Robert Mason and the staff of NASA's Airborne Sciences Office for technical support while on the Lear Jet. Gerry Stasavage and Westy Dain receive special thanks for their aid in building the new dewar and the microcomputer system. We are grateful to Dennis Ward, Janet Simpson, and Alan Moorwood for useful conversations. This work was supported by NASA grant NGR 33-010-182.

REFERENCES

Aitken, D. K., Griffiths, J., Jones, B., and Penman, J. M. 1976, *M.N.R.A.S.*, 174, 41P.
Balick, B. 1976, *Ap. J.*, 208, 75.
Balick, B., and Sneden, C. 1976, *Ap. J.*, 208, 336.
Baluteau, J. P., Bussoletti, E., Anderegg, M., Moorwood, A. F. M., and Coron, N. 1976, *Ap. J.* (*Letters*), 210, L45.
Bečvář, A. 1964, *Atlas of the Heavens Catalogue* (Cambridge: Sky Publishing House).
Beetz, M., Elsasser, H., Poulakos, C., and Weinberger, R. 1976, *Astr. Ap.*, 50, 41.
Beiging, J. 1975, in H II *Regions and Related Topics*, ed. T. L. Wilson and D. Downes (Berlin: Springer-Verlag), p. 443.
Christensen, P. 1979, in preparation.
Dain, F. W., Gull, G. E. Melnick, G., Harwit, M., and Ward, D. B. 1978, *Ap. J.* (*Letters*), 221, L17.
Dickel, H. R. 1968, *Ap. J.*, 152, 651.
Ekers, R. D., Goss, W. M., Schwarz, U. J., Downes, D., and Rogstad, D. H. 1975, *Astr. Ap.*, 43, 159.
Felli, M., Tofani, G., and D'Addario, L. R. 1974, *Astr. Ap.*, 31, 431.
Forrest, W. J., Houck, J. R., and Reed, R. A. 1976, *Ap. J.* (*Letters*), 208, L133.
Gillett, F. C., Forrest, W. J., Merrill, K. M., Capps, R. W., and Soifer, B. T. 1975*a*, *Ap. J.*, 200, 609.
Gillett, F. C., Jones, T. W. Merrill, K. M., and Stein, W. A. 1975*b*, *Astr. Ap.*, 45, 77.
Grasdalen, G. L. 1974, *Ap. J.*, 193, 373.
Greenberg, L. T., Dyal, P., and Geballe, T. R. 1977, *Ap. J.* (*Letters*), 213, L71.
Lada, C., Dickinson, D. F., and Penfield, H. 1974, *Ap. J.* (*Letters*), 189, L35.
Lemke, D., and Low, F. J. 1972, *Ap. J.* (*Letters*), 177, L53.
MacLeod, J. M. Doherty, L. H., and Higgs, L. A. 1975, *Astr. Ap.*, 42, 195.
Martin, A. H. M. 1972, *M.N.R.A.S.*, 157, 31.
Matthews, H. E., Harten, R. H., and Goss, W. M. 1978, preprint.
McCarthy, J. F., Forrest, W. J., and Houck, J. R. 1979, in preparation.
Mezger, P. G., and Smith, L. F. 1976, *Astr. Ap.*, 47, 143.
Moorwood, A. F. M., Baluteau, J. P., Anderegg, M., Coron, N., and Biraud, Y. 1978, *Ap. J.*, 224, 101.
Morrison, D., and Simon, T. 1973, *Ap. J.*, 186, 193.
Panagia, N. 1973, *A.J.*, 78, 929.
Pauls, T., Downes, D., Mezger, P. G., and Churchwell, E. 1976, *Astr. Ap.*, 46, 407.
Peimbert, M., and Torres-Peimbert, S. 1977, *M.N.R.A.S.*, 179, 217.
Petrosian, V. 1970, *Ap. J.*, 159, 833.
Rank, D. M., Dinerstein, H. L., Lester, D. F., Bregman, J. D., Aitken, D. K., and Jones, B. 1978, *M.N.R.A.S.*, 185, 179.
Schraml, J., and Mezger, P. G. 1969, *Ap. J.*, 156, 269.
Scott, P. F. 1978, *M.N.R.A.S.*, 183, 435.
Simpson, J. P. 1975, *Astr. Ap.*, 39, 43.
Smithsonian Astrophysical Observatory. 1966, *Star Catalog* (Washington: Smithsonian Institution).
Webster, W. J., and Altenhoff, W. J. 1970, *Ap. Letters*, 5, 233.
Webster, W. J., Altenhoff, W. J., and Wink, J. E. 1971, *A.J.*, 76, 677.
Wollman, E. R., Geballe, T. R., Lacy, J. H., Townes, C. H., and Rank, D. M. 1977, *Ap. J.* (*Letters*), 218, L103.
Wright, E. L. 1976, *Ap. J.*, 210, 250.
Wynn-Willians, C. G., Becklin, E. E., and Neugebauer, G. 1974, *Ap. J.*, 187, 473.

W. J. FORREST, J. R. HOUCK, and J. F. MCCARTHY: Center for Radiophysics and Space Research, Space Sciences Building, Cornell University, Ithaca, NY 14853.

THE ASTROPHYSICAL JOURNAL, 233:611–620, 1979 October 15

16–39 MICRON SPECTROSCOPY OF OXYGEN-RICH STARS

WILLIAM J. FORREST, JOHN F. MCCARTHY, AND JAMES R. HOUCK
Center for Radiophysics and Space Research, Cornell University
Received 1979 February 12; accepted 1979 April 27

ABSTRACT

Airborne observations of the 16–39 μm spectra of 10 oxygen-rich stars with excess emission in the infrared have been obtained. The stars show excess emission attributed to circumstellar dust grains in the 16–39 μm region in the form of a broad hump peaking near 18 μm and falling smoothly to longer wavelengths. The emission is similar in character to the emission from the Trapezium region of the Orion Nebula, indicating the grain materials are quite similar in these objects. The existence of a feature in the 20 μm region is consistent with the O–Si–O bending resonance expected for silicate material. The lack of any sharp structure in the spectra indicates the silicate is in an amorphous, disordered form. A simple model of small grains of carbonaceous chondrite silicate material in a diffuse circumstellar envelope is shown to give a good qualitative fit to the observed 8–39 μm circumstellar spectra. Comparison of the observed spectra with the model spectra indicates the grain emissivity falls as $1/\lambda^2$ from 20 to 40 μm.

Subject headings: infrared: spectra — stars: circumstellar shells — stars: late-type

I. INTRODUCTION

At wavelengths longward of 8 μm, the spectra of many cool stars show an excess in flux which has been attributed to circumstellar dust emission (Gillett, Low, and Stein 1968; Woolf and Ney 1969). The circumstellar nature of this excess emission has been confirmed by spatially resolving the shells from the star (Zapalla *et al.* 1974; McCarthy, Low, and Howell 1977; Sutton *et al.* 1977) and its identification with dust supported by the lack of any fine structure in high-resolution spectra (Gammon, Gaustad, and Treffers 1972; Treffers and Cohen 1974). Less certain are the chemical and physical composition of the dust grains, their temperatures and spatial distribution about the star, and the wavelength dependence of the opacity of the grains. These characteristics are important to an understanding of the process of grain formation and mass loss from the stars. Further, infrared spectroscopy has shown that the grains around oxygen-rich stars are quite similar to an important component of the interstellar dust grains. Thus information on the composition and opacity of the circumstellar dust grains has important applications to the understanding of other galactic infrared sources.

The present study of the 16–39 μm spectra of oxygen-rich stars provides new information about the dust grains in the cimcumstellar envelopes. If the 10 μm emission feature in circumstellar spectra is due to a Si–O stretching resonance in silicate grains, as suggested by Woolf and Ney (1969), a second O–Si–O bending resonance is expected in the 20 μm region. The shape of the 20 μm resonance depends on the chemical/physical composition of the silicate material. For instance, well-ordered silicates, as are found on the Earth and Moon, all show fine structure in the 20 μm region. The instrumentation and observations are presented in §§ II and III and discussed in § IV. A simple shell model of silicate grains is compared with the observed spectra in § V.

II. INSTRUMENTATION

The observations were made with helium-cooled Ebert-Fastie spectrometers, using telescopes aboard NASA aircraft operating between 41,000 and 45,000 foot (12,505 m and 13,725 m) altitude. The two-channel spectrometer covers the wavelength range 16–39 μm (Forrest, Houck, and Reed 1976). A Si:As detector was used for the 16–23 μm band with a resolution 0.5 μm FWHM. Prior to 1977 the 21–39 μm band used a Ge:Ga photoconductor built by W. J. Moore with a resolution of 1.2 μm FWHM. In 1977 February this was replaced by a more sensitive Ge:Zn detector configured to give a resolution of 1.0 μm FWHM. The 10-channel spectrometer covers the wavelength range 16–30 μm and employs 10 Si:Sb photoconductors with an Intel 8080 microprocessor-based data system which demodulates the signals of 10 detectors simultaneously. This spectrometer and the data system are described more fully in a separate paper (McCarthy, Forrest, and Houck 1979). The spectral resolution was 0.2 μm FWHM for all the observations except for the spectrum of VY CMa, for which $\Delta\lambda = 0.5$ μm FWHM. The spectrometers were used in conjunction with the 91 cm telescope of the NASA Gerard P. Kuiper Airborne Observatory (KAO) and the 30 cm telescope of the NASA Lear Jet (VY CMa only). The beam size of approximately 30″ on the KAO and 2.7–3.2 on the Lear Jet was large enough to include most of the flux from these compact sources. Standard sky chopping using the oscillating secondary was employed.

TABLE 1

STARS INCLUDED IN THE OBSERVING PROGRAM

Name (1)	IRC (2)	AFGL (3)	Spectrum (4)	Variability (5)	Bolometric Excess[a] (6)
α Ori	+10100	836	M2 Iab	SRc	s
X Her	+50248	...	M6e	SRb	s
μ Cep	+60325	2802	M2e Ia	SRc	s
RX Boo	+30257	1706	M7e–M8e	SRb	s
R Cas	+50484	3188	M6e–M8e	M	s
NML Tau	+10050	529	M6e–M10e	M	m
PZ Cas	+60417	3138	M3 Ia[b]	SRa	m
VY CMa	−30087	1111	M5 Ib pec	Lc	l
IRC +10420	+10420	2390	F8–G0 I[c]	...	l
OH 26.5+0.6	...	2205	...	...	l

[a] The bolometric excess is the fractional amount of the total luminosity which appears in excess of that expected from the star alone as described in the text: s = small = 0 to 0.05; m = moderate = 0.05 to 0.5; l = large = 0.5 to 1.0.

NOTE.—The spectral type and variability type are taken from Kukarkin *et al.* (1969) except as noted: [b] Humphreys 1970; [c] Humphreys *et al.* 1973.

III. OBSERVATIONS

The program stars are listed in Table 1 along with their 2 micron sky survey number (IRC, Neugebauer and Leighton 1969), their AFGL sky survey number (AFGL, Price and Walker 1976), the spectral and variable type, and an estimate of the fractional amount of the total emission which is in excess of that expected from the star alone ("bolometric excess"). The stars were selected on the basis of their brightness at 20 μm, the presence of the 10 μm "silicate" feature, and spectral evidence in the visible of an oxygen-rich atmosphere (O/C > 1). With the exception of IRC +10420 all the stars are luminous, red-giant stars probably in an advanced stage of stellar evolution. IRC +10420 is an unusual and luminous G0 I star with large excess emission from dust (Humphreys *et al.* 1973). OH 26.5+0.6 shows evidence of having the thickest dust shell of the stars in this group, with strong absorption at 10 μm and a very cool energy distribution. It is thought to be a Mira variable red giant which is losing mass rapidly (Forrest *et al.* 1978). The stars are arranged here in order of increasing optical depth of the circumstellar material, as judged from their fractional bolometric excesses (column [6]). The method used in deriving this "bolometric excess" is described more fully in § IV.

The observations reported here were obtained between 1976 January and 1978 May. The line-of-sight water-vapor column density was monitored aboard the KAO and ranged from 5 to 20 μm precipitable water vapor. The absence of water-vapor features in the derived spectra shows that the absorption features have been adequately removed by the normalization procedure. Shortward of 17 μm, absorption due to terrestrial CO_2 affects the spectrum, and it was necessary to make small differential corrections to account for this. For spectral calibration, the Moon was observed with the same instruments. The Moon was assumed to radiate as a blackbody at a temperature appropriate for the phase of and position of the beam on the Moon as judged by the 10 μm measurements of Geoffrion, Korner, and Sinton (1960). For the absolute flux calibration on the KAO, ground-based measurement of the 20 μm flux from non-variable sources were used as follows: 1976 May, NGC 7027 ($F_{20\,\mu m} = 6.2 \times 10^{-16}$ W cm^{-2} μm^{-1}, Becklin, Neugebauer, and Wynn-Williams 1973); 1976 November, α Ori ($F_{20\,\mu m} = 1.43 \times 10^{-15}$ W cm^{-2} μm^{-1}, Morrison and Simon 1973); 1977 June, μ Cep ($F_{20\,\mu m} = 5.8 \times 10^{-16}$ W cm^{-2} μm^{-1}, Morrison and Simon 1973); 1978 May, α Her ($F_{20\,\mu m} = 3.7 \times 10^{-16}$ W cm^{-2} μm^{-1}, Morrison and Simon 1973). For the Lear Jet and 1978 January KAO observations, Mars was used as the flux standard at 20 μm, using the model of Wright (1976).

The spectra derived under these assumptions are shown in Figures 1*a*–1*e*. The flux levels have been normalized for convenient display. In Table 2 the spectra are listed. Column (1) gives the number of the spectrum which identifies the spectrum in the appropriate figure. Columns (2) and (3) give the name of the star and the date of the observation. Column (4) gives the spectrometer and telescope used, and column (5), labeled $F_{20\,\mu m}$, gives the flux level of the horizontal tick next to the identification numbers in the figures; it is also the approximate flux level observed at 20 μm. In the cases where the infrared excess is small (Table 1), a considerable fraction of the flux observed is from the stellar photosphere. To estimate the amount expected from the stellar photosphere alone, photometry from 0.84 to 5 μm was fitted with a blackbody of temperature appropriate to the spectral type and extrapolated to 20 μm. This flux will be denoted $F_{20\,\mu m}$(star); the ratio $F_{20\,\mu m}$(star)/$F_{20\,\mu m}$ is given in column (6). As an example of the probable contribution of the stellar photosphere, the blackbodies for RX Boo (spectrum no. 3; Fig. 1*b*) and μ Cep (spectrum no. 7, Fig. 1*a*) are included.

Also included in the figures are ground-based, broad-band measurements of the nonvariable sources made by other observers. The agreement is quite good

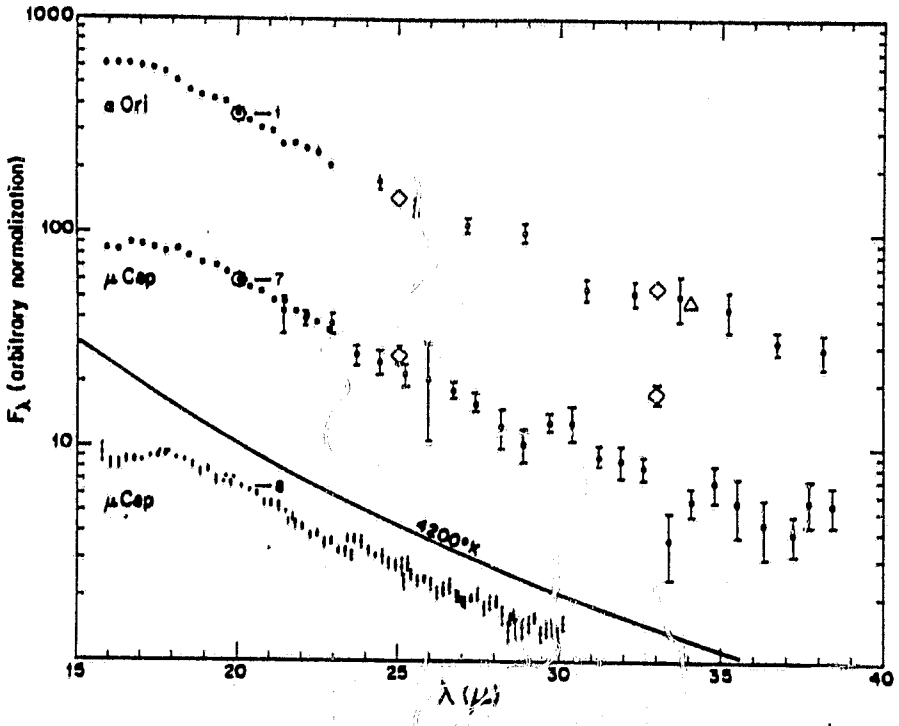

FIG. 1a

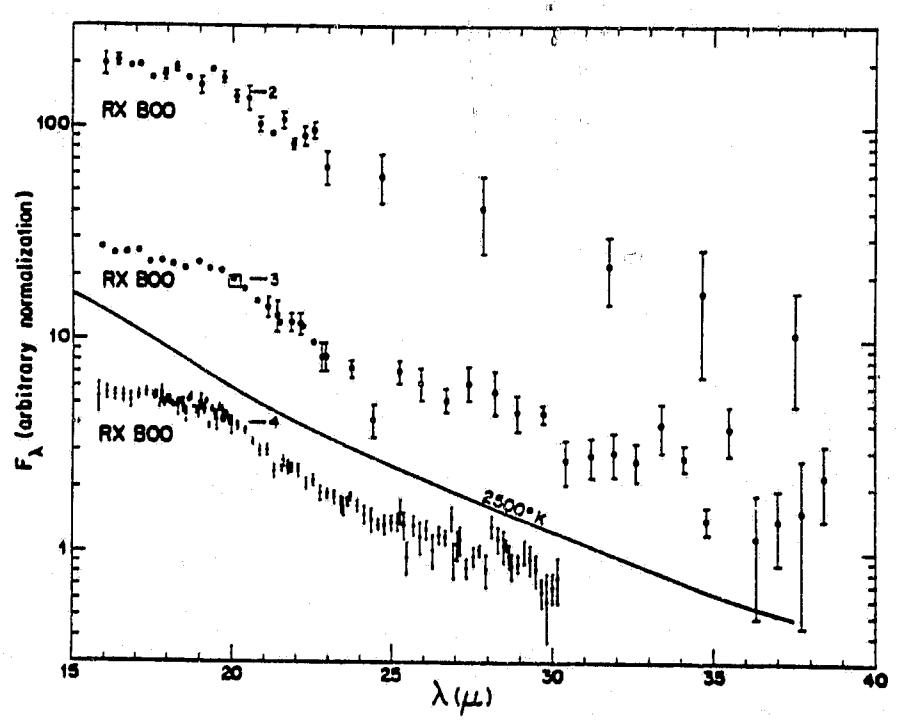

FIG. 1b

FIG. 1.—(*a*) The observed 16–39 μm spectra of the oxygen-rich supergiants α Ori and μ Cep. The flux calibration and other relevant data are given in Table 2. In this and the other figures, statistical error bars representing ±1 σ of the mean are shown where large enough to plot. The smooth curve is a 4200 K blackbody extrapolated from the 4–8 μm data of Russell *et al.* and represents an estimate of the probable contribution of the star to the total observed flux from μ Cep (spectrum no. 7) as described in the text. The large open symbols are ground-based broad-band observations from the following sources: *open squares*, Morrison and Simon 1973; *diamonds*, Hagen, Simon, and Dyck 1975; *triangle*, Low, Rieke, and Armstrong 1973. The lower diamond at 33 μm refers to the μ Cep spectrum below it (spectrum no. 7). (*b*) The observed 16–39 μm spectra of the oxygen-rich red-giant star RX Boo. The flux calibration and other relevant data are given in Table 2. The smooth curve is a 2500 K blackbody extrapolated from shorter wavelengths and represents our estimate of the stellar contribution to the spectrum just above. *Open square*, ground-based 20 μm measurement of Morrison and Simon 1973.

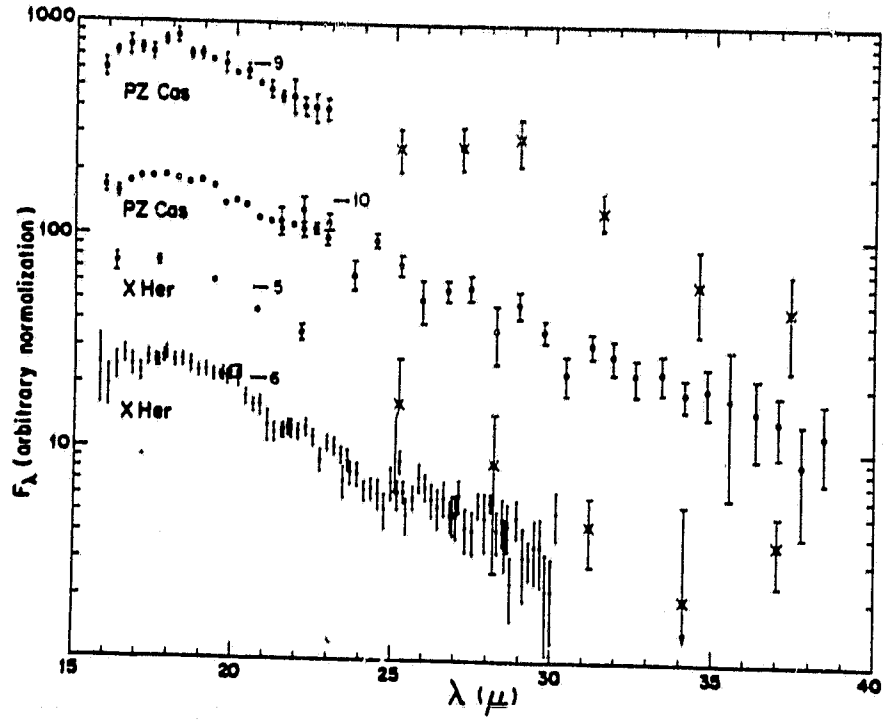

FIG. 1c

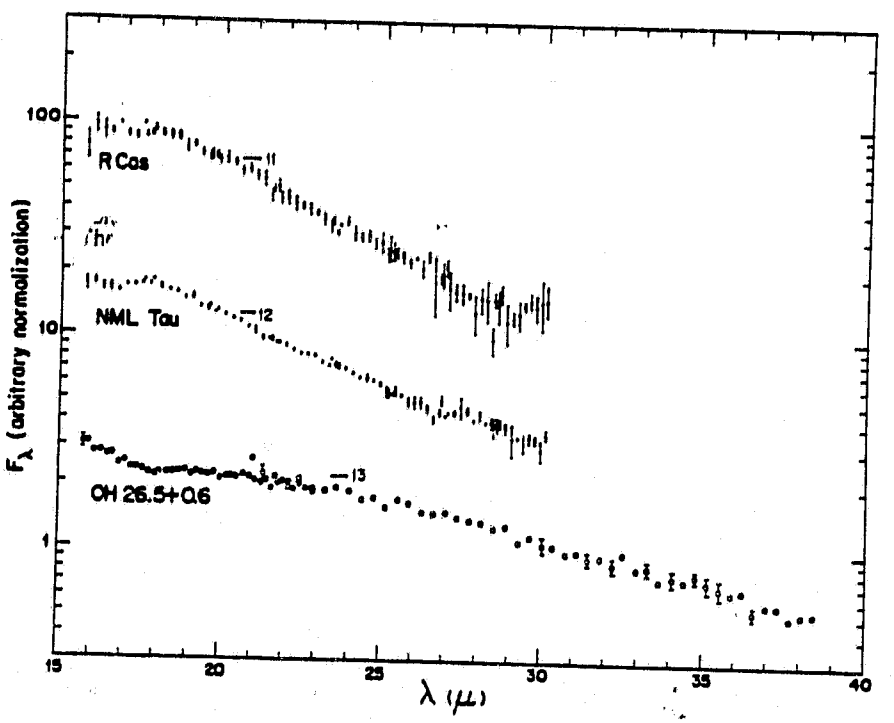

FIG. 1d

FIG. 1.—(*c*) The observed 16–39 μm spectra of PZ Cas (M3 Ia) and X Her (M6e). The flux calibration and other relevant data are given in Table 2. *Open square*, a broad-band 20 μm measurement of X Her by Morrison and Simon 1973. (*d*) The 16–39 μm spectra of the Mira variables R Cas, NML Tau (= IK Tau), and OH 26.5+0.6. The flux calibration and other relevant data are given in Table 2. Some of the OH 26.5+0.6 data here have been reported previously by Forrest *et al.* 1978.

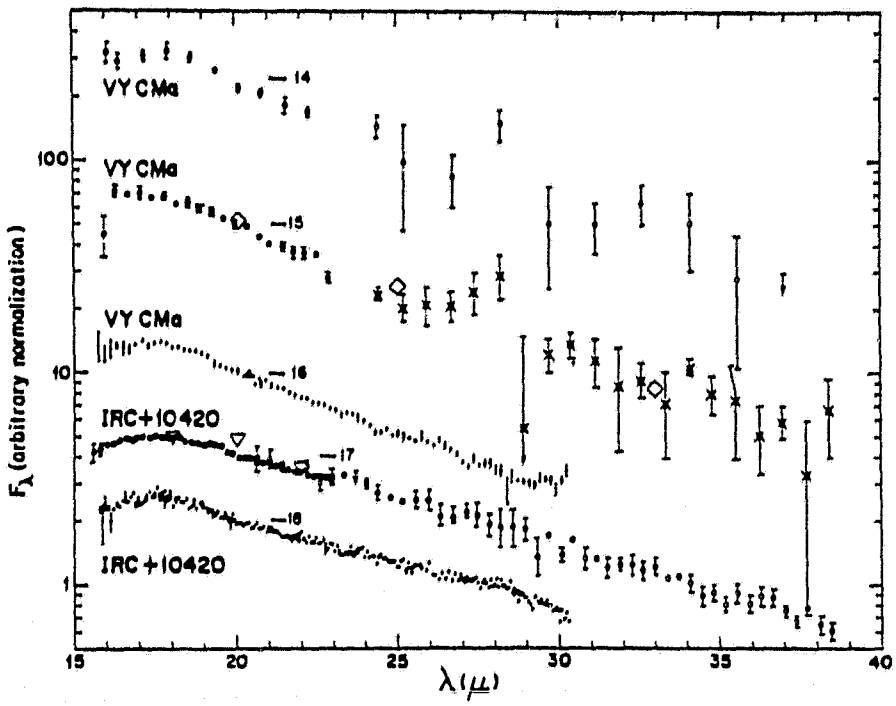

FIG. 1*e*.—The 16–39 μm spectra of the supergiant stars VY CMa and IRC +10420. The flux calibration and other relevant data are given in Table 2. Broad-band observations by Hagen *et al.* (*diamonds*) of VY CMa and by Humphreys *et al.* (*upside down triangles*) of IRC +10420 are included.

in all cases except for the 33 μm observation of μ Cep (Fig. 1*a*, spectrum no. 7) reported by Hagen, Simon, and Dyck (1975). Their flux level is approximately a factor of 2 higher than was observed here, though the 25 μm flux levels agree within the errors. A second spectrum of μ Cep taken in 1978 January from 16 to 30 μm (spectrum no. 8 in Fig. 1*a*) agrees quite well in shape and flux with the 16–39 μm spectrum taken in 1977 June in the region of overlap. Since μ Cep is not variable in the infrared at 20 μm (Morrison and Simon 1973) and has not displayed any large variations in visual flux from 1974 to 1978 (Mattei 1978), the

TABLE 2

OBSERVING LOG AND FLUX LEVELS AT 20 MICRONS

Spectrum, Figure (1)	Name (2)	Date (3)	Notes[a] (4)	$F_{20\,\mu m}$ (W cm^{-2} μm^{-1}) (5)	$F_{20\,\mu m}$(star)/$F_{20\,\mu m}$[b] (6)
1, 1*a*	α Ori	1976 Nov	2, KAO	1.45×10^{-13}	0.41
2, 1*b*	RX Boo	1976 May	2, KAO	3.8×10^{-16}	0.32
3, 1*b*	RX Boo	1977 Jun	2, KAO	3.9×10^{-16}	0.31
4, 1*b*	RX Boo	1978 May	10, KAO	4.0×10^{-16}	0.30
5, 1*c*	X Her	1977 Jun	2, KAO	2.15×10^{-16}	0.33
6, 1*c*	X Her	1978 May	10, KAO	2.1×10^{-16}	0.33
7, 1*a*	μ Cep	1977 Jun	2, KAO	5.8×10^{-16}	0.17
8, 1*a*	μ Cep	1978 Jan	10, KAO	6.4×10^{-16}	0.16
9, 1*c*	PZ Cas	1976 Nov	2, KAO	2.9×10^{-16}	< 0.1
10, 1*c*	PZ Cas	1977 Jun	2, KAO	3.7×10^{-16}	< 0.1
11, 1*d*	R Cas	1978 Jan	10, KAO	6.8×10^{-16}	0.22
12, 1*d*	NML Tau	1978 Jan	10, KAO	1.28×10^{-15}	< 0.1
13, 1*d*	OH 26.5+0.6	1977 Jun	2, KAO	1.08×10^{-15}	< 0.1
14, 1*e*	VY CMa	1976 Jan	2, Lear	6.8×10^{-15}	< 0.1
15, 1*e*	VY CMa	1976 Nov	2, Lear	7.7×10^{-15}	< 0.1
16, 1*e*	VY CMa	1977 Sep	10, Lear	8.0×10^{-15}	< 0.1
17, 1*e*	IRC +10420	1976 May	2, KAO	2.25×10^{-16}	< 0.1
18, 1*e*	IRC +10420	1978 May	10, KAO	2.0×10^{-15}	< 0.1

[a] Notes: 2 = 2 detector 16–39 μm spectrometer; 10 = 10 detector 16–30 μm spectrometer; KAO = NASA C-141 KAO 91 cm telescope; Lear = NASA Lear Jet 30 cm telescope.

[b] An entry < 0.1 in column (6) means the star contributes less than 10% of the observed flux at 20 μm.

discrepancy is probably not due to source variability. It is felt that the measurements reported here are sufficiently reliable to rule out the factor of 2 excess for μ Cep at 33 μm reported by Hagen *et al.* This point could be settled by an independent measurement of the 33 μm flux level of μ Cep, though this would be difficult to do from the ground because of the large and time-variable opacity of terrestrial water vapor at these wavelengths.

IV. DISCUSSION

All the stars in this study radiate in excess of what would be expected from the star alone in the 16–40 μm band (Table 2). The probable source of this emission is circumstellar dust heated by stellar radiation. The character of this radiation is a smooth, blackbody-like continuum at long wavelengths with leveling off or downturn shortward of 18 μm, most evident in the cases where the dust emission dominates (e.g., μ Cep, Fig. 1*a*; PZ Cas, Fig. 1*c*; VY CMa and IRC +10420, Fig. 1*e*; NML Tau, Fig. 1*d*). As this downturn is more rapid than can result from blackbody emission, it indicates that the opacity of the dust grains is not gray at these wavelengths. We interpret this as an emission feature due to a grain resonance in this region. The spectrum of OH 26.5+0.6 (Fig. 1*d*) shows an absorption feature at around 18 μm which is due to radiation transfer effects in the extremely thick shell surrounding the star, as discussed by Forrest *et al.* (1978). When the optical depth is large, a local minimum in flux is observed where the grain emissivity peaks due to the decrease in dust temperature with distance from the star.

The spectrum of RX Boo (Fig. 1*b*), an M8e semiregular variable, is somewhat different from the other stars in that the emission is almost flat out to 20 μm and then decreases. Taking into account the stellar contribution at these wavelengths (Fig. 1*b*, smooth curve), this indicates the dust emission peaks at approximately 19 μm as compared with the peak at approximately 17.5 μm seen in the other stars. This could be due to a different composition of dust grains around this star. Interestingly, the 10 μm spectrum of this star (obtained in 1972 [Gillett and Forrest 1978], not shown here) is somewhat atypical of M type stars in that the excess peaks longward of 9.7 μm and decreases less rapidly beyond the peak. R Leo (Forrest, Gillett, and Stein 1975) shows a similar behavior.

Elitzur (1978) has proposed a mechanism for the excitation of the main line maser emission of OH at 1665 and 1667 MHz which is seen from many cool oxygen-rich red-giant stars. In the present study, the cool stars with thinner circumstellar shells, such as RX Boo, X Her, and R Cas, are typical of this class of object. In his model, the ground-state inversion results from a nonequilibrium population of upper rotational levels due to pumping by a radiation field which falls more steeply than $I_\lambda \propto 1/\lambda^5$. These upper levels are populated by photons at wavelengths near $\lambda = 35$, 53, 79, or 119 μm. Of the stars that have been studied, the emergent spectra of the optically thinnest sources with the hottest apparent dust temperatures (i.e., with a small infrared excess given in Table 1) goes approximately as $F_\lambda \propto (1/\lambda)^4$ from 30 to 40 μm. In those stars with thick shells the observed flux falls off more slowly than this. Thus it is not obvious that radiation excitation involving 35 μm photons as proposed by Elitzur (1978) will work. Closer to the star or at longer wavelengths the dust spectrum will probably be steeper, but this can be offset by a greater contribution from the star whose spectrum is probably a blackbody in the Rayleigh-Jeans limit and therefore goes at $(1/\lambda)^4$.

The emission from the dust alone around the stars μ Cep, PZ Cas, VY CMa, and IRC +10420 from 8 to 38 μm is shown in Figure 2. These stars were chosen because of the large contrast between the dust emission and the estimated stellar emission at these wavelengths.

For μ Cep, the stellar spectrum and excess emission from 8 to 13.5 μm was taken from Russell, Soifer, and Forrest (1975). Those authors discussed the possibility that some of the emission shortward of 8 μm could be from the circumstellar envelope. The stellar spectrum in the 16–40 μm region was assumed to be the continuation of the blackbody fit to the 5.5–8 μm data and is shown as the smooth curve in Figure 1*a*. The difference between the observed flux and this blackbody is attributed to circumstellar emission and is plotted in Figure 2. Integrated over wavelength, the circumstellar emission constitutes less than 0.05 of the total emission from μ Cep (bolometric excess <0.05; Table 1), indicating a relatively thin circumstellar shell. The subtraction process is most uncertain near 8 μm

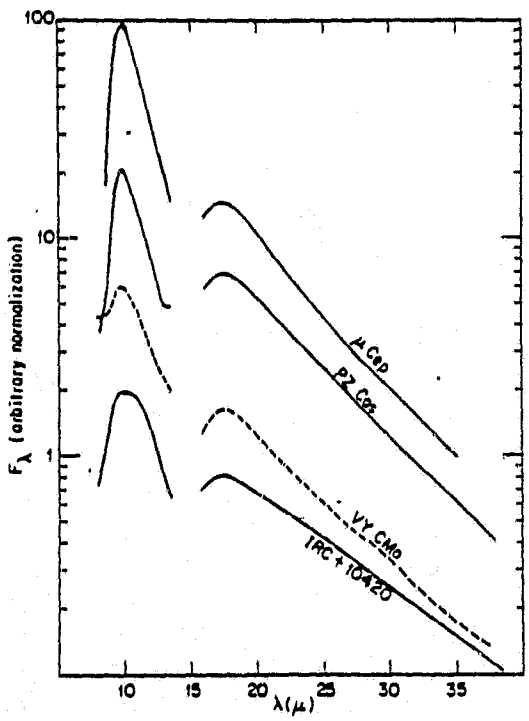

FIG. 2.—The excess emission from μ Cep, PZ Cas, VY CMa, and IRC +10420 as described in the text.

where the stellar continuum can contribute a major fraction of the observed flux.

PZ Cas was observed from 16 to 39 μm at the suggestion of F. C. Gillett (1976), who had obtained an 8–13 μm spectrum in 1975 November showing a very large dust emission feature peaking at 9.7 μm. Using the broad-band measurements from the IRC (Neugebauer and Leighton 1969) and AFGL (Price and Walker 1976) in conjunction with the 8–13 and 16–39 μm spectra, it was found that the energy distribution could be fitted by a 2500 K blackbody shortward of 5 μm plus an infrared excess longward of 8 μm. The blackbody was assumed to represent the stellar continuum and was subtracted to give the infrared excess shown in Figure 2. Integrated over wavelength, the infrared excess constituted approximately 0.16 of the total flux observed (bolometric excess $\approx$ 0.16; Table 1), indicating a moderately thick circumstellar shell. Again, this process is most uncertain near 8 μm where the stellar continuum can supply a major fraction of the observed flux. Beyond 10 μm the stellar continuum represents less than 10% of the observed flux. There is an additional uncertainty in the ratio of 10 to 20 μm emission because the photometry and spectrometry were done at different times and this source appears to vary in the infrared (Table 2; Price and Walker 1976).

For the stars VY CMa and IRC +10420, the optical depth of the circumstellar shell is large enough to modify the stellar spectrum, and a different procedure to estimate the infrared excess was necessary. In these cases the total observed emission was integrated over all wavelengths. In the absence of a circumstellar shell, the spectrum of the star was assumed to be a blackbody of temperature appropriate for the spectral type (6000 K for IRC +10420, 2500 K for VY CMa) with the same integrated luminosity as the observed luminosity. Any emission above this flux level is certainly circumstellar excess. For VY CMa the infrared excess integrated over wavelength constitutes at least 0.5 of the total flux (bolometric excess $\geq$ 0.5; Table 1), while for IRC +10420 the bolometric excess was at least 0.88. For IRC +10420, the star can contribute at most 2% of the flux observed at 8 μm and beyond, so no subtraction was necessary and the total observed flux is plotted in Figure 2. For VY CMa, the star may contribute as much as 12% to the flux observed at 8 μm, but this fraction decreases to less than 4% at 10 μm and beyond. Since the contribution of the star to the observed spectrum is uncertain when the optical depth and geometry of the circumstellar shell are uncertain, the total observed flux is plotted in Figure 2. It is believed to be primarily due to circumstellar emission, but there may be some stellar contribution near 8 μm.

From the derived spectra of 8–39 μm circumstellar emission shown in Figure 2, the similarity of the circumstellar dust is apparent. There is a peak of emission near 18 μm with a smooth continuum falling toward longer wavelengths, indicating a resonance in the grain material near 18 μm. At shorter wavelengths there is the familiar and more prominent 9.7 μm emission feature. The existence of these two resonances is in qualitative agreement with the silicate hypothesis which predicts a feature in the 10 μm region due to the Si–O stretching resonance and a feature in the 20 μm region due to the O–Si–O bending resonance.

The smoothness of the spectra indicates the grain material is different than well-ordered lunar and terrestrial silicates which typically show sharp structure, especially in the 20 μm region (see Knacke and Thomson 1973; Zaikowski, Knacke, and Porco 1975). The shape of these spectra is quite similar to that observed in the Trapezium region of the Orion Nebula (Forrest and Soifer 1976; Forrest, Houck, and Reed 1976), but with a higher apparent temperature. This is consistent with the idea that the cool oxygen-rich red-giant stars are the source of an important component of the interstellar dust seen in Orion.

V. SHELL MODEL

a) The Model

In order to make a more detailed comparison of the observed circumstellar spectra in Figure 2 and the theoretical emission, some simple models have been considered. In the case where the shell optical depth is not large, the theoretical emission is particularly simple because each grain is observed without attenuation and the radiation field which determines the grain temperature falls as $1/R^2$ beyond a few stellar radii. As there are no sharp resonances in the observed spectra, it is not possible at this time to unambiguously identify the grain material which is responsible for the emission. However, the existence of the two features near 10 and 20 μm is consistent with silicate emission, and this will be used as a working hypothesis for the present models. It will be shown that using measured grain emissivities from a likely silicate material and a realistic density distribution in the circumstellar envelope gives a good fit to the observed optically thin spectra.

Of the laboratory measurements available at present, the silicate materials which appear most similar to the observed 8–40 μm spectra are the carbonaceous chondrite meteorites Vigarano and Murchison measured by Penman (1976) (see Forrest, Houck, and Reed 1976). This is physically reasonable because this type of meteorite is believed to represent relatively unprocessed material from the primitive solar nebula. Other carbonaceous chondrite materials (Zaikowski and Knacke 1975) and an artificially produced amorphous silicate material (Day 1974) show a close similarity to the 10 μm feature, but the second peak occurs at longer wavelengths than the feature observed here and by Forrest, Houck, and Reed (1976). Penman measured the reflectance from polished samples and applied the Kramers-Kronig principle to derive the optical constants from 5 to 40 μm. The emissivities of small spherical grains were calculated using Mie theory. For the present comparison, the emissivities of equal parts of the Vigarno and Murchison material have been taken from Penman (1976); the resultant mass opacity, κ_λ, is shown at the top of Figure 3. The peak mass opacity of approximately 2800 cm^2 g^{-1} occurs at

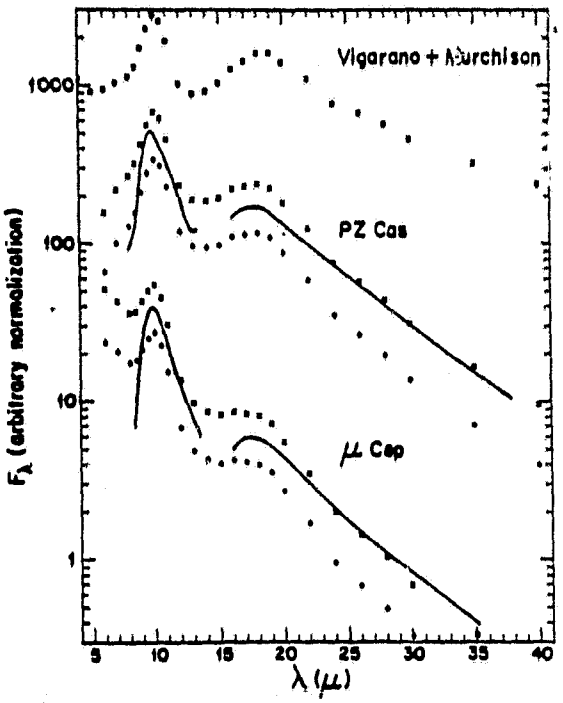

FIG. 3.—Model fits to the excess emission from PZ Cas and μ Cep (*solid lines*) as described in the text. The crosses are for a density distribution $\rho_d = \rho_0/R^2$ and the diamonds for a density $\rho_d = [1/R^2(1 - R_0/R)^{1/2}]$. The assumed inner temperatures are, from the top, 400 K, 340 K, 1250 K, and 860 K, as noted in Table 3. The squares are the opacity (κ_λ, cm^2 g^{-1}) of the meteorite mixture used in calculating the emergent spectra. The peak opacity of 2800 cm^2 g^{-1} occurs at 10 μm.

10 μm, and a second peak with approximately 1650 cm^2 g^{-1} opacity occurs near 18.5 μm.

The flux from a grain of mass m_i, mass opacity κ_λ, at a temperature T_i, and a distance D away from the Earth, will be

$$F_\lambda^i = \frac{m_i \kappa_\lambda}{D^2} B_\lambda(T_i) , \qquad (1)$$

where $B_\lambda(T)$ is the Planck blackbody function (W cm^{-2} μm^{-1} sr^{-1}). If the circumstellar shell is optically thin at infrared wavelengths, each grain will be seen independently, and the total flux observed will be

$$F_\lambda = \frac{\kappa_\lambda}{D^2} \sum m_i B_\lambda(T_i) . \qquad (2)$$

Thus the emergent spectrum is determined by the density of grains in the shell versus distance from the star $\rho_d(R)$ and the grain temperature as a function of distance from the star $T_d(R)$. The temperature of a grain will be determined by energy balance, $\dot{E}_{in} = \dot{E}_{out}$. In the present case $\dot{E}_{out}$ will be dominated by thermal radiation, so

$$\dot{E}_{out} = 4\pi m_i \int_0^\infty \kappa_\lambda B_\lambda(T_i) d\lambda . \qquad (3)$$

If the circumstellar shell is optically thin in the near-infrared (1–5 μm), $\dot{E}_{in}$ will be dominated by the stellar radiation field, which falls as $1/R^2$ more than a few stellar radii from the photosphere. Therefore $\dot{E}_{in} = \dot{E}_0(R_0/R)^2$, where $\dot{E}_0$ is the power input at a distance $R = R_0$ from the star.

These equations thus define the run of temperature versus distance from the star. In order to evaluate equation (3), it is necessary to know the grain opacity κ_λ at all wavelengths. From 5 to 40 μm, the opacities from Penman (1976) shown in Figure 3 were used. Shortward of 5 μm, it was assumed the optical constants were constant versus wavelength and the particles were small so

$$\kappa_{\lambda < 5\,\mu m} = \kappa_{5\,\mu m}\left(\frac{5\ \mu m}{\lambda}\right) .$$

Beyond 40 μm, it was assumed that the imaginary part of the dielectric constant ϵ_2 fell as $1/\lambda$ so that

$$\kappa_{\lambda > 40\,\mu m} = \kappa_{40\,\mu m}\left(\frac{40\ \mu m}{\lambda}\right)^2 .$$

At the temperatures of most interest in the circumstellar shells between 100 and 1000 K, more than half of the Planck emission falls between 5 and 40 μm, so it is believed these approximations are not critical to the results. Numerical integration of equation (3) showed that $\dot{E}_{out} \propto T^{4.4}$ from $T = 160$ to 1600 K and $\dot{E}_{out} \propto T^{6.1}$ below 160 K.

The density distribution in the circumstellar shell is less certain. The mass-loss rate from a star is given by

$$\dot{M} = 4\pi R^2 \rho(R) v(R) , \qquad (4)$$

where $\rho(R)$ is the total density and $v(R)$ is the outflow velocity. Since both the gas and the dust mass-loss rates have been observed to be fairly constant from stars of this type (see Forrest, Gillett, and Stein 1975; Weymann 1963) and the circumstellar absorption lines (Deutsch 1960; Weymann 1963) and OH emission lines (Wilson and Barrett 1972) indicate the outflow velocity is constant with time, it is expected that $\rho \propto 1/R^2$ in the outer parts of the envelope. Since dust grains are not expected to condense where the density is very low and the dust is momentum coupled to the gas (Gilman 1972), one also expects the dust density $\rho_d \propto 1/R^2$ in the outer parts of the envelope. Close to the point where dust grains begin to condense, neither the velocity nor the fractional amount of dust is well known. Fortunately, it will be shown that at the wavelengths of interest beyond 8 μm, the shape of the emergent spectrum does not depend strongly on the density distribution near the region of condensation. The point at which dust begins to condense will be denoted $R_0 \gtrsim r_*$, where r_* is the stellar radius. Theory (Jones and Merrill 1976) and observation (Zappala *et al.* 1974) indicate $R_0/r_* \gtrsim 3$ for the type of stars considered here. For the purposes of this calculation, it has been assumed that all the dust condensation occurs at R_0 (see Menietti and Fix 1978). Then if radiation pressure on the grains determines the flow

velocity, the dust velocity will be of the form

$$v_d(R) \approx v_d(R_0) + v_\infty \left(1 - \frac{R_0}{R}\right)^{1/2}, \qquad (5)$$

where $v_d(R_0)$ is the initial velocity and $v_d(R_0) + v_\infty$ is the final outflow velocity. Two cases have been considered: $v_d(R_0) \gg v_\infty$, which leads to a $\rho_d \propto 1/R^2$ shell structure, and $v_d(R_0) = 0$, for which

$$\rho_d \propto \frac{1}{R^2(1 - R_0/R)^{1/2}}$$

is infinite at R_0 but quickly approaches $1/R^2$ beyond $2\,R_0$.

In a preliminary run of the model with $\rho_d \propto 1/R^2$ and $T_0 = 500$ K, an interesting effect was discovered when the model was run out to outer limits of $10\,R_0$, $100\,R_0$, and $1000\,R_0$. Though 99% of the total flux comes from within $100\,R_0$, this region contributes only 90% of the flux at 40 μm and approximately half the flux at 80 μm. Even though the temperature is low ($\sim$35–76 K) in the outer layers of this shell, the mass is large, and this region dominates the emission at longer wavelengths. Farther from the star than approximately $1000\,R_0$, two effects are important in determining the emergent spectrum beyond 100 μm. First, heating by the interstellar radiation field will set a minimum temperature of the grains. With the grain emissivity used here, a grain radius of 0.1 μm, $Q_{abs} = 1$, and the interstellar radiation field given by Allen (1973), the minimum temperature is approximately 30 K in the galactic plane. Second, when a mass of interstellar matter equal to that in the circumstellar shell has been swept up, the structure of the shell will be significantly different than the $\rho \propto 1/R^2$ assumed here. For a space density of 1 H atom cm^{-3}, an outflow velocity of 10 km s^{-1}, and a mass-loss rate of $10^{-5}\,M_\odot$ yr^{-1}, this happens after approximately 3×10^5 years at a distance $R > 10^4\,R_0$ from the star. Since we are interested in the emergent spectrum from 5 to 40 μm, these effects will not be important and it is sufficient to integrate out to $1000\,R_0$.

With the density in the shell fixed, the only free parameter in the model is T_0, the dust temperature at the distance R_0 from the star where dust forms. This temperature has been varied in order to fit the observed ratio of $F_{10\,\mu m}/F_{18\,\mu m}$ for the shells around PZ Cas and μ Cep (Fig. 2). The temperatures are given in Table 3 and the resulting spectra are compared to the observed spectra in Figure 3. Also given in Table 3 is the temperature a thin isothermal shell would have in order to give the observed ratio $F_{10\,\mu m}/F_{18\,\mu m}$.

b) Discussion

From Figure 3 it is seen that the models give a good fit to the observed spectra. In particular, the shape and position of the 10 and 18 μm emission features are reproduced. This provides further support to the hypothesis (Woolf and Ney 1969) that silicate grains are responsible for much of the excess emission from oxygen-rich red-giant stars. It also indicates that the grains around these stars are probably made of a disordered, amorphous form of silicates similar to that found in the carbonaceous chondrite meteorites.

From Figure 3 it is seen that there is little difference between the emergent spectra for the two density distributions considered here. This shows that the emergent spectrum is not particularly sensitive to the density distribution near $R = R_0$, where it is least well known. Thus it is felt that the discrepancies between the model and observed fluxes shortward of 9 μm and longward of 20 μm are not due to density effects alone.

Short of 9 μm, the models predict more flux than is seen. This could be due to either lower emissivity of the circumstellar grains at these wavelengths or an overestimate of the stellar continuum which was subtracted to derive the excess emission. For both PZ Cas and μ Cep, the 8–10 μm spectrum had the approximate shape of the model spectrum *before* subtracting the stellar contribution. This indicates that the circumstellar silicates probably have a sharper feature than the silicates measured by Penman (1976). However, some of the observed 6–8 μm continuum could be due to the hot grains in the inner part of the shell. A measurement of the size of the emitting region at different wavelengths could clarify this point.

Longward of 20 μm, the models predict less flux than is observed. This indicates that the emissivity of the circumstellar grains falls less rapidly than the silicates measured by Penman (1976). The observed spectra would be fitted by an emissivity which fell as $1/\lambda^2$ from 20 to 40 μm rather than the $1/\lambda^{2.6}$ dependence of the Vigarano and Mirchison mixture used here.

The values found here for the dust emissivity and dust temperatures in the shell are consistent with the model of Elitzur (1978) for producing main line OH maser emission mentioned earlier. However, a detailed comparison for specific stars is necessary to see whether the shell optical depths are large enough to produce a sufficiently intense incident flux with a steep enough spectrum in the masing region.

TABLE 3

MODEL DUST TEMPERATURES

STAR	$F_{10\,\mu m}/F_{18\,\mu m}$ (observed)	T_0		
		Thin Shell	$\rho_d = \rho_0/R^2$	$\rho_d = [\rho_0/R^2(1 - R_0/R)^{1/2}]$
PZ Cas	2.95	270 K	400 K	340 K
μ Cep	6.9	470 K	1250 K	860 K

VI. CONCLUSIONS

The study of the 16–39 μm emission from oxygen-rich red-giant stars and IRC +10420 with excess emission at 10 μm has revealed:

1) The stars show excess emission in the 16–39 μm region in the form of a broad hump peaking near 18 μm and falling smoothly to longer wavelengths.

2) Except for possibly RX Boo, the emission from these stars is quite similar in character and qualitatively like the emission seen in the Trapezium region of the Orion Nebula (Forrest, Houck, and Reed 1976). This indicates the grain material are quite similar in these objects.

3) Lack of further structure in the 20 μm region prevents an unambiguous identification of the circumstellar material. The observed spectra are consistent with emission from small grains of silicate material similar to the carbonaceous chondrite meteorites in a diffuse circumstellar envelope. Comparison of the spectra with a simple model indicates that the grain emissivity falls as $1/\lambda^2$ from 20 to 40 μm and suggests that some of the observed 6–8 μm continuum could be due to emission from hot grains in the inner part of the circumstellar envelope.

4) The spectra of μ Cep do not show the 33 μm emission feature reported by Hagen *et al.*

We would like to thank the pilots and staff of the NASA Lear Jet and C-141 Kuiper Airborne Observatory and Gerry Stasavage for their assistance in this project. We thank Daniel A. Briotta, Ray W. Russell, and E. E. Salpeter for useful discussions and F. C. Gillett for suggesting the observation of PZ Cas and providing its 8–13 μm spectrum. This work was supported by NASA grants NGR 33-010-182 and NGR 33-010-081.

REFERENCES

Allen, C. W. 1973, *Astrophysical Quantities* (3d ed.; London: Athlone Press).
Becklin, E. E., Neugebauer, G., and Wynn-Williams, C. G. 1973, *Ap. Letters*, **15**, 87.
Day, K. L. 1974, *Ap. J. (Letters)*, **192**, L15.
Deutsch, A. J. 1960, *Stellar Atmospheres*, ed. J. L. Greenstein (Chicago: University of Chicago Press), p. 543.
Elitzur, M. 1978, *Astr. Ap.*, **62**, 305.
Forrest, W. J., *et al.* 1978, *Ap. J.*, **219**, 114.
Forrest, W. J., Gillett, F. C., and Stein, W. A. 1975, *Ap. J.*, **195**, 423.
Forrest, W. J., Houck, J. R., and Reed, R. A. 1976, *Ap. J. (Letters)*, **208**, L133.
Forrest, W. J., and Soifer, B. T. 1976, *Ap. J. (Letters)*, **208**, L129.
Gammon, R. H., Gaustad, J. E., and Treffers, R. R. 1972, *Ap. J.*, **175**, 687.
Geoffrion, A. R., Korner, M., and Sinton, W. M. 1960, *Lowell Obs. Bull.*, **5**, No. 1, 1.
Gillett, F. C. 1976, private communication.
Gillett, F. C., and Forrest, W. J. 1978, private communication.
Gillett, F. C., Low, F. J., and Stein, W. A. 1968, *Ap. J.*, **154**, 677.
Gilman, R. C. 1972, *Ap. J.*, **178**, 423.
Hagen, W., Simon, T., and Dyck, H. M. 1975, *Ap. J. (Letters)*, **201**, L81.
Humphreys, R. M. 1970, *A.J.*, **75**, 602.
Humphreys, R. M., Strecker, D. W., Murdock, T. L., and Low, F. J. 1973, *Ap. J. (Letters)*, **179**, L49.
Jones, T. W., and Merrill, K. M. 1976, *Ap. J.*, **209**, 509.
Knacke, R. F., and Thomson, R. K. 1973, *Pub. A.S.P.*, **85**, 341.
Kukarkin, B. V., *et al.* 1969, *General Catalog of Variable Stars* (Moscow: Academy of Sciences of USSR Press).
Low, F. J., Rieke, G. H., and Armstrong, K. R. 1973, *Ap. J. (Letters)*, **183**, L105.
Mattei, J. A. 1978, AAVSO Observations, private communication.
McCarthy, D. W., Low, F. J., and Howell, R. 1977, *Ap. J. (Letters)*, **214**, L85.
McCarthy, J. F., Forrest, W. J., and Houck, J. R. 1979, *Ap. J.*, in press.
Menietti, J. D., and Fix, J. D. 1978, *Ap. J.*, **224**, 961.
Morrison, D., and Simon, T. 1973, *Ap. J.*, **186**, 193.
Neugebauer, G., and Leighton, R. B. 1969, *Two Micron Sky Survey* (NASA).
Penman, J. M. 1976, *M.N.R.A.S.*, **175**, 149.
Price, S. D., and Walker, R. G. 1976, AFGL-TR-76-0208.
Russell, R. W., Soifer, B. T., and Forrest, W. J. 1975, *Ap. J. (Letters)*, **198**, L41.
Sutton, E. C., Storey, J. W., Betz, A. C., and Townes, C. H. 1977, *Ap. J. (Letters)*, **217**, L97.
Treffers, R. R., and Cohen, M. 1974, *Ap. J.*, **188**, 545.
Weymann, R. 1963, *Ann. Rev. Astr. Ap.*, **1**, 97.
Wilson, W. J., and Barrett, A. H. 1972, *Astr. Ap.*, **17**, 385.
Woolf, N. J., and Ney, E. P. 1969, *Ap. J. (Letters)*, **155**, L181.
Wright, E. L. 1976, *Ap. J.*, **210**, 250.
Zaikowski, A., and Knacke, R. F. 1975, *Ap. Space Sci.*, **37**, 3.
Zaikowski, A., Knacke, R. F., and Porco, C. C. 1975, *Ap. Space Sci.*, **35**, 97.
Zappala, R. R., Becklin, E. E., Matthews, K., and Neugebauer, G. 1974, *Ap. J.*, **192**, 109.

WILLIAM J. FORREST, JAMES R. HOUCK, and JOHN F. MCCARTHY: Center for Radiophysics and Space Research, Cornell University, Space Sciences Building, Ithaca, NY 14853

#55

THE ASTROPHYSICAL JOURNAL, 242:965–975, 1980 December 15

THE GALACTIC CENTER: 16–30 MICRON OBSERVATIONS AND THE 18 MICRON EXTINCTION

J. F. MCCARTHY, W. J. FORREST, D. A. BRIOTTA, JR., AND J. R. HOUCK
Center for Radiophysics and Space Research, Cornell University
Received 1980 April 24; accepted 1980 June 24

ABSTRACT

Low resolution 16–30 μm spectra of three regions in Sgr A West have been obtained, and the area has been scanned in two colors, 19 μm and 28 μm, with 30″ resolution. The 18 μm silicate feature is clearly seen in absorption as a broad depression present in all three spectra. Two-component models of the continuum have been constructed and fitted to the spectra. The most plausible models assume silicate grains for both components and derive a 19 μm optical depth for the absorbing dust of $\sim$2. Comparison with far-infrared data suggest that the absorbing component is in fact made up of two parts: one local to the galactic center, and the other distributed along the 10 kpc line of sight, with the local component constituting roughly one-third of the total. Extension of the models to $\lambda < 15$ μm shows that additional sources of emission are necessary to explain the observed flux at shorter wavelengths, and that the ratio of optical depths in the 9.7 and 18 μm silicate features may be as large as 2–3. The total dust mass column density in the line if sight is estimated to be $\sim 1.4 \times 10^{-3}$ g cm^{-2}. The local component is within $\sim$2 pc of the galactic center and has a mass of $\sim 20\ M_{\odot}$.

No 18.7 μm [S III] emission has been detected, which is consistent with normal S III/H II abundance and an 18.71 μm dust extinction optical depth of 2.1 or more, in agreement with the most plausible continuum models. Indirect arguments suggest that the S/H abundance is no more than a factor of 2 higher than in the solar neighborhood. Comparison with the Brackett-γ flux suggests that the S/H abundance is lower than this.

Subject headings: galaxies: Milky Way — galaxies: nuclei — infrared: spectra

I. INTRODUCTION

Within the galactic center, ionized gas, stars, and heated dust are in close proximity to each other. The ionized gas is observed in the thermal radio continuum source called Sgr A West, in many infrared and radio recombination lines of hydrogen and helium, and in infrared fine-structure lines such as [Ne II] 12.8 μm and [O III] 88 μm (Ekers *et al.* 1975; Neugebauer *et al.* 1978; Mezger and Smith 1976; Lacy *et al.* 1979; Dain *et al.* 1978). Sgr A West is also a strong infrared continuum source. In the near-infrared ($\lambda \lesssim 3 \mu$m), the flux is mainly due to the late-type stars clustered at the core, attenuated by the intervening interstellar dust (Becklin and Neugebauer 1968). From 3 μm to 1 mm, the strong infrared continuum is produced primarily by thermal radiation from clouds of dust grains. In the mid-infrared ($3\ \mu\text{m} \lesssim \lambda \lesssim 20\ \mu$m), ground-based high-resolution maps show several compact continuum sources (Becklin *et al.* 1978*a*; Rieke, Telesco, and Harper 1978). Some, for example IRS 7, are identified at late-type supergiant stars, but others, such as IRS 1, are not well understood. Some evidence exists that they are compact clumps of ionized gas with associated dust (Lacy *et al.* 1979). The 8–13 μm spectra of all the sources in Sgr A West are dominated by deep 9.7 μm absorption features which are attributed to attenuation by cold foreground silicate grains of the background continuum from warm dust (Woolf 1973; Willner 1976). At $\lambda \sim 50$ μm, available maps have lower spatial resolution, and only two sources are identified (Harvey, Campbell, and Hoffmann 1976; Rieke, Telesco, and Harper 1978). One, Sgr A West (NE), is coincident with the thermal radio source and the compact mid-infrared sources. The other, Sgr A West (SW), has a much colder spectrum. Although NE and SW are approximately the same brightness at 50 μm, at 10 μm SW is much dimmer, and to date only a single compact source has been detected in it (Lebofsky 1979).

In this paper we will address several questions of current interest. First, what is the amount and distribution of the dust, both within the galactic center and along the line of sight? What is the physical temperature of the grains? What can we conclude about the emissivity spectrum of the grains, and what does this

imply about the composition of the grains? As for the ionized gas, what is its ionization structure and what are the elemental abundances in it? What is the nature of the infrared continuum sources?

To attack these questions, we have obtained low-resolution 16–30 μm spectra of three positions in the Sgr A West region. In addition, we have mapped the area in two colors (19 and 28 μm) with a spatial resolution of 30″ (1.5 pc at 10 kpc); these results are presented in § II. In § III, upper limits to the 18.71 μm [S III] flux are given and interpreted in terms of the dust extinction and the ionization structure and elemental abundances of the ionized gas. Section IV discusses the continuum emission and proposes models to explain it. An 18 μm absorption feature is observed and identified as a resonance of silicate minerals present in dust grains. Section V examines the results of the continuum models, determines the consequences of extending the models to other wavelengths, and discusses the relative strengths of the 9.7 μm and 18 μm silicate features and the shape of the silicate spectrum for $\lambda > 16$ μm. In § VI, we present our conclusions.

II. OBSERVATIONS AND RESULTS

Observations of the galactic center were made during two flight series on NASA aircraft flying at altitudes of more than 12 km. In both series the instrument used was a 10-channel liquid helium cooled grating spectrometer described by McCarthy, Forrest, and Houck (1979). The first observations were performed in 1977 September on the Lear Jet, and the second set in 1978 May using the Kuiper Airborne Observatory (KAO). Relevant observational parameters are summarized in Table 1. Standard beam-switching and data-reduction techniques were used. In the calibration spectrum of Mars from the 1978 May series, a narrow water vapor feature was noted at 29.8 μm and was suppressed with a 15% correction to the calibration.

A continuum spectrum from 16 to 30 μm was obtained in the Lear Jet series. The 2.7 field of view ("big beam") was large enough to contain the entire Sgr A West source, which has a FWHM diameter of ~30″ in the 16–30 μm range. During the 1978 May KAO series, 16–30 μm spectra were obtained of both far-infrared sources, NE and SW, at a resolution of 30″. For the SW spectrum, the beam was nearer the position of Harvey, Campbell, and Hoffman (1976) than that of Rieke, Telesco, and Harper (1978), but at 24 μm this source was not clearly separated from the peak (NE). The reduced spectra are shown in Figure 1. In both of the KAO spectra there are systematic errors at $\lambda > 20$ μm. The first, type, so-called scalloping, appears as a wavelike variation with a period of 2 μm and a peak-to-peak amplitude of 10–15% of the flux. This appears to be due to phase differences between channels, aggravated by the high chopper frequency (35 Hz). Also, two peaks at 26.5 and 28.2 μm show the effect of incompletely canceled water vapor features. None of these features appear to be real properties of the source spectra.

TABLE 1

OBSERVATIONAL PARAMETERS

PARAMETER	FLIGHT SERIES 1977 Sept	1978 May
Aircraft	Lear	C-141 (KAO)
Telescope	30 cm	91 cm
Beam diameter (FWHM)	2.7	30″
Chopper throw	8′	90″
Spectral resolution (FWHM)	0.5 μm	0.2 μm
Standard spectrum	Moon	Mars
Flux standard	Mars	Mars, α Her, IRC+10420

Several comments may be made here: First, all the spectra have a broad depression centered at ~19 μm. We attribute this feature to absorption of radiation by a foreground cloud of cold silicate grains of the background radiation from hot dust. Below we report on more specific models of this continuum. Second, a comparison of the Sgr A West (NE) and Sgr A West (2.7) big beam spectra shows that the central 30″ contains from one-half to one-fourth of the total flux from the entire galactic center region, indicating that the source is not much larger than the 30″ beam. Furthermore, since the color temperature of the big-beam spectrum is lower than that of the NE source, the outer regions of the source must be colder than the center, and the source diameter must increase with wavelength. Both of these effects are confirmed by our data. Ground-based 21 μm maps (Becklin *et al.* 1978*a*) show that the galactic center contains a number of compact sources in addition to an extended component, but they contribute only about 20% of the flux in a 30″ beam. Therefore, these compact sources are not vital to our understanding of the present spectra. Third, the SW source and the big beam spectra have virtually the same shape, suggesting that the Lear Jet spectrum might be modeled as a source similar to the SW one but filling roughly one-tenth of the big beam's solid angle. Fourth, none of the spectra show evidence of [S III] 18.71 μm emission from the ionized gas, although this is a common characteristic of other galactic H II regions (McCarthy, Forrest, and Houck 1979; McCarthy 1980).

In 1978 May we also observed 14 positions at two different wavelengths (18.9 and 27.8 μm) and constructed a map of the Sgr A West region. The points are arranged in a rough cross with the long arm approximately parallel to the galactic equator and with the NE source located at the intersection of the arms. Individual points are separated by ~12″, which is

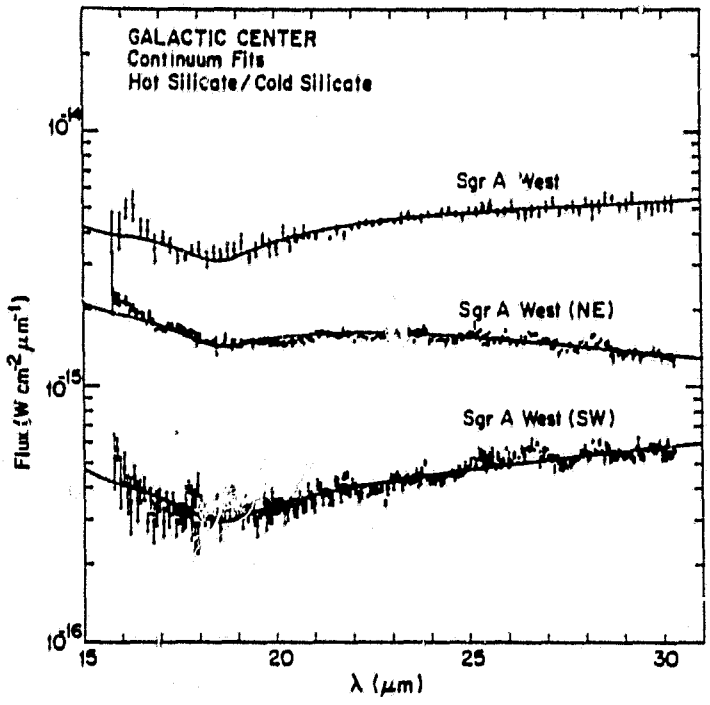

FIG. 1.—Reduced spectra of the galactic center. The top spectrum was taken with a 2.7′ beam and includes the entire source. The middle spectrum was centered on the peak 24μm source in a 30″ beam, which approximately coincides with the NE source. The bottom spectrum, also with a 30″ beam, is of a point near the SW source. The curves are model fits to the data. The model consists of optically thin dust obscured by a cold dust cloud with optical depth of order unity. Both clouds are assumed to consist of silicate dust grains.

slightly less than a beam radius. The chopper throw was sufficiently large that the flux in the reference beams was negligibly small. In the course of the mapping we measured the NE source three times (positions 1, 4, and 14), and these results can be used to gauge the effects of guiding jitter. At the position of the NE source the graphs show an average of these three measurements.

Beam positioning on the KAO was done with a ρ-θ offset stage, and by peaking up on the 24 μm continuum source. The offset guide star was an anonymous star which is located 135″ from the NE source (1950 position $17^h42^m20^s.3$, −28°58′41″ from Palomar plates). Inaccuracies in the computed field rotation angle dominate the relative positional uncertainties which are estimated at ∼3″. The uncertainty in the absolute positions depends on the position of the guide star (known to ∼±10″) and the absolute error in the rotation angle. Computing the rotation angle has been a constant source of trouble in the past, and it is difficult to estimate its uncertainty. Since the peak flux of the 19 μm map agrees well with ground-based measurements, we have corrected the derived position of the NE source to agree with IRS 1. This correction was then made to all the other map positions and to the positions of the full spectra. It corresponds to an error in the calculated field rotation angle of 5°, or ∼12″ on the sky. It should be noted that the beam position of the SW spectrum does not agree well with the positions of Harvey, Campbell, and Hoffman (1976) or Rieke, Telesco, and Harper (1978). At best we were pointed at the edge of the source and included about half of its solid angle. However, we did include most of the weak and extended 10 μm emission associated with this source.

The maps are shown in Figure 2 and the raw data are listed in Table 2. The fluxes have an effective bandwidth of 2 μm since they were derived from an analog average of all 10 detector signals. Again, the quoted flux uncertainties are one standard deviation of the mean as derived from the scatter of several integrations.

In Table 2B and Figure 2, two quantities are derived from the raw fluxes and graphed. The first is the color temperature, and the second is the ratio of the observed flux to the flux expected from a blackbody which has the observed color temperature and which fills the beam. This second parameter is a very crude measure of the source's apparent optical depth. One must be careful about simplistic interpretations of these quantities, however. Since there is an obvious spectral feature, the spectrum is not that of a blackbody, and the color temperature does not correspond to the temperature of dust in the source. Furthermore, it is often the case in H II regions that a distribution of temperatures is necessary to explain the spectrum adequately.

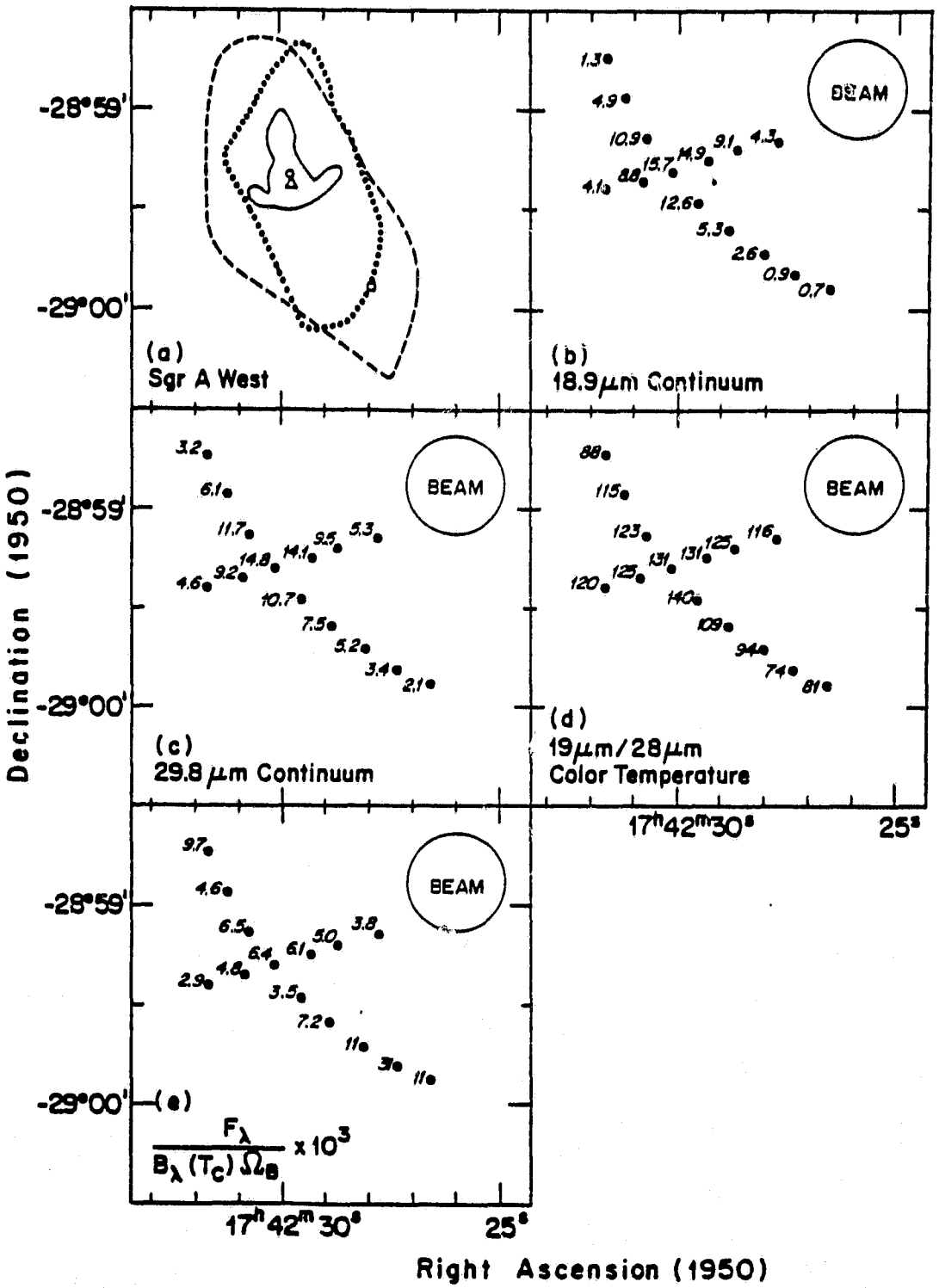

FIG. 2.—(*a*) Features in Sgr A West. *Circle*, IRS1 20 μm peak (Becklin *et al.* 1978*a*). *Solid line*, Outermost contour of 20 μm map of Becklin *et al.* (1978a). *Triangle*, *square*, and *dashed line*, 53 μm peaks of NE and SW sources, and 53 μm half max contour (Harvey *et al.* 1976). *Dotted line*, Half max 5 GHz contour of WORST map (Ekers *et al.* 1975). (*b*) The 18.9 μm continuum of Sgr A West. The units are 10^{-16} W cm^{-2} μm^{-1}, and in these units a typical error is ±0.3. Beam size = 30″, effective bandpass = 2.0 μm. (*c*) The 29.8 μm continuum. Units are 10^{-16} W cm^{-2} μm^{-1}, and a typical uncertainty is ±0.2. (*d*) The 19 μm/28 μm color temperature map of Sgr A West derived from Figs. 2*b* and 2*c*. Units are kelvins, and typical errors are ±3 K. (*e*) A map of the ratio of the observed flux to the flux from a blackbody of the derived color temperature which fills the beam. This quantity is a crude measure of the apparent optical depth and is dimensionless. The plotted numbers are to be multiplied by 10^{-3}, and a typical error is ±5%.

TABLE 2

SAGITTARIUS A WEST MAP

A. OBSERVED QUANTITIES

POSITION No.	POSITION		CONTINUUM FLUX (10^{-16} W cm^{-2} μm^{-1})		NOTES
	R.A. (1950)	Decl. (1950)	at 18.9 μm	at 27.8 μm	
1	17^{h}42^{m}30^s.1	−28°59′20″	16.1±0.2	14.9±0.2	a
2	31.3	58 56	4.9±0.1	6.1±0.2	
3	30.8	59 08	10.9±0.6	11.7±0.2	
4	30.2	59 18	15.8±0.2	14.9±0.2	a
5	29.6	59 28	12.6±0.1	10.7±0.4	
6	28.9	59 36	5.3±0.8	7.5±0.1	
7	28.1	59 43	2.6±0.2	5.2±0.1	
8	27.4	59 49	0.9±0.1	3.4±0.1	b
9	26.6	59 53	0.7±0.1	2.1±0.1	
10	31.7	58 44	1.3±0.2	3.2±0.4	
11	30.2	59 18	...	...	a,d
12	28.7	59 12	9.1±0.3	9.5±0.1	
13	29.4	59 15	14.9±0.3	14.1±0.2	
14	30.2	59 18	15.3±0.3	14.7±0.1	a
15	30.9	59 21	8.8±0.2	9.2±0.2	
16	31.7	59 24	4.1±0.1	4.6±0.3	
17	27.8	59 09	4.3±0.2	5.3±0.2	
NE avg....	30.4	59 20	15.7±0.4	14.8±0.1	a,c
(NE).....	30.2	59 16	14.5±1.0	14.5±1.0	a,e
(SW).....	28.3	59 39	3.3±0.5	5.6±0.5	b,e
2:7.....	...	...	34±2	51±4	e

B. DERIVED QUANTITIES

POSITION No.	19 μm/28 μm COLOR TEMPERATURE (K)	$\frac{F_\lambda}{B_\lambda(T_c)\Omega_B} \times 10^{3f}$	NOTES
1	133±1	6.0±0.1	a
2	115±2	4.6±0.1	
3	123±3	6.5±0.3	
4	131±2	6.4±0.1	a
5	140±3	3.5±0.2	
6	109±8	7.2±0.8	
7	94±3	11±0.4	
8	74±3	31±0.9	b
9	81±5	11±0.6	
10	88±6	9.7±0.8	
11	...	...	a,d
12	125±2	5.0±0.2	
13	131±2	6.1±0.2	
14	130±2	6.5±0.1	a
15	125±2	4.8±0.1	
16	120±4	2.9±0.2	
17	116±3	3.8±0.2	
NE avg....	131±2	6.4±0.2	a,c
(NE).....	127	7.1	a,e
(SW).....	99	8.9	b,e
2:7.....	106	1.5	e

Notes to Table 2:

[a] Sgr A West (NE).

[b] Near Sgr A West (SW).

[c] Average of #1, #4, and #14.

[d] No measurements made.

[e] Complete spectra.

[f] F_λ is the observed flux, $B_\lambda(T_c)$ is the Planck function for the derived color temperature T_c, and Ω_B is the solid angle of the beam.

The scans through the source show that, as suggested by the full spectra, the color temperature drops as the beam is moved off the NE source, but the ratio of the flux to the equivalent blackbody flux is nearly constant except for an increase near the SW source. This illustrates that the SW source has a cold spectrum.

Our spatial resolution is barely good enough to resolve Sgr A. On the NE-SW arc the apparent FWHM at 19 μm is $\sim$40″ while it is 48″ at 28 μm. Similarly, on the E-W line the source shows a FWHM of roughly 36″ at 19 μm and 40″ at 28 μm. Along both axes the source is wider at 28 μm than at 19 μm, and it is slightly elongated along the galactic plane, in agreement with other maps. It is also apparent that the position of peak flux lies between positions 1 and 13, slightly to the west of the NE spectrum position.

III. [S III] UPPER LIMITS

No unresolved emission lines are seen in any of the three spectra. This is surprising, because at this resolution the 18.71 μm [S III] line is commonly observed in galactic H II regions (McCarthy, Forrest, and Houck 1979; McCarthy 1980). In Table 3 we present 3 σ upper limits to the line flux. Using a simple method described by McCarthy, Forrest, and Houck (1979), we have calculated the expected line fluxes. This model uses the observed thermal radio continuum flux as a measure of the mass of ionized gas and assumes that the S III/H II abundance ratio observed in Orion (Peimbert and Torres-Peimbert 1977) may be applied to Sgr A West. Furthermore, emissivities are calculated in the low density limit ($n_e < 6000$ cm^{-3}), and 18.71 μm extinction is neglected. As shown in Table 3, the predicted line fluxes are 3 to 8 times higher than observed.

There is evidence for clumps of $n_e \sim 10^4$ cm^{-3} embedded in the lower density ($n_e \sim 10^3$ cm^{-3}) ionized gas (Lacy *et al.* 1979; Ekers *et al.* 1975; Rodriguez and Chaisson 1978). However, these clumps contribute only about one-fourth of the total radio flux, and they cannot explain the low observed [S III] fluxes.

The 18.71 μm extinction to the ionized gas is likely to be considerable. Continuum models, presented below, give τ(19 μm) up to 2.4, which is high enough to bring the predicted fluxes into agreement with the observed upper limits. Therefore, our data are consistent with normal S III/H II abundance and large dust extinction [τ(18.71 μm) $\geq$ 2.1].

Compared to other galactic H II regions, the ionization structure of Sgr A West is peculiar, and the abundances of heavy elements may be higher than near the Sun. Within large uncertainties, the He II/H II ratio is normal (0.095 $\pm$ 0.040), but the line profiles suggest that He/H might be abnormally high (Mezger and Smith 1976). From observations of [Ar III] 8.99 μm, [Ar II] 6.98 μm, [O III] 88 μm, and [Ne II] 12.8 μm, there is clear evidence for an unusually cool radiation field (Lacy *et al.* 1979; Willner *et al.* 1979; Dain *et al.* 1978). Furthermore, the [Ar II] and [Ne II] fluxes suggest overabundances of these elements. Under these conditions of partial helium ionization and low Ar III/Ar II ratio, theoretical models suggest that S III/S $\geq$ 0.5 (Balick and Sneden 1976; Pipher, private communication). Since normal H II regions have S III/S near unity (McCarthy 1980), the S/H abundance ratio can be no more than a factor of 2 above the value in the Sun's neighborhood, as long as these theoretical H II region models are correct.

The above estimate of S III abundance in the galactic center depends on an estimate of the amount of ionized gas within our 30″ beam based on the radio map of Ekers *et al.* (1975). The data of Neugebauer *et al.* (1978) on the emission of Brackett-γ (Bγ) from the ionized gas indicate that the gas may be more centrally condensed than indicated by the radio map. Using the Bγ results of Neugebauer *et al.* (1978) in a 32″ beam to estimate the amount of ionized gas in our beam results in an estimate n (S III)/n (H) $\leq 1.5 \times 10^{-5}$ exp[τ(18.7 μm) $-$ τ(2.16 μm)] for an electron temperature $T_e \geq 5000$ K. As discussed by Neugebauer *et al.* (1978), the extinction to the ionized gas in the galactic center is around $\tau_{2.16\ \mu m} \approx 2.5$. There may be additional local extinction. Then, if we estimate $\tau_{18.7\ \mu m} \approx \frac{1}{2}\ \tau_{9.7\ \mu m} \approx \frac{1}{2}\ \tau_{2.16\ \mu m} \approx 1.25$, the abundance is n (S III)/n (H) $\leq 0.4 \times 10^{-5}$. This is less than one-quarter the "cosmic" abundance of sulfur (Allen 1973), and indicates either a low sulfur abundance or a dominance of

TABLE 3

[S III] UPPER LIMITS

SPECTRUM	CONTINUUM (10^{-15} W cm^{-2} μm^{-1})	S_ν(5GHz) (Jy)	LINE FLUX (10^{-16} W cm^{-2}) Observed	Predicted	Observed / Predicted
Sgr A West.....	3.40 $\pm$ 0.04	26	< 1.9	5.8	< 0.33
Sgr A West (NE)...	1.475 $\pm$ 0.006	6	< 0.16	1.33	< 0.12
Sgr A West (SW)...	0.307 $\pm$ 0.004	4	< 0.22	0.89	< 0.25

NOTE.—5 GHz radio continuum fluxes are based on the WORST map of Ekers *et al.* (1975). Observed line fluxes are 3σ upper limits.

the S II ion. This is surprising in view of the high abundance of Ar II and Ne II which have similar ionization potentials. A low sulfur abundance seems to be indicated. Because the extinction at 4.05 μm is closer to that at 18.7 μm, a better estimate of the S III abundance could be made if Bα measurements were made in a 30″ beam.

IV. CONTINUUM EMISSION AND MODELS

The most striking feature of the continuum spectra is the 18 μm depression, which we attribute to absorption by cold silicate grains along the line of sight. The 18 μm silicate feature is commonly observed in oxygen-rich stars (Forrest, McCarthy, and Houck 1979) and in H II region/molecular cloud complexes. It is due to O–Si–O bending motions in the grains. In both types of sources, the feature is seen over a range of optical depths running from $\tau \ll 1$ in emission to $\tau \geq 1$ in absorption. From models of the circumstellar shell emission of oxygen-rich stars an empirical emissivity function for interstellar silicate grains has been found (Forrest, McCarthy, and Houck 1979). This function is plotted in Figure 3 and discussed in more detail below.

To explain the 18 μm feature as absorption, we need to assume at least two components to the dust: one to do the emitting and the other the absorbing. The emission is from a hot, optically thin cloud of dust grains at the galactic center. The absorption is by cold silicate grains with 18 μm optical depth of order unity between us and the galactic center. These grains may be interstellar or they may be local to the galactic center or, most likely, a little of each. Using simple radiative transfer theory, the flux received at the earth is:

$$F = B(T_1)\,[1-\exp(-\tau_1)]\,\exp(-\tau_2)\,\Omega + B(T_2)\,[1-\exp(-\tau_2)]\,\Omega.$$

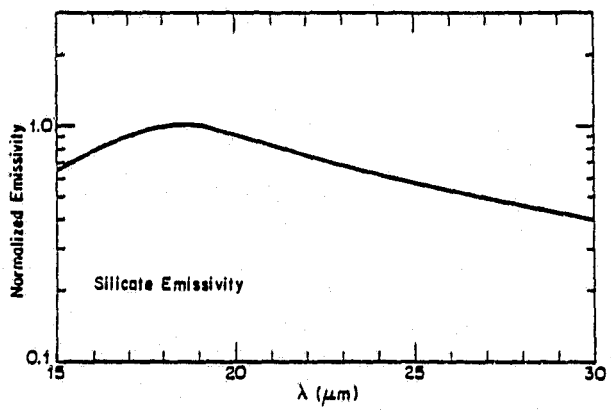

FIG. 3.—Normalized emissivity assumed for the interstellar silicate grains. This emissivity fits the spectra of circumstellar shells. Beyond 19 μm, it follows a λ^{-2} law.

Here T_1 and T_2 are the temperatures of the hot and cold grains, respectively; τ_1 and τ_2 are the wavelength-dependent optical depths; Ω is the solid angle of the beam; and $B(T)$ is the Planck blackbody function. Our model explicitly includes the emission from the cold, absorbing component since far-infrared observations show that the cold dust can be responsible for a significant fraction of the emission at 30 μm. Note that this model also assumes that both components fill the beam, an assumption which should be more reliable for the KAO spectra.

This is the simplest model which can produce the observed absorption feature, and it is easy to criticize it. Due to the observed nonuniform distribution of late-type stars and ionized gas, it seems clear that there will be a continuous distribution of dust temperatures. The split into two components is then only an approximation which will work to the extent that two temperatures dominate over all the others. We shall see, however, that the model does remarkably well in explaining the 16–30 μm data, and with only minor modification it can be extended to longer wavelengths.

The emission of the hot dust is not known, but we can make reasonable guesses which will span the possibilities. Three alternatives have been considered. In the first, the grain emissivity was taken to be constant, producing a blackbody spectrum for the hot dust cloud. This is rather implausible on physical grounds, since either the grains would have to be large (radius > 5 μm) compared to typical interstellar dust or the cloud itself would need to be dense enough to be optically thick. The second alternative used the previously mentioned empirical silicate emissivity function for the hot dust, resulting in an emission spectrum similar to that of the Trapezium. For $\lambda > 19$ μm the emissivity falls as λ^{-2}, and for $\lambda < 19$ μm it follows the emissivity of the carbonaceous chondrite meteorites Vigarno and Murchison as measured by Penman (1976). This curve was found to be a good fit to the silicate emission spectra of circumstellar shells (Forrest, McCarthy, and Houck 1979). Since the temperature of the circumstellar dust is not known independently, the shell spectra do not uniquely determine $\tau(9.7\ \mu\text{m})/\tau(19\ \mu\text{m})$. The present models are less sensitive to temperature effects and may allow us to determine $\tau(9.7\ \mu\text{m})/\tau(19\ \mu\text{m})$. For a final alternative, we considered a grain emissivity which was proportional to λ^{-1}. This produces a smooth spectrum qualitatively similar to a blackbody spectrum of higher temperature. One would expect such an emissivity from small grains (radius $\ll 5$ μm) with a constant complex index of refraction. Such a grain emissivity is often mentioned in the literature, but it is not yet well justified observationally. On observational grounds, the silicate emissivity must be considered the most likely, but the others should not be ignored.

The two-component model has four free parameters, T_1, τ_1, T_2, τ_2, and the best fit values were found by

TABLE 4

CONTINUUM FITS

SPECTRUM	χ^{2a}	HOT DUST Type[b]	HOT DUST $T(K)$	HOT DUST $\tau(19\,\mu m)$	COLD DUST Type[b]	COLD DUST $T(K)$	COLD DUST $\tau(19\mu m)$
Sgr A W (NE) ...	0.68	Si	184	9.0×10^{-3}	Si	50.4	2.1
Sgr A W (SW) ...	1.59	Si	184	2.5×10^{-3}	Si	49.9	2.4
Sgr A (2:7)	0.78	Si	154	1.6×10^{-3}	Si	41.8	2.4
Sgr A W (NE) ...	0.68	$1/\lambda$	149	6.8×10^{-3}	Si	53.8	0.84
Sgr A W (SW) ...	1.59	$1/\lambda$	139	1.7×10^{-3}	Si	54.9	0.78
Sgr A (2:7)	0.78	$1/\lambda$	125	1.5×10^{-3}	Si	42.8	1.09
Sgr A W (NE) ...	0.59	BB	187	2.6×10^{-3}	Si	49.3	0.9
Sgr A W (SW) ...	1.48	BB	189	6.0×10^{-4}	Si	52.4	1.1
Sgr A (2:7)	0.76	BB	150	5.8×10^{-4}	Si	39.9	1.2

[a] All χ^2 computed assuming $\sigma(\lambda_i)=\max[\sigma_m(\lambda_i)$ from observations, $0.05F_\lambda]$.
[b] Si = silicate emissivity, $1/\lambda = 1/\lambda$ emissivity, BB = blackbody (ϵ = constant).

minimizing χ^2, which is defined in the usual way. To allow for the instrumental effects, guiding noise, and other systematic errors, the uncertainties in the individual points were constrained to be greater than or equal to a predetermined minimum error of 5% of the flux at that point. The fitting algorithm was a grid search procedure adapted from Bevington (1969), which continued until χ^2 changed by less than 1% between iterations. It was found that the absorption feature in the SW spectrum was marginally significant statistically even though it is clear enough to the eye.

The results of the fits are summarized in Table 4. The hot silicate/cold silicate fit is graphed in Figure 1; the other two types of fit produce curves which are nearly indistinguishable from that shown. It can be seen that the models give good fits to the spectra of the galactic center. This supports the plausibility of the two component model.

V. DISCUSSION OF CONTINUUM MODELS

All of the fits fail to produce as rapid a turnup at 16 μm as observed. This can be ascribed to two causes: First, as mentioned above, a more realistic model would include a gradient of temperatures. Addition of a third component of higher temperature would tend to increase the 16 μm flux preferentially; but since the turnup is so sharp, it is unlikely that this is the main effect. The other possibility is that the true silicate emissivity is in fact more sharply peaked than assumed. In order to explain the discrepancy, the value of the emissivity at 16 μm would have to be reduced by a factor of $\sim$0.8.

Table 4 shows that the statistical significance of the fits is similar for all models, with the blackbody fits having slightly smaller χ^2. In general, this means that we cannot say anything definite about the intrinsic spectrum of the hot dust or about its composition. A comparison of the NE and SW results shows that for a given type of fit the values of T_1, T_2, and τ_2 are nearly identical. Although the observed spectra are quite different in both shape and normalization, this difference appears to be due to the amount of hot dust in the source (i.e., τ_1), with the NE source containing 3 to 4 times more hot dust than SW. Together with the similarity of τ_2, this suggests that the cold spectrum of SW might be better understood as due to the lack of a central heat source rather than an increase in mid-infrared dust extinction in front of an otherwise normal H II region, as suggested by Rieke, Telesco, and Harper (1978). The equilibrium temperature of dust grains at a projected distance of 30″ from the NE source is estimated to be 30–60 K if the grain heating is due to radiation from the NE source. The SW source may be a local concentration of the "cold" dust near the galactic center.

Note that the silicate models require about twice as much cold dust optical depth as the others. In the silicate models the hot dust cloud's spectrum has a silicate emission feature, and more absorbing dust is required to hide it. Similarly, the silicate models require the highest optical depths of hot dust, while the λ^{-1} fits the need somewhat less, and the blackbody fits need least of all, only about one-third of the silicate values. Finally, for all emissivity types, the cold dust is at temperatures near 50 K for the NE and SW sources and near 40 K for the 2:7 beam.

It is interesting to extend this model to other wavelengths to see if we can make it fail. To do so, we need a set of observations at comparable spatial resolution and covering a broad wavelength range. Luckily, the galactic center is a popular object, and Sgr A West (NE) has been examined at 30″ resolution from 3.5 μm to 175 μm (Harvey, Campbell, and Hoffman 1976; Sutton, Becklin, and Neugebauer 1974; Willner *et al.* 1979). These data are plotted in Figure 4. Unfor-

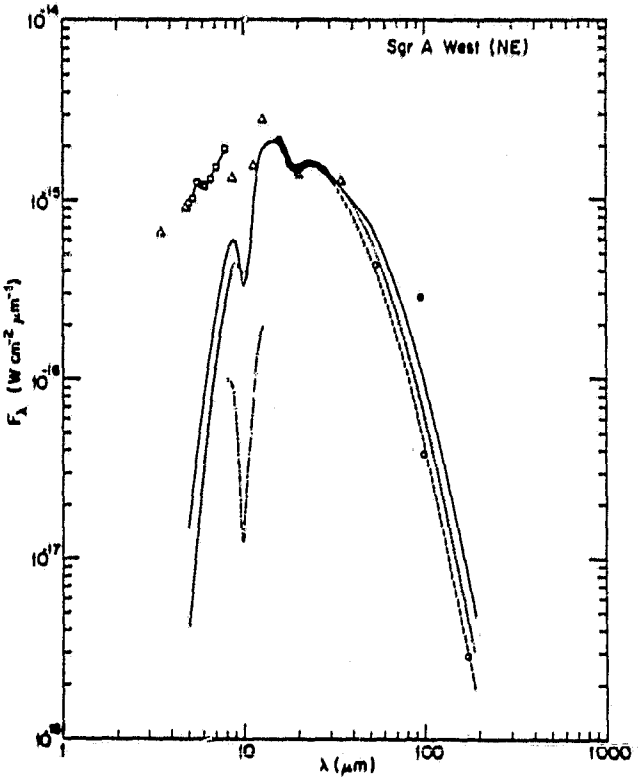

FIG. 4.—Observations of Sgr A West (NE) with a 30″ beam, and models of the dust emission spectrum. *Hatched area*, this paper. *Circles*, Harvey *et al.* (1976). *Squares*, Willner *et al.* (1979). *Triangles*, Sutton *et al.* (1974). *Dot-dash line*, 8–13 μm spectrum of Woolf (1973), multiplied by 0.1 for clarity. This spectrum was obtained with a 22″ beam and is shown here to demonstrate the depth of the 9.7 μm silicate feature. *Light solid line*, best fit two component model with both components consisting of silicate grains. *Dotted line*, best fit two component model with hot dust having $1/\lambda$ emissivity. *Dashed line*, three component model. See text for description.

tunately, due to experimental difficulties the 8–13 μm spectrum has not been measured with a 30″ beam. The closest existing measurement is by Woolf and Gillett (Woolf 1973) with a 22″ beam. It is plotted in Figure 4 multiplied by 0.1 for clarity. The spectrum of Aitken, Jones, and Penman (1974) with a 13″ beam and 15″ N–S throw is similar in shape. However, Willner (1976) measured a number of compact sources at 10 μm with a 5″ beam, including one spot (labeled "IRS 10") which was in fact mainly the 10 μm extended source. This spectrum shows a much shallower 9.7 μm silicate feature than the Woolf data. The lack of 30″ data in the 10 μm window is particularly unfortunate because with it a direct comparison of the 9.7 and 18 μm silicate emissivities would be possible.

The models are compared with the existing data in Figure 4. Here we have assumed the silicate emissivity used by Forrest, McCarthy, and Houck (1979) for $\lambda < 16$ μm. Only two of the two-component fits are shown; the hot blackbody fit is similar to those plotted. All the models fit well in the 16–30 μm region, as they should, and all have similar failings as they are extended outside this range.

Two serious problems with the model are the lack of emission at shorter wavelengths and the lack of contrast in the 9.7 μm silicate absorption feature. The former indicates that there are additional sources of emission at shorter wavelengths. The latter may indicate that the 9.7 μm opacity is larger relative to the 19 μm opacity than has been assumed here. From the shape of the spectrum a temperature of about 400 K for the emitting material is indicated. A ratio of $\tau_{9.7\ \mu m}/\tau_{19\ \mu m}$ of about 2.5 rather than the 1.7 assumed is required to duplicate the depth of the 9.7 μm absorption seen by Woolf. Such a ratio is consistent with values estimated from [S III] observations in obscured H II regions (McCarthy 1980). However, the complicated nature of the Sgr A source prevents a definite conclusion from being reached at this time. The data of Rieke, Telesco, and Harper (1978) and Becklin *et al.* (1978*a*) indicate the compact sources contribute an increasingly large fraction of the flux from Sgr A at wavelengths shorter than 20 μm. Therefore, to model Sgr A realistically at shorter wavelengths requires a knowledge of the intrinsic spectra of these sources.

In the far-infrared, all the two component models lie above the observations by factors of 1.2 to 3, but a simple and plausible explanation can be found. Harvey, Campbell, and Hoffmann (1976) fit their data with 60 K grains having a λ^{-2} emissivity and a 53 μm optical depth of 0.082. By using the λ^{-2} law, $\tau(19\ \mu m) = 0.58$, or roughly one-third of the optical depth needed to explain the 18 μm feature in the silicate model [note, however, that $\tau(53\ \mu m)$ is in better agreement with the blackbody and $1/\lambda$ fits]. This suggests that one should try three component models in which the new component acts only as an absorber. In order not to be observed in the far infrared, the dust must be either very cold ($T \sim 10$ K) or extended (so chopping techniques would not detect it) or both. These properties are exactly what one would expect of interstellar grains lying far from hot stars, so we identify the third component with the interstellar extinction in the galactic plane between the Sun and the galactic center. The second component is now interpreted as a local concentration of cool dust ($T \sim 60$ K) in the galactic center itself, and the ratio of column densities of local to line-of-sight dust is estimated at $\sim$1:2, provided the hot dust grains are silicates. In Figure 4, a crude fit of this model is plotted, assuming $T_2 = 59$ K, $\tau_2 = 0.6$, and $\tau_3 = 1.5$. The parameters of the hot dust are the same as those of the two-component silicate model.

On the basis of infrared polarimetry, Knacke and Capps (1977) arrived at a similar qualitative picture for the dust distribution. Observing that the 11.5 μm

polarization vector is roughly perpendicular to that at 2.2 μm, they hypothesized that two dust components were involved. One is local to the galactic center and is responsible for the 11.5 μm polarization. It is probably identical with our cool ($T \sim 60$ K) local dust. On the other hand, Knacke and Capps suggested that the 2.2 μm polarization is caused by another component distributed along the line of sight. We identify this dust with our third, purely absorbing, component.

The three component model is also supported by the similarity of the values of τ_2 for all three spectra. This fact suggests a screen rather than a shell of absorbing material. Furthermore, the [S III] upper limits favor the models with hot silicate dust because of their higher dust optical depths. Finally, the far-infrared maps show a concentration of cold dust near the galactic center, and the existence of interstellar dust in the line of sight is well established.

Since we have now derived estimates of $\tau(19\ \mu\text{m})$, we are in a position to discuss the optical properties of the dust. The visual extinction to the late-type stars in the core has been estimated as $\sim$30 mag from the near-infrared colors (Becklin and Neugebauer 1968; Becklin *et al.* 1978*b*). From the observed Bγ flux at 2.17 μm, the extinction to the ionized gas is consistent with $A_V = 30$ mag within large uncertainties (Neugebauer *et al.* 1978). However, several lines of evidence suggest that A_V is not constant over the region (Lebofsky 1979; Rieke, Telesco, and Harper 1978), and we will consider $A_V = 30$ mag as a lower limit. From our models, we can set an upper limit of $\tau(19\ \mu\text{m}) \leq 2.1$ for the central 30″. Together, these give a lower bound of $A_V/\tau(19\ \mu\text{m}) \geq 14$. Immediately this shows that the 18 μm feature is no stronger than the 9.7 μm one, since $A_V/\tau(9.7\ \mu\text{m}) = 14$ toward VI Cyg No. 12 (Gillett *et al.* 1975). One might be tempted to derive a firmer number by assigning $A_V = 30$ mag and $\tau(19\ \mu\text{m}) = 1.5$ to the interstellar extinction, yielding $A_V/\tau(19\ \mu\text{m}) = 20$. This is risky, however, since the stars and gas appear to be embedded in the far infrared source.

At this point, we can make an order of magnitude estimate of the dust mass column density in the line of sight. This quantity, which we will call μ, is related to τ by $\mu = \tau/\kappa_\lambda$, where κ_λ is the optical cross section per unit mass, as long as κ_λ is constant along the line of sight. The value of κ_λ is not well known, but at 9.7 μm it is thought to be $\sim 3 \times 10^3$ cm^2 g^{-1} (Forrest, McCarthy, and Houck 1979). Since $\kappa_\lambda(9.7\ \mu\text{m})/\kappa_\lambda(19\ \mu\text{m}) \sim 2$, $\kappa_\lambda(19\ \mu\text{m}) \sim 1.5 \times 10^3$ cm^2 g^{-1}. Therefore, the total mass column density of dust toward the galactic center is $\sim 1.4 \times 10^{-3}$ g cm^{-2}, as long as both the hot and cold components are made of silicate grains. If the three component model is correct, then the mass column density in the interstellar medium (ISM) is $\mu(\text{ISM}) \sim 1.0 \times 10^{-3}$ g cm^{-2}, and the local component has $\mu(\text{local}) = 0.4 \times 10^{-3}$ g cm^{-2}. At 10 kpc, our 30″ beam covers an area of 1.6×10^{37} cm^2, so the dust mass contained in this portion of Sgr A West is of order 3 $M_\odot$. As shown by the 53 μm map of Harvey, Campbell, and Hoffman (1976), the cold local dust is in fact spread over a region roughly 90″ × 45″ in extent, corresponding to a local dust mass of order 20 $M_\odot$.

VI. SUMMARY AND CONCLUSIONS

In this paper we have presented three 16–30 μm continuum spectra and two-color scans of the galactic center. Comparison with high spatial resolution maps shows that in our data the extended background emission dominates over the compact sources. The map has a spatial resolution of 30″ and shows that the source is slightly elongated along the galactic plane with a diameter of $\sim$40″ or 2 pc.

No [S III] 18.71 μm line emission has been detected from Sgr A West. This is consistent with large dust extinction [$\tau(18.71\ \mu\text{m}) \geq 2.1$] and normal S III/H II abundances. Indirect arguments suggest that S III/S $\geq$ 0.5 is reasonable, and that the S/H abundance is no more than a factor of 2 higher than in the solar neighborhood. A comparison with the Bγ flux suggests a lower S/H abundance. Measurements of Bα in a 30″ beam should allow more stringent limits on the S III abundance to be made.

All three 16–30 μm continuum spectra show a broad depression centered at about 18 μm, which we attribute to absorption by cold silicate dust grains. In order to investigate the properties of the dust, we have constructed two component models for the continuum and have fitted them to the data. In these models a hot optically thin cloud of dust lies behind a cold cloud of silicate dust grains with an optical depth of order unity. Three types of emissivities for the hot dust were considered: a constant emissivity, a $1/\lambda$ emissivity, and a silicate emissivity. The derived dust parameters are listed in Table 4. All three types gave good fits, but the silicate type is the most plausible on physical grounds. The success of the models demonstrates that the assumed silicate emissivity is reasonable. Furthermore, the presence of the 18 μm feature supports the hypothesis that silicate minerals are indeed responsible for the 9.7 μm feature observed in the spectra of many objects.

In extending this silicate model to $\lambda > 30$ μm, we find that a simple and natural modification improves the fit greatly. If one-third of the absorbing dust is local to the galactic center, and the rest is distributed along the line of sight ("interstellar"), then we can account for published photometry to 175 μm. The temperature of the local dust is raised slightly, to $\sim$60 K, and the interstellar component is too cold and/or too extended to be observed.

Below $\lambda \sim 16$ μm, the silicate model predicts a flux consistently below the observed values. This discrepancy requires the presence of additional emission sources at shorter wavelengths.

The silicate model also fails to duplicate the observed depth of the 9.7 μm absorption feature. The assumed value of 1.7 for the ratio $\tau(9.7\ \mu m)/\tau(19\ \mu m)$ may be too low. A better value would lie between 2 and 3. Finally, a lower limit of 14 may be set on the ratio of visual to 19 μm extinction, $A_V/\tau(19\ \mu m)$.

In the line of sight to the galactic center, the total dust mass column density is $\sim 1.4\times10^{-3}$ g cm^{-2}. This value assumes that silicate grains make up both components; other models will lower this estimate by a factor of 2 or 3. In the three component model, the interstellar dust mass column density is $\sim 1.0\times10^{-3}$ g cm^{-2} along the 10 kpc line of sight. The total dust mass local to the galactic center (within about 2 pc) is $\sim 20\ M_\odot$.

We thank the pilots and crews of the Kuiper Airborne Observatory and the Lear Jet for their support. Gerry Stasavage and Westy Dain were instrumental in the building and testing of our spectrometer and data system. This work was supported by NASA contracts NGR 33-010-081 and NGR 33-010-182.

REFERENCES

Aitken, D. K., Jones, B., and Penman, J. M. 1974, *M.N.R.A.S.*, **169**, 35P.
Allen, C. W. 1973, *Astrophysical Quantities* (3d ed.; London: Athlone).
Balick, B., and Sneden, C. 1976, *Ap. J.*, **208**, 336.
Becklin, E. E., Matthews, K., Neugebauer, G., and Willner, S. P. 1978*a*, *Ap. J.*, **219**, 121.
———. 1978*b*, *Ap. J.*, **220**, 831.
Becklin, E. E., and Neugebauer, G. 1968, *Ap. J.*, **151**, 145.
Bevington, P. R. 1969, *Data Reduction and Error Analysis for the Physical Sciences* (New York: McGraw-Hill).
Dain, F. W., Gull, G. E., Melnick, G., Harwit, M., and Ward, D. B. 1978, *Ap. J.* (*Letters*), **221**, L17.
Ekers, R. D., Goss, W. M., Schwarz, U. J., Downes, D., and Rogstad, D. H. 1975, *Astr. Ap.*, **43**, 159.
Forrest, W. J., McCarthy, J. F., and Houck, J. R. 1979, *Ap. J.*, **233**, 611.
Gillett, F. C., Jones, T. W., Merrill, K. M., and Stein, W. A. 1975, *Astr. Ap.*, **45**, 77.
Harvey, P. M., Campbell, M. F., and Hoffman, W. F. 1976, *Ap. J.* (*Letters*), **205**, L69.
Knacke, R. F., and Capps, R. W. 1977, *Ap. J.*, **216**, 271.
Lacy, J. H., Baas, F., Townes, C. H., and Geballe, T. 1979, *Ap. J.* (*Letters*), **227**, L17.
Lebofsky, M. J. 1979, *A.J.*, **84**, 324.
McCarthy, J. F. 1980, Ph.D. dissertation, Cornell University.
McCarthy, J. F., Forrest, W. J., and Houck, J. R. 1979, *Ap. J.*, **231**, 711.
Mezger, P. G., and Smith, L. F. 1976, *Astr. Ap.*, **47**, 143.
Neugebauer, G., Becklin, E. E., Matthews, K., and Wynn-Williams, C. G. 1978, *Ap. J.*, **220**, 149.
Peimbert, M., and Torres-Peimbert, S. 1977, *M.N.R.A.S.*, **179**, 217.
Penman, J. M. 1976, *M.N.R.A.S.*, **175**, 149.
Rieke, G. H., Telesco, C. M., and Harper, D. A. 1978, *Ap. J.*, **220**, 556.
Rodriguez, L. F., and Chaisson, E. F. 1978, *Ap. J.*, **228**, 734.
Sutton, E., Becklin, E. E., and Neugebauer, G. 1974, *Ap. J.* (*Letters*), **190**, L69.
Willner, S. P. 1976, Ph.D. dissertation, California Institute of Technology.
Willner, S. P., Russell, R. W., Puetter, R. C., Soifer, B. T., and Harvey, P. M. 1979, *Ap. J.* (*Letters*), **229**, L65.
Woolf, N. J. 1973, in *Interstellar Dust and Related Topics*, ed. J. M. Greenberg and H. C. van de Hulst (Boston: D. Reidel), p. 485.

D. A. Briotta, W. J. Forrest, and J. R. Houck: Space Sciences Building, Cornell University, Ithaca, NY 14853

J. F. McCarthy: Hughes Aircraft Company, Building 541, Mail Station B322, P.O. Box 92919, Airport Station, Los Angeles, CA 90009.